Dissertation
Submitted to the
Combined Faculties for Natural Sciences and for Mathematics
of the Ruperto-Carola University of Heidelberg, Germany
for the degree of
Doctor of Natural Sciences

Presented by
M.Sc, Andrea Boni
Born in Feltre, Italy
Oral Examination: 21.01.2015

Inner nuclear membrane protein targeting studied by quantitative live cell imaging and RNAi screening

Referees: Prof. Dr. Iain Mattaj
                                    Prof. Dr. Oliver Gruss

This work has been carried out at the European Molecular Biology Laboratory in Heidelberg from October 2010 to June 2014 under the supervision of Dr. Jan Ellenberg.

Contribution:

Antonio Politi developed the mathematical model for INM protein targeting

Summary

During interphase of cycling cells, the surface of the nuclear envelope (NE), consisting of inner and outer nuclear membrane (I/ONM) fused at each nuclear pore complex (NPC) approximately doubles. This organelle growth requires homeostatic synthesis and delivery of lipids and proteins to maintain a fully functional NE and prepare for the next nuclear division. INM proteins reside specifically in the INM and carry out several essential functions. They constitute a heterogeneous class of transmembrane proteins and are delivered by the probably least understood cellular membrane trafficking pathway. How targeting of the different classes of INM proteins is achieved and how many trafficking and regulatory mechanisms exist is currently not well understood. One reason is that unlike for other trafficking pathways such as membrane secretion, it has so far been impossible to visualize INMP trafficking in live cells.

To address this point in the first part of my project I have developed a novel INMP trafficking reporter system (named Target-INM) that allows the acute release of INM proteins from the ER to the INM. The system is based on trapping INM proteins in the ER with a cleavable retention domain that can be removed by acute activation of a protease. I applied this generic reporter strategy to a set of INM proteins (LBR, Lap2beta, Tor1AIP1, Man1 and Sun1) that represent the major transmembrane protein classes and could image and quantify their synchronous delivery from the ER to the INM in interphase with high spatial and temporal resolution.

Exploiting this assay, I screened by siRNA knockdown and automated high resolution confocal time-lapse microscopy 96 candidate genes for their requirement in LBR targeting. These genes include nucleoporins, importins, lamins as well as NE and ER membrane proteins. I identified several genes that affect LBR INM targeting. Together with Antonio Politi, a postdoc in the lab, I developed a mathematical model of the INM protein targeting process that I used to fit the kinetic signatures of the different transport phenotypes and cluster the scoring genes into three major phenotypic classes providing evidences for the basic principle governing INM protein targeting. Comparing the genetic requirements for targeting of the different INMP protein classes should now put us in a position to define the number of molecularly distinct trafficking pathways from the ER to the INM.

Zusammenfassung

Während der Interphase teilungsaktiver Zellen, verdoppelt die Kernhülle (KH), die aus einer inneren und äußeren Membran (I/ANM) besteht, welche an den Kernporen fusionieren, in etwa ihre Oberfläche. Dieses Organellenwachstum setzt homöostatische Synthese und Anlieferung von Lipiden und Proteinen voraus, um die KH voll funktionsfähig zu halten und sie für die nächste Kernteilung vorzubereiten. INM Proteine halten sich spezifisch in der INM auf und führen verschiedene essentielle Funktionen aus. Sie bestehen aus einer heterogenen Klasse von Transmembranproteinen und werden über den wahrscheinlich bisher am wenigsten verstandenen zellulären Membrantransportweg angeliefert. Wie die gezielte Anreicherung verschiedener Klassen von INM Proteinen bewerkstelligt wird und wie viele Transport-und Regulationsmechanismen es gibt, ist bisher nicht bekannt. Ein Grund ist, dass es bisher nicht, wie bei anderen Transportwegen wie Membransekretion, möglich war, INMP-Transport in lebenden Zellen zu visualisieren.

Um diesen Punkt zu adressieren, habe ich im ersten Teil meines Projektes ein neues INMP Transport-Reportersystem (Target-INM) entwickelt, dass die akute Freigabe von INM Proteinen vom Endoplasmatischen Reticulum (ER) in die INM erlaubt. Das System basiert auf dem Einschließen von INM Proteinen im ER mit einer abspaltbaren Retentionsdomäne, die durch akute Aktivierung einer Protease entfernt werden kann.Ich habe diese generische Reporterstrategie auf ein Set von INM Proteinen angewendet (LBR, Lap2beta, Tor1AIP1, Man1 und Sun1), die die Hauptklassen von Transmembransproteinen repräsentieren, und konnte ihre synchrone Bewegung vom ER in die INM in Interphase mit hoher räumlicher und zeitlicher Auflösung am Mikroskop aufnehmen und quantifizieren. Mit diesem Assay habe ich mit siRNA Knockdown und automatisierter hochauflösender Konfokalmikroskopie 96 Kandidatengene auf ihre Notwendigkeit in LBR targeting gescreent. Diese Gene beinhalten Nukleoporine, Importine, Lamine und auch KH und ER Membranproteine. Ich habe verschiedene Gene indentifiziert, die LBR INM targeting beeinflussen. Zusammen mit Antonio Politi, einem Postdoc aus dem Labor, habe ich ein mathematisches Model vom INMP Targeting-Prozess entwickelt, das ich benutzt habe um kinetische Signaturen verschiedener Transport-Phänotypen zu fitten und die Treffer-Gene in drei große phänotypische Klassen zu

unterteilen, die Hinweise auf grundlegende Prinzipien von INM Protein-Targeting liefern. Der Vergleich genetischer Vorraussetzungen für das Targeting verschiedener INMP Proteinklassen sollte uns nun in die Lage versetzen, die Anzahl der molekular verschiedenen Transportwege vom ER zur INM defnieren zu können.

Table of Contents

3 Material and Methods

4 Discussion

1 INTRODUCTION

1.1 The Nuclear Envelope (NE): an overview

One of the characteristic features of the eukaryotic cell is the presence of a nucleus. This highly organized structure is delimited from rest of the cell by a double membrane system called the nuclear envelope (NE). The NE can be separated into two different compartments: the *Outer Nuclear Membrane* (ONM), which is continuous with the endoplasmic reticulum (ER) and has a similar protein composition, and the *Inner Nuclear Membrane* (INM) that faces the nucleoplasm and is more specialized in proteins composition and function. The 40-50 nm lumen between the ONM and the INM is the perinuclear space (PNS). The *nuclear lamina*, a dense meshwork of intermediate filament proteins termed *lamins* and their associated proteins, lies directly underneath the INM. Another characteristic of the INM is the presence of a large set of transmembrane proteins called *Inner Nuclear Membrane Proteins* (INMPs), which have essential functions in the stability of the nuclear structure and genome organization. The Nuclear Pore Complexes (NPCs) are inserted in a region, called *pore membrane* (PoM) where the ONM and the INM are fused, to ensure selective transport of proteins and ribonucleoproteins as well as passive diffusion of charged ions via its central channel (Figure 1.1).

Despite its stable structure during interphase, during an open mitosis the NE can become very dynamic and flexible and undergo complete disassembly, which is reversed with the reformation of the NE in the two daughter cells. Moreover the nuclear envelope surface almost doubles between G1 and G2 of cycling cells in preparation for the next division. Postmitotic NE reassembly as well as NE growth during interphase require remodeling of membranes, reformation of protein complexes (e.g.NPC and lamin filaments) and trafficking of many membrane proteins to rebuild a fully functional NE (see paragraph 1.3.1).

Recently the NE is no longer considered just a physical barrier to separate the nuclear and cytoplasmic processes of the cell but a fundamental player in genome regulation and an interface between external stimuli and the cytoskeleton on the one and the genome on the other side due to the functions of many INMPs (Dauer and Worman, 2009).
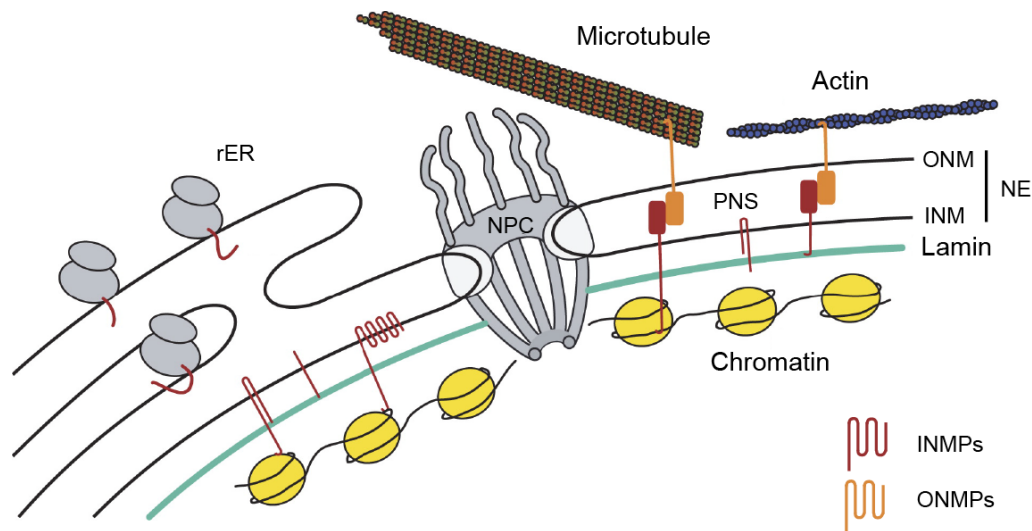
Figure 1.1 Schematic representation of Nuclear Envelope (NE) structure and its main components. The NE is composed of the Outer Nuclear Membrane (ONM) and the Inner Nuclear Membrane (INM). The ONM is continuous with the rough endoplasmic reticulum (rER). The ONM and INM fuse to each other in regions where the Nuclear Pore Complexes (NPCs) are inserted. The space between the ONM and INM is called the Perinuclear space (PNS). Several transmembrane proteins called Inner nuclear Membrane Proteins (INMPs) are localized to the INM where they interact both with lamins or chromatin. Some INMPs can also interact in the PNS with proteins of the ONM that are bound to the cytoskeleton (Adapted from Dultz and Ellenberg, 2007).

1.1.1   The scaffold of the metazoan nucleus: the nuclear lamina

In order to maintain the integrity and the structure of the nucleus, metazoan cells have evolved a 25-50nm thick network of type V intermediate filaments, called lamins (Dechat et al., 2008). Nuclear lamins are the major component of the nuclear lamina and they can be separated into two major types called type A and type B nuclear lamins. The Lamin-A gene (*lmna*) gives rise to four different lamins: two type A and two type C lamins; instead Lamin-B1 and Lamin-B2 originates from two different genes *lmnb1* and *lmnb2*. Lamins were believed to be specific to animal metazoans with no homologous genes present in fungi and plants (Mans et al., 2004). Recently lamin orthologues were found in several amoebozoan species, such as the NE81 genes in Dictyostelium (Kruger et al., 2012).

The protein structure of lamins reassembles that of other intermediate filaments

consisting of a central rod domain with four α-helical coiled-coil segments flanked by a small globular N-terminal domain and a larger immunoglobin-like C-terminal domain. Individual monomer can then associate to form coiled-coil homodimers that are described to form high order lattice structures by head to tail and side to side association at least *in vitro* (Aebi et al. 1986). Both types of lamins undergo a series of posttranslational modifications; stable association of B-type lamins into the INM depends on its tail where the cystein in the CaaX domain becomes farnesylated and methylated. In contrast to Lamin-B, Lamin-A undergoes an endoproteolytic cleavage that removes the farnesyl and methylated tail; this cleavage occurs after its insertion into the nuclear lamina and thus the mature lamin A is no longer membrane associated. If Lamin-A and Lamin-B can form homopolymers or heteropolymers and whether the more complex nuclear lamina in somatic cells recapitulates the structures described in vitro is still unknown.

At least one type of Lamin-B is expressed ubiquitously whereas embryonic stem cells and some differentiated cell types do not express Lamin-A. The main function of the nuclear lamina is to ensure stability and it largely determines the overall shape of the interphase nucleus. Moreover it provides anchoring sites for the NPCs and substrates for the interactions with many NE proteins (Wilson and Foisner, 2010). Proper localization of lamin binding proteins is fundamental for their roles in gene regulation and signaling in the nucleus and it is dependent on an intact network of lamins. For instance, Lamin-associated domains (LADs) are genomic regions ranging from about 80 kb to 30 Mb that are anchored to the nuclear periphery (Guelen et al., 2008) via interactions with lamin binding proteins or lamin directly. Many of the genes within a LAD are transcriptional inactive suggesting a direct role of nuclear lamina in gene regulation and chromatin organization (Akhtar and Gasser, 2007; Heessen and Fornerod, 2007). Mutations in lamin genes lead to a class of human diseases called laminophaties such as Emery-Dreifuss muscular dystrophy and Hutchinson-Gilford progeria. This disease class presents with a wide range of organ and cellular phenotypes consistent with the multiple roles of lamins both in NE structure maintenance and genome regulation.

1.1.2   The nuclear pore complex (NPC): structure and functions

Trafficking across the NE is finely regulated by a large macromolecular complex, called the nuclear pore complex (NPC). The NPC is composed of multiple subcomplexes that assemble themselves in a structure of about 50 MDa in yeast (Rout et al., 2000) and 110 MDa in vertebrates (Reichelt et al., 1990). Studies by electron microscopy reveal a conserved architecture of the NPC across different species (Hinshaw et al., 1992; Akey and Radermacher, 1993, Beck et al., 2004; Beck et al., 2007). It has a cylindrical structure with pseudo eight-fold symmetry that can be divided in two main parts: a central core part in the plane of the nuclear membrane and the two peripheral structures: a filamentous structure toward the cytoplasmic side and a basket-like structure toward the nucleoplasm. The central core is formed by three main ring structures, the nucleoplasmic, spoke and cytoplasmic rings that create a central channel with a minimum diameter of about 50 nm; an additional peripheral approximately 10 nm channel is believed to exist between the NPC and pore membrane (PoM) (Reichelt et al., 1990; Hinshaw et al. 1992) (Figure 1.2 A).

Despite its huge molecular size the NPC is composed of only approximately 30 proteins, called nucleoporins (Nups), present in a multiple of eight copies in each NPC. Some Nups, like Nup107-160, Nup93 and Nu62 localize symmetrically to the central core of the NPC; other Nups instead form the cytoplasmic filaments (Nup358 or RanBP2) and the nuclear basket (Tpr) (Brohawn et al., 2009). The anchorage of the NPC to the nuclear membrane is mediated by several transmembrane nucleoporins (e.g. Pom121, ndc1 and gp210) (Figure 1.2B)
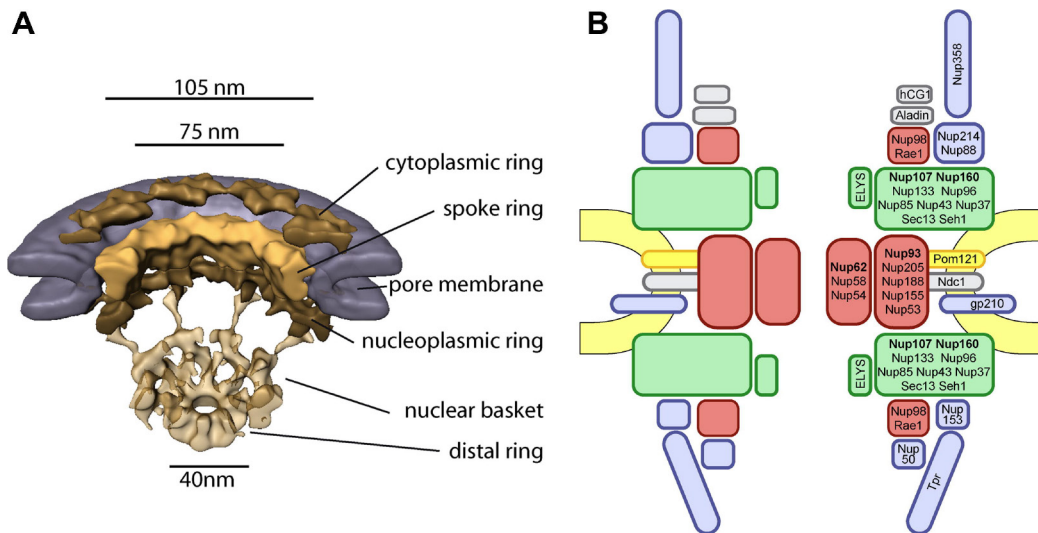
Figure 1.2 (A) Reconstruction of *D. Discoideum* nuclear pore by 3D cryo-EM nuclear pore with the dimensions of the outer and inner diameter and the central channel indicated (Beck et al., 2007). (B) Molecular architecture of vertebrate NPC complex showing the different NPC subcomplexes. (from Antonin et al., 2008).

The central core of the NPC is believed to be a stable structure that does not dissociate during interphase (Rabut et al., 2004). In differentiated cells of *C. elegans* and in rat brain tissue it has indeed been shown to be stable for the entire life (D'Angelo et al., 2009, Savas et al., 2012). In contrast peripheral nucleoporins are more much dynamic and can exchange with the soluble pool of Nups (Rabut et al., 2004).

Assembly of the NPC is a multistep process that occurs in cycling cells with an open mitosis at two cell cycle stages: at the end of mitosis and during interphase. These two assembly processes, although not fully understood, differ both in terms of molecular requirements and timing. Postmitotic assembly occurs in a relative short time frame to re-establish an import competent NPC within 10 minutes (Dultz et al., 2008). On the other hand interphase assembly, which takes place on a sealed NE membrane, is a slower process characterized by the initial accumulation of transmembrane nucleoporin at the assembly site (Dultz et Ellenberg, 2010, Doucet et al., 2010) and requires on the order of one hour.

The NPC, although freely permeable to small molecules, metabolites and ions smaller than 50 kDa, acts as a highly selective barrier for macromolecules. Facilitated transport across the NPC of soluble cargos larger than 50-60 kDa is an efficient process that occurs in a number of steps: 1) The Nuclear Localization Signal (NLS) or Nuclear Export Signal (NES) in the cargo are first recognized by nuclear transport factors (NTFs) 2) The NTFs–cargo complex docks to the NPC by interaction with specific Nups and translocate through the NPC. 3) Once the target compartment is reached, the complex dissociates and the cargo molecule is released. Directionality of the transport is ensured by a gradient of RanGTP/RanGDP across the nuclear envelope that promotes the association or dissociation of the NTF with their cargo molecules (Weiss et al., 2003 Stewart, 2007).

The family of nuclear transport factors or karyopherins includes around 20 members. Among them, are importin-ß and its adaptor importin-α that take part in nuclear import, as well as the exportin CRM1 which is involved in the process of nuclear export. Importin-ß binds its NLS cargo protein in the cytosol and translocates to the nucleus through the interactions in the NPC central channel. The interaction surface is mediated by Nups enriched in FG repeats that are multiple hydrophobic regions made of FG, FXFG or GLFG peptides. In the nucleus the binding of RanGTP to importin-ß induces the release of the NLS cargo protein from importin-ß (Stewart, 2007). Based on the fact that the Ran GTP exchange factor (RanGEF) RCC1 is chromatin associated, a higher concentration of RanGTP is found in the nucleus and this imposes the directionality of the transport process. In contrast the association of the export factors CRM1 with its cargo is enhanced by the presence of RanGTP allowing the exportin-cargo-RanGTP complex to exit the nucleus (Fornerod et al., 1997; Matsuura and Stewart, 2004). Once in the cytoplasm hydrolysis of GTP promoted by RanGAPs triggers the disassembly of the complex and the release of the cargo. Therefore transport across the NPC itself does not require energy consumption and it is powered simply by diffusion whereas directionality is assured by a steep gradient of Ran in the GTP- or GDP-bound state across the NE that favors assembly of export complexes in the nucleus and import complexes in the cytoplasm.

Apart from the essential function in nucleocytoplasmatic transport, the NPC is emerging as an important element in gene regulation. It has been shown that some

nucleoporins associated with active genes in yeast might facilitate export of mRNA in a model the called *gene-gating hypothesis* (Casolari et al., 2004). Moreover different Nups display cell-specific expression; for instance, in embryonic stem cells (ESCs) the transmembrane nucleoporin gp210 is absent but becomes expressed and incorporated into the NPC in differentiated cells: preventing its incorporation into the NPC blocks the expression of genes required for differentiation without affecting nuclear transport (D'Angelo et al., 2012). The role of Nups that are not incorporated in the NPC has been also examined. Recently two works demonstrated that nucleoplasmic Nups bind directly to chromatin and are involved in the regulation of transcription of cell-cycle and developmental genes (Capelson et al., 2010; Kalverda et al., 2010). Many other functions have been described for the NPC and specific Nups ranging from the coordination of cell cycle progression, to the maintenance and repair of chromatin (reviewed in Strambio-De-Castillia et al., 2010).

1.2 Nuclear Membrane Proteins

The Outer Nuclear Membrane (ONM) is an extension of and shares many of its components with the endoplasmic reticulum (ER) to which it is connected with tubules and cisternae at multiple sites. However a subset of membrane proteins is exclusively localized to the ONM. Moreover the Inner Nuclear Membrane (INM) contains both a specific class of INM proteins and has a specialized lipids composition (Ledeen and Wu, 2006). Many studies have tried to identify the complete repertoire of NE proteins both by microscopy screen (Rolls et al., 1999) and by mass spectrometry (Dreger et al., 2001; Schirmer et al., 2003; Murthi and Hopper, 2005). Recently it has become clear that the NE proteome greatly differs between cell types and tissues (Korfali et al., 2010, 2012, Wilkie et al., 2011, reviewed in Wong et al., 2014) and although many of these proteins have not yet been characterized in detail this variability likely reflects multiple roles of NE proteins in cell identity and differentiation.

1.2.1   Outer Nuclear Membrane Proteins (ONMPs)

The presence of several proteins that exclusively localized to the ONM raised

some intriguing questions: what prevents ONM proteins from diffusing back to the peripheral ER? Are they tethered within the ONM or do diffusion barriers exist between the ONM and the ER?

Starr and Han (2002) found that the localization of *C. Elegans* Anc-1, a large type II ONM protein, was dependent on Unc-84, an INM protein, via the interaction of their respective luminal domains in the perinuclear space (PNS). The interaction depends on a conserved C-terminal domain, named KASH that was then described to be present also in the ONM protein Klarsicht from *Drosophila* and Syne-1 and Syne-2 in humans (also referred as Nesprin 1 and Nesprin 2). Recently two studies defined the structural basis of the KASH-SUN interaction demonstrating that the SUN proteins arrange as homotrimer able to bind three KAS peptides (Sosa et al., 2012; Zhou et al., 2012). Protein containing KASH domains belong to a family that in mammals is encoded by the Nesprin 1-3 genes and consists of a number of alternatively spliced isoforms (Zhang et al., 2001). Nesprin 1-2 give rise to two very large proteins Nesprin 1 Giant (Nesp1G 1.000kDa) and Nesprin 2 Giant (Nesp2G 800kDa) as well as other smaller isoforms believed to be localized in the INM too (Mislow et al., 2002). Nesp1G and Nesp2G have a typical domain organization with a large cytoplasmic N-terminal tail containing an actin binding domain (ABD), followed by multiple spectrin repeats and a C-terminal PNS tail with the conserved KASH domain. The more recently discovered Nesprin-3 (Nesp3) and Neprin-4 (Nesp4) bind respectively the cytoskeleton protein plectin (Wilhelmsen et al., 2005) and the motor protein kinesin-1 (Roux et al., 2009). Localization of all Nesprin proteins to the ONM is dependent on the interaction in the PNS with the Unc-84-related INM proteins, Sun1 and Sun2 (Padmakumar et al., 2005). The macromolecular assembly containing Nesprin and Sun is known as the LINC complex (for <u>L</u>inker of the <u>C</u>ytoskeleton and <u>N</u>ucleoskeleton) since Sun1 and Sun2 are INM proteins that bind several nuclear proteins, including A-type lamins (Crisp et al., 2006)(Figure 1.3). The LINC complex is crucial for a number of different nuclear process. For example pronuclear migration along microtubules in *C. elegans*, the movement of telomeres in the nucleus during meiosis and mechanotransduction of signals from the extracellular matrix to the genome all rely on an intact LINC complex (reviewed in Tapley and Starr, 2013). Recently the Nesprin-4 gene was identified to carry a disease causing mutation in a family with hereditary hearing loss; indeed Nesprin-4 knockout mice are normal except for specific hearing loss phenotypes (Horn et al., 2013). Consistent with a

proposed role of the LINC complex, cochlea cells these mice exhibit several defects in nuclear positioning and degenerated stereocilia.
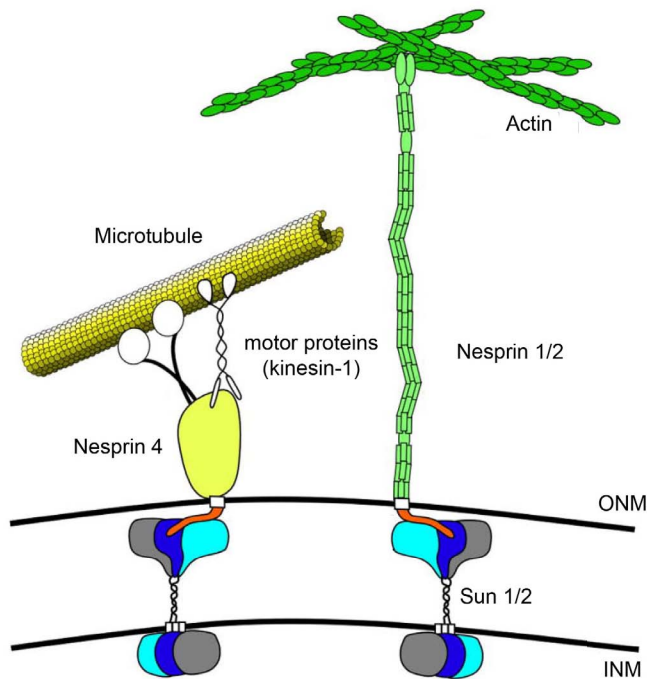
Figure 1.3 Interaction of SUN and KASH proteins across the NE. SUN protein trimers (light blue, dark blue, and grey) bind the KASH domain of Nepsrin in the perinuclear space. Nespin 4 recruits microtubule motor proteins to the surface of the nucleus, while Nepsrin 1 and Nesprin 2 are able to bind actin filaments (Adapted from Tapley and Starr, 2013).

1.2.2   Inner Nuclear Membrane Proteins (INMPs)

Recently there has been increasing interest in Inner Nuclear Membrane proteins (INMPs) because of the link between INMPs and a variety of genetic diseases. However, so far only a subset of 15 INMPs is well characterized in term of membrane topology, domain organization and functions. They are mostly type II membrane proteins with the N-terminus facing the nucleoplasm and multiple structural features in terms of the number of transmembrane (TM) and size of the N-terminal domains (Table 1.1). INMPs are part of a fundamental network for nuclear structure stability, spatial organization of the genome and gene regulation via direct or indirect interaction with nuclear binding partners, such as lamins and chromatin proteins (Burke and Stewart, 2006) Moreover INMPs have been implicated in important signaling pathways inside the nucleus (Worman et al., 2006).

Name	Number of TMD	Size of the nucleoplasmic domain (aa)
Emerin	1	223(Nt)
Man1	2	474(Nt)/213(Ct)
Lap2β	1	410(Nt)
TMEM43/LUMA	4	30(Nt)/11/11(Ct)
Sun1	1	315(Nt)
Sun2	1	212(Nt)
LBR	8	211(Nt)
LEM2	2	212(Nt)/105(Ct)
Nurim	6	4(Nt)/17/27/28(Ct)

Table 1.1 Table including some of the well characterized INMPs. Transmembrane Domain (TMD), N-terminus (Nt), C-terminus (Ct). For multipassing INMPs the size of each nucleoplasmic domain is indicated. Note the large variability of the nucleoplasmic domain size among different INMPs. (Source Lusk et al., 2011 and UniProtKB/Swiss-Prot)

Lamin-associated polypeptide2 (LAP2), LAP1 and lamin B receptor (LBR) are by far the most abundant lamin binding proteins in the INM. The family of LAP2 proteins includes the alternative spliced isoforms LAP2 β, γ, δ and ε (Harris et al., 1995; Harris et al., 1994; Furukawa et al. 1995). With a total molecular weight ranging from 38 to 50 kDa they are characterized by the presence of one transmembrane region and a large N-terminal nucleoplasmic domain that binds lamins (Harris et al., 1994; Harris et al., 1995; Furukawa et al. 1995). LAP2 proteins share a conserved 43 amino acid motif, known as the LEM domain (named after Lap2, Emerin and MAN1), which mediates interaction with the DNA-binding protein BAF (barrier-to-autointegration factor), an important sequence-independent DNA cross-linking protein implicated in nuclear assembly, chromatin organization and cell cycle progression (Margalit et al., 2007). The LEM domain is also found in other INMPs such as Emerin a small 34 kDa single pass INM protein (Bione et al., 1994; Manilal et al., 1996), MAN1, a double pass transmembrane protein with both N and C termini exposed to the nucleoplasm (Lin et al., 2000), the Ankyrin repeat and LEM domain-containing protein 2 (ANKLE2) and LEM2/3. Domains that bind DNA or chromatin proteins are present in several LEM-containing proteins; the complex network of interactions between

lamins, LEM proteins, BAF and other nuclear factors is responsible for the connection between chromatin and NE thereby regulating signaling and transcription (reviewed in Wilson and Foisner, 2010).

Lamin B receptor (LBR) is probably the most well characterized INM protein. Initially discovered due to its capacity to bind specifically to Lamin-B (Worman et al., 1990), LBR also binds via 200aa N-terminal domain the MeCP2, HA95 and heterochromatin (HP1) proteins. The interaction seems to be regulated by cell cycle phosphorylation at many arginine/serine rich regions (Nikolakaki et al., 1997). On the other hand the C-terminal domain is believed to function as a sterol reductase given the high sequence homology with various sterol reductases.

A additional class of INM proteins is characterized by the presence of the SUN domain which is found in the homologues proteins Sad1 and UNC-84 in *S. pombe* and *C. elegans* respectively (Malone et al., 1999). Five different SUN proteins are present in mammals, two of which SUN1 and SUN2 are localized specifically to the INM (Hodzic et al, 2004; Padmakumar et al, 2005). The N-terminal domain extends into the nucleoplasm and binds to the nuclear lamina. Whereas the conserved C-terminal SUN domains reside in the PNS and interact with the KASH domain of Nesprin ONM proteins forming the LINC complex. SUN2 forms stable homotrimers through coiled-coil regions adjacent to its SUN domain (Sosa et al., 2012; Zhou et al., 2012) and it also heteroligomerizes with SUN1 (Wang et al, 2006; Lu et al, 2008).

A visual screen for nuclear envelope-localizing proteins (Rolls et al., 1999) first identified Nurim as a new INM protein (Rolls et al., 1999). Interestingly this multispanning transmembrane protein lacks the large N-terminal domain required for binding to the nuclear lamina and chromatin; the tight association of Nurim within the INM is dependent on its C-terminal domain through the binding with a currently unidentified protein in the nucleus (Hofemeister and O'Hare, 2005). LUMA has been recently added to the INMPs panel following its identification in a proteomic screen (Dreger et al., 2001). Characterization of the LUMA protein revealed that it has four transmembrane domains with both N and C termini in the nucleoplasmic face of the nuclear membrane. LUMA can oligomerize through its transmembrane domains and interact with Emerin participating in controlling its distribution in the NE (Bengtsson and Otto, 2008).

Small isoforms of Nesprin 1 and 2 are also reported to localize to the INM (Mislow et al., 2002; Zhang et al., 2001). They contain a LEM-like domain but their localization

to the INM depends on interaction with A-type lamin and Emerin being unable to bind BAF directly.

1.2.3   The role of INMPs in disease

It is now clear that INMPs have many other functional roles apart from the maintenance of nuclear structure and stability. The genome is non-randomly distributed inside the cell nucleus; various studies have identified self-associated topological domains (TADs) described as subchromosomal regions that self-interact while having few contact sites with neighboring TADs (Dixton et al., 2012). Moreover Lamin Associated Domains (LADs) are defined as large chromatin domains that are in contact with the nuclear lamina. Although it has been shown that TADs are fairly conserved between cell types as well as between embryonic stem cells and more differentiated cell types, LADs can substantially change. Many LADs contain developmentally regulated and cell-type specific genes that need to be activate in a specific temporal framework. Various studies have shown how genome-nuclear lamin interactions reorganize during neuronal differentiation (Peric-Hupkes et al., 2010) or during myogenesis (Yao et al., 2011) allowing expression of developmentally regulated genes. Interestingly, establishment of this chromatin configuration requires the presence of different INMPs such as Lap2b (Zullo et al., 2012) and LBR (Solovei et al., 2013). These evidences are also supported at the molecular level since LBR can form a quaternary complex with the heterochromatin protein (HP1) and under-acetylated core histones H3/H5 (Polioudaki et al., 2001). Moreover the binding of LBR with the methyl binding protein MeCP2 (Guarda et al., 2009) and methylated histones (Hirano et al., 2012) can play a direct role in positioning DNA and heterochromatin to the nuclear periphery. In the same way LAP2β can repress transcription by interacting with the repressor GCL and inducing deacetylation of histone H4 through the histone deacetylase HDAC3 (Nili et al., 2001; Somech et al., 2005). Given the cell type differences in NE proteome composition and that several INMPs are differentially expressed in different tissues (reviewed in Wong et al., 2014) it has been proposed that cell specific chromatin organization relies significantly on the composition of the NE. Indeed overexpression screening of several NE proteins influence the localization of chromosomes inside the nuclei and

the chromatin compaction state (Korfali et al., 2010, Zuleger et al., 2013).

Apart from their roles in overall genome regulation some INMPs may more directly modulate specific functions and pathways inside the cell. Martins et al., 2003 proposed that LAP2β is involved in regulation of DNA replication. During interphase, LAP2β interacts with HA95 and stabilizes the replication factor Cdc6 preventing its proteasome degradation thereby promoting DNA replication. An involvement of the INM protein MAN1 in the regulation of TGF-β/BMP signaling during the dorsoventral axis determination in *Xenopus* embryos came initially from two different studies (Osada et al., 2003; Raju et al., 2003). The TGF-β/BMP signaling cascade is propagated inside the cell by the phosphorylation of members of the signal transducers family, Smad. MAN1 interacts via its C-terminal domain with all Smad family members thereby inhibiting the TGF-β/BMP signaling by sequestration of the Smad factors to the INM; indeed downregulation of MAN1 by RNAi enhances the TGF-β (Lin et al., 2005; Pan et al., 2005). In addittion some plasma membrane growth factor receptors (such as Amphiregulin and Heparin-binding EGF-like growth factor) have been demonstrated to traffic between the plasma membrane to the INM regulating general transcription and inducing heterochromatin formation. (Heida et al., 2008; Isokane et al., 2008). These new studies and the function of MAN1 in the TGF-β/BMP signaling identify the NE as an important interface between external stimuli and the genome.

Laminopathies are a class of diseases linked to mutations in the LMNA gene; however some of the INMPs, like Emerin, MAN1 and LBR are also disease associated. Mutations in the emerin gene cause the *X-linked Emery-Dreifuss muscular dystrophy (EDMD)*, the third most common form of X-linked muscular dystrophy. EDMD is characterized by muscle wasting, differentiation defects of myoblast into myotubes, cardiomyopathy and cardiac conduction defects. Loss of emerin from the NE can lead to disregulation of the MyoD induction of myogenesis (Melcon et al., 2006). Several diseases (osteopoikilosis, Buschke-Ollendorf syndrome, and melorheostosis) with severe sclerosing bone dysplasias and skin abnormalities are caused by mutations in the MAN1 gene. In affected families, deletions of the C-terminal domain of MAN1 disrupt the interaction with Smad family proteins; this can cause enhancement of the TGF-β/BMP signaling (as discussed above) that is also implicated in the regulation of bone density and homeostasis (Hellemans et al., 2004).

LBR mutations have been linked to two different types of diseases; impairment of the sterol reductase domain leads to the Pelger–Huet anomaly which is associated with abnormal nuclear shape and chromatin organization in neutrophil cells (Hoffmann et al., 2002). Interestingly LBR expression increases during the differentiation of precursors into granulocytes and supports the nuclear shape and chromatin changes necessary for neutrophil differentiation. Complete loss of LBR expression gives rise to the lethal HEM/Greenberg skeletal dysplasia (Waterham et al., 2003).

1.3 Nuclear Envelope Dynamics in Mitosis and Interphase

The nuclear envelope (NE) undergoes dramatic changes during the cell cycle of a metazoan eukaryotic cell. To allow chromosome segregation during an open mitosis the cytoplasmic mitotic spindle has to have access to the chromatin and this is achieved by the complete disassemble of the NE. As a consequence the NE must be regenerated in the two daughter cells in order to re-establish the nuclear compartmentalization and functions. Although less dramatic, changes in the structure of the NE also occur during interphase; the nuclear surface as well as the number of NPCs almost doubles in order to let the cell to properly progress through multiple cell divisions. NE remodeling in both mitosis and interphase is thus a highly dynamic and essential process that involves many molecular players and requires a fine level of regulation.

1.3.1   NE Remodeling During Mitosis: Role of Nuclear Membrane Proteins

NE disassembly during mitosis is a multi-step process that requires disruption of polymers and macromolecular complexes (e.g. nuclear lamina and NPCs), removal of membranes and trafficking of membrane proteins with both high temporal and spatial coordination. The process called nuclear envelope breakdown (NEDB) marks the entry in mitosis. (Terasaki et al., 2001; Dultz et al., 2008). NEBD begins with the removal of several nucleoporins from the NPC; this causes the initial loss of the permeability barrier of the NE and generates several fenestrations allowing the influx of molecules (Lenart et al., 2003). After substantial fenestration of the NE, mitotic

factors have access to the nucleus allowing NE disassembly to progress. Depolymerization of the nuclear lamina is the following step after NEBD and is largely mediated by the cyclin-dependent kinase 1 (Cdk1) phosphorylation of A/C lamins and importantly of INMPs like LAP2 β and LBR (Courvalin et al., 1992; Dreger et al., 1999).

Although chromatin condensation starts before NEBD, the rate of condensation increases dramatically upon NEBD (Hirota et al., 2004). In addition phosphorylation of chromatin proteins that are associated to the NE, such as BAF, reduces their affinity for the LEM protein family (LAP2, Emerin and MAN1) (Nichols et al., 2006). Lamina depolymerization and phosphorylation of INM and chromatin proteins trigger the complete absorption of NE membranes and the redistribution of INMPs into the ER (Ellenberg et al., 1997; Yang et al., 1997). NEDB is further facilitated by microtubule dependent tearing by the attachment of microtubule filaments to the outer face of the nucleus (Beaudouin et al.,2002). In addition depletion of the INM proteins SUN1 and SUN2 has been shown to delay removal of membrane from chromatin and to affect mitotic progression (Turgay et al., 2014). A similar phenotype is displayed by a series of proteins, called reticulons, that are able to bend and tubulate the ER (Voeltz et al., 2006). Depletion of a specific class of reticulons (i.e. YOP-1 and RET-1) not only leads to abnormal ER structure but delays NEBD (Audhya et al., 2007). In metaphase the bipoloar spindle is established such that the minus ends of microtubules are focussed at the two centrosomes and the plus ends interact with the chromosomes at their kinetochores. Interestingly NE components play an unexpected mitotic role; some Nups can be detected in association with the kinetochores (Loïodice et al., 2004) and are suggested to be involved in the spindle assembly checkpoint (Guttinger et al., 2009).

The reassembly of the NE (NER) occurs around the segregated chromatin in late anaphase and is concluded during telophase. NER is a delicate process that must ensure the enclosure of the whole set of chromosomes into a sealed NE with functional NPCs and an intact lamina network. A spatial signal for reformation of the NE around chromatin is mediated by high levels of RanGTP produced by the chromatin associated factor RCC1 (Hetzer et al., 2002). One of the first events in NE reformation is the binding of the Nup107-160 complex to the surface of naked chromatin (Dultz et al., 2008). In the mitotic cytoplasm the Nup107-160 complex is

sequestered by importin-β. Binding of importin-β to RanGTP allows the release of Nup107-160 and the initiation of the assembly of NPCs on chromatin (Harel et al., 2003). In addition NER is a process that implicates the reorganization of the mitotic ER from tubules into NE sheets (Anderson and Hetzer, 2008). The initial coating of chromatin by the tips of ER tubules is believed to be supported by the presence of NE membrane proteins, such as the pore membrane Nups NDC1 and POM121, able to bind the preformed NPCs on chromatin (Anderson et al., 2009). Moreover a major role is played by INMPs trough their ability to bind directly to chromatin and/or nuclear factors. It has been shown that several INM proteins can bind DNA directly due to the presence of a basic extralumen domain (Ulbert et al., 2006). For instance LBR is able to target membranes to the naked chromatin surface in *Sea urchin* (Chaudhary and Courvalin, 1993; Collas et al., 1996) and it has been demonstrated to be recruited into chromatin early after anaphase in live cells (Ellenberg et al., 1997). A model for LBR-mediated targeting of membrane during NE reassembly suggests that importin-β is bound to the phosphorylated form of LBR in the mitotic ER. Upon approaching chromatin, importin-β is then release from the LBR due to the presence of high level of RanGTP and LBR dephosphorylated. LBR can now bind DNA and the heterochromatin protein HP1 and efficiently recruits membranes around chromatin (Ma et al., 2007; Lu et al., 2010). A role is also described for the chromatin protein BAF and LEM containing INMPs in the formation of a continuous NE membrane. during NEBD BAF is phosphorylated by the vaccinia-related kinase 1 (VRK1) causing its dissociation from the chromatin; reversal of this phosphorylation state during NE reassembly leads to the recruitment of LEM containing INMPs (LAP2 β, emerin and MAN1) to chromatin through an interaction with BAF interaction (Nichols et al., 2006). Interestingly Lem4 (also known as ANKLE2) interacts both with the phosphatase PP2A and VRK1 and controls the dephosphorylation of BAF during mitotic exit inhibiting VRK1 and enhancing PP2A activity (Asencio et al., 2012) Importantly at this early stage of NE reassembly the bulk of the nuclear lamins are not yet reassembled thus targeting of INMPs to the reforming NE is largely dependent on interactions with chromatin and chromatin proteins (Newport et al.1990).

Another point to consider is the topological rearrangement from the mitotic tubular ER into the spherical NE sheet. Although INM proteins play a role in this transition by spreading the ER membrane around the chromatin the implication of ER-shaping

proteins has been considered in different studies. The current proposal is that different ER tubule and edge binding proteins, the reticulons Rtn3-4 and DP1, are displaced from the forming NE to allow formation of the NE sheets. Indeed overexpression of reticulons inhibits NE formation and their depletion of these by siRNA accelerates NE formation in vivo (Anderson and Hetzer, 2008). How reticulons are displaced from the forming NE is still an open question.

1.3.2 NE Remodeling during Interphase

The nucleus of a cycling cell doubles its volume during interphase in order to maintain nuclear size in the two daughter cells. This process requires the integration of additional nucleoplasmic material, new membranes and lamina components. Strikingly NE growth, as well as the increase in NPCs, is not a direct consequence of DNA replication because inhibitors of DNA replication do not interfere with these processes (Maul et al., 1973, Dultz et al., 2010). *De novo* assembly of NPCs assembly in interphase leads to the increase of the total number of NPC from about 2000 in the G1 phase to 4000 in G2 in HeLa cells (Maul et al., 1972). Interphase assembly requires insertion of the NPC into an intact NE membrane and nuclear lamina and only recently is it clear that this mechanism differs from postmitotic assembly (Doucet et al., 2010; Dultz et al., 2010). The INM protein Sun1 has been implicated in NPC assembly during interphase in two different studies; Sun1 associates with NPCs (Liu et al., 2007) and its depletion from mammalian cells reduces interphase NPC assembly (Talamas et al., 2011).

A continuous delivery of membranes to the NE is necessary; however is not clear how this process happens *in vivo*. At least *in vitro* disruption of the connections between the NE and peripheral ER prevents nuclear expansion suggesting a pathway for membrane trafficking between the ER tubules to the ONM (D'Angelo et al., 2006). Nuclear membrane expansion can be mediated by farnesylated nuclear proteins as suggested in studies in *Xenopus*; for example overexpression of lamin B can lead to nuclear membrane growth in *Xenopus* oocytes (Prufert et al., 2004; Ralle et al., 2004). Moreover it has been suggested that lipid metabolism can play a role in nuclear envelope growth. In yeast abnormal proliferation of the nuclear membrane has been reported in deletion mutants that affect the balance between phosphatidic acid (PA)

and its dephosphorylated form diacyl glycerol (DAG) (Han et al., 2008; O'Hara et al., 2006). In addition the PA phosphatase lipin is implicated in lamina disassembly during mitosis (Gorjanacz and Mattaj, 2009, Mall et al 2012). Since the lamin network is very stable during interphase (Daigle et al., 2001) it is possible that membrane growth requires partial and local disassembly of the lamin network. Thus factors implicated in the depolymerization of the nuclear lamina during mitosis, such as PKC-isoforms and lipin could be important for local rearrangements in interphase. Not only membranes but also nuclear membrane proteins must be targeted to the NE during interphase. Although these proteins are co-translationally inserted into the ER membranes and can diffuse to the ONM, the NPC poses a diffusional barrier for those proteins that have to reach the INM. The mechanism of targeting INM proteins during interphase is still largely unknown and a detailed overview of the current knowledge will be discussed in the next section.

1.4 Targeting of INM Proteins In Interphase

As discussed previously after NEBD INMPs are distributed into the mitotic ER and they are responsible via their interactions with chromatin to reshape the ER into the NE during NE reassembly. In this manner INMP targeting is achieved and directly linked to a functional role in nuclear assembly (Antonin et al., 2008). Although INMPs carry out essential functions in interphase, surprisingly the INM is one of the least understood destination compartments in membrane trafficking. How targeting of proteins to this compartment is achieved and regulated is poorly understood especially when compared to the transport of soluble nuclear proteins across the NPC. Moreover substantial differences in the mechanism of targeting to the INM can exist between different resident proteins, given the great variability of the INMPs in terms of the number of transmembrane regions, size and domains organization of the nucleoplasmic domains. The first model to be proposed, called *diffusion-retention,* implies that once INMPs reach the INM by lateral diffusion from the ER, the interactions with the lamina or chromatin prevents them from diffusing back. It is now becoming clear that this model cannot fully explain the more recent experimental

findings; INM protein targeting must be considered as a *multi-step process* that includes diffusion from the ER to the ONM, NPC translocation and INM retention and/or mobility. Moreover different model organisms (yeast, mammalian cell and *Xenopus* oocytes), and methodologies (*in vitro* biochemistry or *in vivo* imaging) have been employed to study INM protein targeting therefore a comprehensive view of the targeting mechanisms for different INMPs has so far not been achieved.

1.4.1   Insertion of INM Proteins in the membrane

Protein insertion into the lipid membrane is a regulated process mediated by two well conserved systems: the Sec61 and GET (Guided-entry of a Tailed Anchor protein) system. The components of these two systems are located in the ER and ONM but possibly also at the INM (Deng et al., 2006). Insertion of membrane proteins with single (monotopic) and multiple (polytopic) transmembrane segments occurs co-translationally via the Sec61 system. Whereas the GEF pathway is used by proteins with a single transmembrane segment and a short luminal tail. Most of the well characterized INMPs are polytopic or contain large lumenal domains which make them likely to be inserted co-translationally via the Sec61 system; only emerin and Lap2β in principle can use the GEF system. Which of the two pathways are actually required for different INMPs has not been directly investigated. Moreover it is believed that INMP insertion occurs at the cytoplasmic ER-ONM surface but very small monotopic INMPs could as well transported as soluble chaperoned proteins into the nucleus first and then be directly inserted into the INM destination compartment.

1.4.2   The *Diffusion-Retention* Model

As discussed in the previous section, most INMPs are likely incorporated into the ER membrane with a topology determined by their primary structure. Since the ER meshwork is continuous with the NE, INMPs can diffuse laterally from ER membranes via the ONM and the pore membrane into the INM where they are retained by interactions with chromatin, lamins or other nuclear factors. Powell and Burke (Powell and Burke, 1990) first formulated this diffusion retention hypothesis of targeting. By fusing rat and mouse cells they could follow the exchange of LAP1 with

species specific antibodies after formation of the heterokaryons. Instead when murine cells lacking Lamin A and C were used for formation of heterokaryons the exchange between nuclei was not observed. Based on this evidence they concluded that 1) lamin A confers retention of LAP1 at the INM and 2) that the protein by laterally diffusing in the peripheral ER of the heterokaryons can reach the INM via the NPC. In agreement with the diffusion retention model several studies observed differential mobility of INMPs in the ER and at the INM (Ellenberg et al., 1997, Ostlund et al., 1999, Wu et al., 2002). The work of Ellenberg et al. (1997) showed by quantitative Fluorescence Recovery After Photobleaching (FRAP) that the ER fraction of an LBR tagged with GFP is highly mobile in interphase in contrast to a less mobile pool of LBR localized in the INM that is assumed to be bound to Lamin-B and other nuclear proteins. Although the same behavior has been reported for Emerin (Ostlund et al., 1999) and MAN1 (Wu et al., 2002), the mobility of INMPs at the INM is very variable and this is likely to be caused by differences in binding affinities for their nuclear substrates (lamins and chromatin proteins) (Ostlund et al., 2006) (Figure 1.4 A).

In the diffusion-retention model the INMPs can freely diffuse across the pore membrane (PoM); indeed some small viral membrane proteins can access the INM but do not accumulate at this site likely due to the lack of retention (Bergmann and Singer, 1983) suggesting that free diffusion occurs across the PoM. However by artificially increasing the size of the nucleoplasmic domain of an INM protein up to 60-70 kDa the accumulation at the INM can be prevented leading to its retention in the ER (Soullam and Worman, 1995; Wu et al., 2002). Notably the N-terminal domain of all known INMPs does not exceed 60kDa and ranges from the 40aa of Nurim to the more than 400aa of LAP2β or MAN1. It has therefore been suggested that the 10 nm channel that has been postulated between the NPC and the PoM (Beck et al., 2004) acts as a sterical restriction diffusion barrier to membrane proteins which have large cytoplasmic domains.

Several studies have tried to investigate the presence and the requirement of targeting signals and it is now clear that these signals are different among different INMPs. A chimeric protein harboring the N-terminal nucleoplasmic domain of LBR fused to a transmembrane segment was shown to be sufficient to localize to the INM, suggesting the presence of targeting signals in the N-terminal region (Soullam and Worman,

1995). The same has demonstrated for MAN1, LAP2β and emerin (Furukawa et al, 1995; Ostlund et al., 1999; Wu et al., 2002). However the N-terminal domain is not the only determinant of INM protein targeting since transmembrane domains also have a role in the targeting of LBR (Soullam and Worman, 1993, 1995) and nurim (Rolls et al., 1999).

All of these studies have been done by assessing the steady state localization of deleted or mutated fluorescencely tagged INMP chimeras. Therefore it is difficult to distinguish whether the identified targeting signals have a role in post-mitotic or during interphase targeting and the relative contribution of these signals in the two targeting processes.

1.4.3 NPC permeability barrier for membrane proteins

As discussed previously, artificially increasing the size of the nucleoplasmic domain of an INM protein above 60-70 kDa prevents its accumulation in the INM (Soullam and Worman, 1995; Wu et al., 2002, Ohba et al., 2004). These studies indicate that the NPC imposes a size dependent diffusional barrier for membrane proteins. This barrier can prevent large proteins resident in the ER from entering the INM as well as limiting the diffusion of INMPs.

The NPC is also an efficient barrier to diffusion of soluble inert objects larger than 5 nm in diameter, typically globular proteins larger than 50-60 kDa. Different models have been proposed to explain the permeability barrier to soluble molecules. Although it is generally accepted that FG Nups (Nups 54, 58, 62, 98) are needed for barrier formation, the physical arrangement and the relative contribution of FG Nups to the barrier is still unclear. The "selective phase model" predicts that FG Nups bind each other forming a sieve-like FG hydrogel (Frey S and Görlich D. 2007) across which small molecules but not large ones can diffuse. The main alternative model, the "reduction of dimensionality'" model (Peters 2005), assumes that the central NPC channel is narrow enough to prevent three-dimensional random walks of small inert molecules without requiring the interaction between FG domains. The contribution of different FG Nups has been investigated using reconstituted nuclei from *Xenopus* extract (Hülsmann et al., 2012); surprisingly depletion from the extract of the

centrally located Nup62 leaves the NPC barrier largely intact. However Nup98 depletion strongly impairs the permeability. A recombinant Nup98 added to the depleted extract can restore NPC permeability only if it contains cohesive FG domain supporting the "selective phase model".

The first evidence on the nature of NPC permeability for membrane proteins came from a study in reconstituted nuclei of *Xenopus* in which Nup188 was depleted (Theerthagiri et al., 2010). Reconstituted nuclei showed no defect of NPC permeability for soluble molecules but the import rate for integral INM protein reporters was increased twofold. Moreover reporters harboring an artificial nucleoplasmic domain above the 60-70 kDa threshold were able to reach the INM. However depletion of the other inner ring Nup205 does not show the same phenotype in the reconstituted nuclei. The Nup188 phenotype has been recapitulated in mammalian cells following Nup188 KD (Antonin et al.,2011). By contrast, removal of an inner ring Nup (scNup188, scNup170) in *S. cerevisiae*, prevents transport of the INM proteins scHeh1/scHeh2 and scDoa10 without evident changes in nuclear size or NE expansion (King et al., 2006; Deng and Hochstrasser, 2006). So far a systematic analysis on the contribution of different Nups to the permeability of the NPC for membrane proteins is still missing.

1.4.4   Active/facilitated INM protein targeting

The involvement of an active and energy dependent pathway for INM protein targeting has been long debated. By using an artificial reporter based on a truncated form of LAP2β, Ohba et al. (2004) demonstrated that reporter accumulation to the INM is prevented by the depletion of ATP from the cells. Therefore it was suggested that an energy dependent process is required for local rearrangements of the NPC in order to create a transient channel allowing lateral diffusional movement of the INM protein. This could involve kinases and phosphatases acting on NPC components; additionally ATP could be required for the dissociation of heat shock protein family acting on nucleoporins via the activity of ATPases. ATP depletion could lead to stable binding of heat shock proteins to nucleoporins creating a steric impediment to INMPs movement across the NPC

The requirement for energy could also be an indirect indication that some active facilitated/active transport mechanisms exist. Indeed the N-terminal nucleoplasmic domain of LBR contains sequences that resemble NLS able to bind importin-β (Ma et al., 2007). When this domain is expressed as a soluble protein it is efficiently targeted to the nucleus indicating that the NLSs are functional. Several INMPs have predicted NLS sequences in their N-terminal domain (Lusk et al., 2007); NLS sequences have been shown to contribute in the targeting process of SUN2 (Turgay et al., 2010) and the Man1 yeast homologues Heh1 and Heh2 (King et al., 2006). The functional NLS in SUN2 is able to bind the import complex importin-α/importin-βl; however mutations in the sequence prevent localization to the INM only to a minor extent (Turgay et al., 2010). The situation for yeast Heh2 is different. Either deleting or mutating the NLS abolishes targeting of Heh2 to the INM leading to its mislocalization to the ER. Interestingly yeast strains that carry mutations in the yeast transport factors Karyopherin-α and Karyopherin-β show the same phenotypes suggesting that the classical mechanism of NLS facilitated nuclear transport used by soluble nuclear proteins can also play a role in the trafficking of INM proteins (King et al., 2006) (Figure 1.4 B)

Another facilitated targeting mechanism has been proposed for the yeast protein Mps3. Mps3 can bind the NLS-containing protein histone H2Z.A and use it as a "piggyback" system to the INM. (Gardner et al., 2011). Given the large numbers of INMP nuclear binding partners it cannot be excluded that some of them are potential "piggyback" candidates
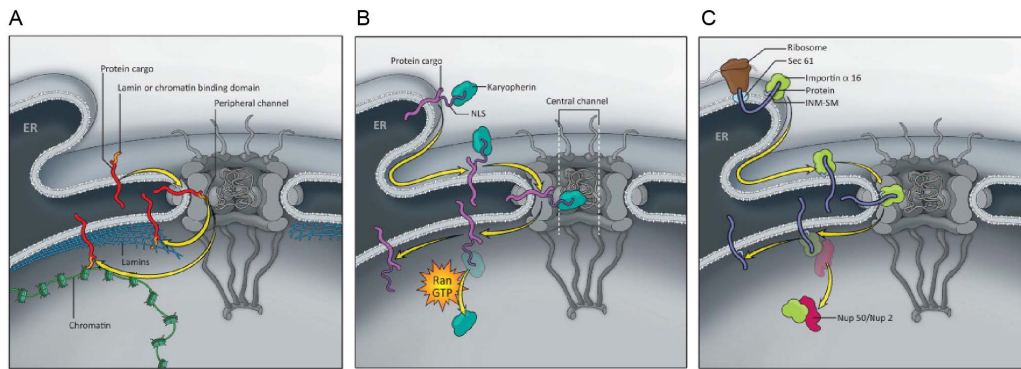
Figure 1.4 Cartoon representation of the three main targeting models (A) In the *diffusion retention model* INM proteins translocate via the peripheral channel of the NPC and then bind to lamins or chromatin. (B) based on the *active/facilitated model* the importin and the RAN system are responsible for the targeting using the central channel of the NPC (C) in the *signal sequence model* the INM-SM on INM protein can be recognized by the importin-α-16 just after translation. Importin-α-16 binding drives INM protein to peripheral NPC channels. The release from the importin-α-16 in the nucleus is mediated by Nup50/Nup2 or other Ran-independent mechanisms. (modified from Katta et al., 2014).

1.4.5   Role of NPC components in INM Protein Targeting

The karyopherin mediated targeting of the yeast protein Heh2 implies that the karyopherins must be able to contact FG Nups to promote translocation of the cargo. These Nups are mostly located in the central channel of the NPC away from the PoM (exceptions are the membrane FG-nucleoporin POM121 and Nup35); Thus whether INMPs can interact with FG-Nups during their transit is unclear. Nup2 and Nup170 are required for targeting of wt Heh2 to the INM (King et al., 2006); moreover yeast strains lacking the GLFG repeats of Nups 100, 145, and 57 show a reduced INM accumulation of a reporter based on Heh2 (Meinema et al., 2011). The reporter used in Meinema et al. (2011) differs from the wt Heh2 by the absence of the LEM domain and the second transmembrane domain; however the reporter containing only the N-terminal bipartite NLS signal, a linker region (LR) and the first transmembrane domain does localize to the INM in a karyopherin dependent manner. The authors have shown that reducing the LR below a threshold length prevents targeting to the INM; moreover the LR is predicted to be an unstructured region typical of disordered proteins. Taken together, this model predicts that the LR region could stretch allowing the NLS, with bound karyopherins, to contact FG-Nups in the central channel of the

NPC. In order to test this model a trapping system based on the rapamycin FRB-FKBP system has been developed between centrally located Nups, Nsp1, and the Heh2 reporters. Upon addition of rapamycin the Heh2 reporter gets trapped in NPC like structures suggesting that it is able to reach the central channel of the NPC in order to contact the Nup-Nsp1 whereas if it was using the lateral channel addition of rapamycin should have no effect. Although the *central channel pathway* is an intriguing hypothesis, how the NPC can accommodate INM protein passage of polypeptides that span from membrane to channel through its scaffold structure is still not addressed. Moreover in the study of Meinema et al. (2011) a more technical issue needs to be clarified. The reporter used in the study could potentially behave as a tail anchored protein rather than a canonical transmembrane protein like the wt Heh2; therefore it cannot be excluded that during the rapamycin trapping experiment the reporter is present as a soluble protein and was not membrane anchored.

In mammalian cells a more systematic analysis of different INMPs has been carried out by looking at the exchange of proteins between the ER and INM after photobleaching. In this study LBR targeting is shown to be affected by the depletion of Nup53 and requires RanGTPase activity. Additionally LBR contains six FG repeats that are believed to interact directly with FG-Nups (Zuleger et al., 2011). FG repeats are particularly enriched in nuclear envelope proteins suggesting that they might enable these proteins to function as their own transport receptors (Kerr and Schirmer, 2011).

1.4.6 Importance of subcellular trafficking in INM protein targeting

Membrane proteins can undertake a number of trafficking pathways to different subcellular compartments before reaching their final destination compartment. Proper targeting is often mediated by the presence of signal sequences in the membrane protein. In this context is worth mentioning some mechanisms that account for the steady state localization of INMPs at the INM.

Several INMPs (SUN2, Emerin, LBR and LEM2) have an arginine rich motif that has been identified as a retrieval signal from the Golgi to the ER. Mutations of this retrieval motif in SUN2 lead to its mislocalization in the Golgi away from the ER membrane indicating that retrieval signals might support efficient delivery of INMPs to the INM (Turgay et al., 2010). Moreover perturbing endosome dynamics by Rab5

GTPase overexpression leads to SUN2 accumulation in endosomal membranes (Liang et al., 2011).

It has been proposed that INM proteins can be already recognized during the process of translation and directed to the INM. The evidence came from baculovirus-derived membrane proteins destined to the inner nuclear membrane (INM) containing a specific stretch of positively charged amino acids (later named INM-SM). The INM-SM located close to the nucleoplasmic face of the transmembrane domain can be recognized by a truncated membrane associated form of importin-α (KPNA-4-16) (Saksena et al., 2004). The INM-SM is found conserved in different INMPs and indeed KPNA4-16 can bind the sorting motif present in the two mammalian INMPs nurim and LBR (Braunagel et al., 2007). The proposed role for the KPNA4-16 is to recognize the INM-SM posttranslationally and mediate an early sorting of the INMPs towards the INM; however how the directionality of the sorting toward the INM is achieved remains undetermined (Figure 1.4 C).

1.4.7 NPC-independent trafficking pathways?

Although it is generally believed that targeting of INMPs occurs via lateral diffusion in the ER membranes, it has been speculated that there is a potential vesicular trafficking pathway for INMPs between the INM and ONM. Treatment of cells with drugs that inhibit membrane fusion events (BAPTA and NEM) has no effect on the targeting of an artificial INM reporter (Ohba et al., 2004); however these drugs block cytoplasmic membrane fusion and it is unknown if they act also on luminal nuclear membrane surfaces. Indeed vescicular trafficking can exist across the NE as demonstrated by the nuclear egress of Herpes Simplex Virus (HSV); during HSV life cycle the mature capsids are assembled inside the nucleus and encapsulated into vesicles close to the nuclear face of the INM. Here, they recruit the endogenous protein kinase-C (PKC) and produce viral Cdc2-like kinases, which together phosphorylate the nuclear lamina triggering its local disassembly. HSV capsids are then observed in the NE perinuclear space and they are finally de-enveloped via membrane fusion with the ONM and released into the cytoplasm (reviewed in Johnson and Baines, 2011). For a long time the virus has been thought to use a membrane disassembly mechanism but a recent a study from Speese et al. (2012)

pointed to the possibility of an endogenous vesicular trafficking pathway for nuclear exit of large RNPs. Interestingly the protein TorsinA, a AAA+ protein with ATPase activity that localizes in the ER-NE lumen, has been implicated in this pathway. Depletion of TorsinA leds to an accumulation of large RNP vesicles in the perinuclear space likely due to a defect in INM scission (Jokhi et al, 2013). It cannot formally be excluded that a similar trafficking pathway for INMPs exists from the ONM to the INM that is dependent on ATP hydrolysis to support TorsinA acitivity.

The studies published to date suggest that the trafficking of INMPs proteins is much more complex than first believed. For several INMPs the steady state localization at the INM is the result of the combination of several targeting signals present in their sequence and the simple *diffusion-retention model* cannot fully explain the complexity of this mechanism. Recent evidence suggests that a *receptor-mediated targeting* exists in yeast but whether the same mechanism is also conserved in mammals has not been yet proven. As well many other questions remain open with the respect to the contribution of Nups in the targeting process and how the NPC can accommodate the transit of very different INMPs, potentially slicing through its structural scaffold during translocation. The intriguing model of a NPC *central channel pathway* should be more carefully investigated. If it is confirmed potentially two trafficking pathways through the central and peripheral channel of the NPC could be undertaken by INMPs depending on their size and the presence of NLS signals. These two pathways would likely require different molecular machinery and have different transport kinetics across the NPC.

1.5 Aim of the research

The Inner Nuclear Membrane (INM) represents one of the least understood destination compartments in membrane trafficking. Compared to the nuclear import of soluble proteins, the mechanism of INM protein targeting in interphase to the nucleus has been poorly investigated. Most of the studies have been carried out in very different model systems (yeast vs mammalian cells) and focused on different INM protein family members making comparison between studies complicated or impossible. Moreover progress in the field is currently limited by the absence of a general assessment of the molecular requirements for INM protein targeting, which could help to differentiate between the existence of different targeting pathways or a single unifying targeting mechanism.

The aim of my PhD project is to fill some of the above mentioned gaps in our knowledge by developing a robust system to image INMP targeting in real time in living mammalian cells that can be combined with siRNA screening technology, in order to elucidate the genetic requirements for the targeting process and provide evidence for which targeting mechanism is used.

I therefore first developed a novel reporter that allows real time imaging of the synchronous targeting of INMPs from the site of synthesis in the ER to the INM with high spatial and temporal resolution in live mammalian HeLa cells. The development, validation of the reporter system and its application to a panel of different INMPs is presented in chapter 2.1 *("Generation of a novel reporter to study INM protein trafficking")*

I then combined the newly developed reporter with a high throughput time-lapse microscopy and liquid handling platform for siRNA screening. This allowed me to target several genes in parallel and asses their contribution in the targeting of the INM protein Lamin B receptor (LBR). The results, shown in chapter 2.2 *("A quantitative assay to study LBR targeting after siRNA gene knock down")*, demonstrates that the developed reporter system is a valuable tool to dissect the genetic requirement for the trafficking of INMPs.

Moreover in collaboration with a postdoc in the lab, Antonio Politi, we took advantage of the large amount of quantitative kinetic INM INMP targeting data of the screen and built a mathematical model for INM protein targeting (2.3 "*A predictive mathematical model for INM proteins targeting*"). The model allowed me to make predictions which step of the targeting process is affecting by a particular gene and to guide functional validation experiments *(2.4 Validation of model prediction).*

2 RESULTS

2.1 Generation of a novel reporter to study INM protein trafficking

In generating a new reporter to study INMPs trafficking I considered the different requirements that it should fulfill in order to be robust and generally applicable. Firstly, the new reporter should allow me to observe synchronous trafficking of a consistent amount of INM protein between ER and the INM by microscopy. The general strategy I employed is based on *trapping* and then the *release* of an INM protein from the ER. Importantly the release step should occur with sufficient temporal resolution and be compatible with live cell experiments. The reporter should allow me to not only observe but also to *quantify* the targeting process with a good dynamic range in siRNA functional screens. Finally, although I started to develop the reporter using Lamin B Receptor (LBR) as a model protein, the general reporter strategy should be applicable to other INMPs in order to allow comparative studies with the same system.

2.1.1   ER trapping of LBR by increasing its N-terminal cytoplasmic domain

 It was shown previously that adding the 60 kDa chicken muscle pyruvate kinase domain (CMPK) to the N-terminus of lamin B receptor (LBR) prevents its targeting to the INM and leads to its retention in the ER (Soullam and Worman, 1995). The fusion of the CMPK domain to the N-terminal domain likely prevents the passage of the LBR through the limited space between the NPC and the pore membrane (PoM). Therefore I took advantage of this and used the LBR as a model protein to develop the new reporter. I used is truncated version (LBR1TM-mEGFP) of the full length human LBR consisting of a nucleoplasmic domain of about 200 aa and the first transmembrane domain. This construct has been shown to retain the full capacity to target to the INM (Soullam and Wormann, 1995). The LBR nucleoplasmic region contains three different domains: the tudor (aa 1-62), RS (aa 53-89) and globular II domain (aa 89-211) (Figure 2.1 A). The tudor and the RS domains are able to bind histones and DNA respectively whereas the globular II domain of LBR interacts with HP1 and the RS domain also interacts with Lamin B.

The CMPK domain was fused to the N-terminus of LBR1TM-EGFP to generate the CMPK-LBR1TM-EGFP. HeLa Kyoto cells were transfected with the CMPK-

LBR1TM-EGFP construct and imaged with confocal microscopy 24h later. As predicted an ER tubular meshwork is clearly visible; this localization is typical for ER membrane proteins that distribute homogenously through the ER membranes. A comparable fluorescence intensity level is also present at the NE, presumably the ONM where the reporter should be able to freely diffuse (Figure 2.1 B).
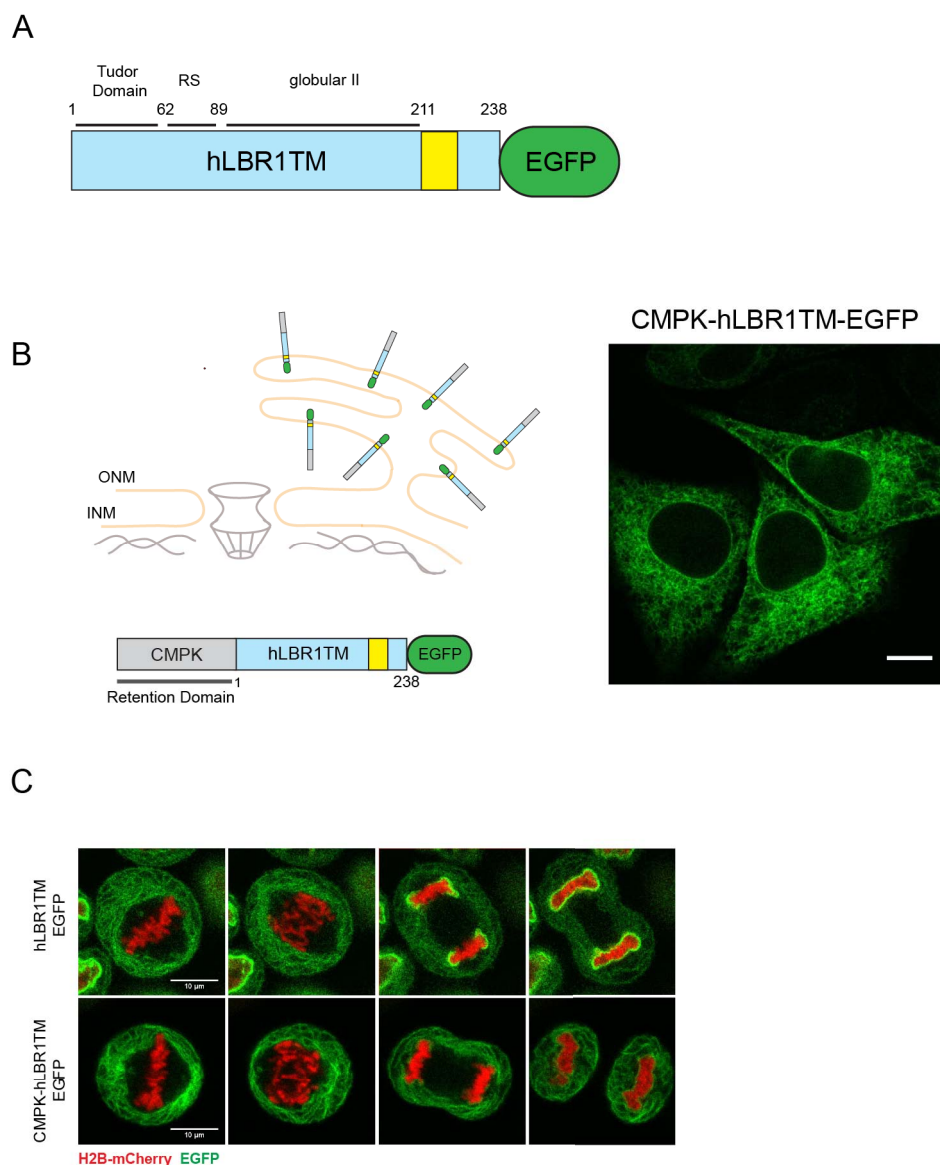
Figure 2.1 Schematic representation of hLBR1TM-EGFP with the three different domains: tudor (aa 1-62), RS (aa 53-89) and globular II domain (aa 89-211). (B) Predicted and *in vivo* localization of the CMPK-LBR1TM-EGFP constructed. Scale Bar 10μm (C) Postmitotic targeting of hLBR1TM-EGFP around telophase nuclei. Note that the accumulation around chromatin is prevented in the presence of the CMPK domain.

Discrimination between the ONM and INM is not possible by confocal microscopy due to its resolution limit (the typical distance between INM and ONM is about 50 nm), and therefore the possibility that some of the reporter is targeted to the INM during interphase cannot be ruled out. Postmitotic INM targeting should also be excluded since the presence of the CMPK also prevents LBR targeting during NE reassembly at the end of mitosis (Figure 2.1 C).

To conclude, fusion of the 60kDa CMPK retention domain is a perfect strategy to *trap* a large amount of LBR protein in the ER membranes.

2.1.2 Inducible cis-cleavage of the retention domain allows INM localization of LBR

The CMPK retention domain needs to be removed in order to release the LBR fraction trapped in the ER. The removal of the CMPK domain can be achieved by a protease that acts at a cleavage site placed between the LBR N-terminus and the CMPK domain. Protease cleavage needs to be specific, fast and inducible. Among different proteases that I considered, the NS3 protease from the Hepatite C Virus (HCV) was determined to be the only one suitable for this purpose.

The HCV genome encodes for a long polyprotein that is cleaved by the NS3 serine protease at four different sites into several functional viral proteins. The NS3 protease and its cleavage site have been chosen for several reasons: first the NS3 protease is well tolerated by the cell as demonstrated in a previous application (time-STAMP) (Lin et al., 2008), a specific and reversible cell-permeable small molecule inhibitor (called BILN2061) has been described (Lamarre et al., 2003) and at least *in vitro* the activity of the NS3 protease seems to be an order of magnitude higher than other proteases such as the TEV protease from tobacco etch mosaic virus (Cabrita et al., 2007; Zhang et al., 1997).

Among the four cleavage sequences in the HCV polyprotein I selected the NS5a/b site. The NS5a/b site is a stretch of about 15aa (ASEDVVCCSMSYTWT) that is recognized and cleaved between the critical residues "CC|SM" by NS3 protease with the highest activity compared to the other sites of the polyprotein (Zhang et al., 1997).

The features described above should ensure high efficiency cleavage by the NS3 protease at NS5a/b site and fast release of CMPK retention domain from LBR.

I therefore cloned the NS5a/b cleavage site between the CMPK retention domain and the N-terminus of LBR; the NS3 protease was then fused to the N-terminal of the CMPK domain allowing cis-cleavage activity at the protease cleavage site. In this manner I expected to achieve controllable localization of the LBR in the ER or INM as a function of protease activity (Figure 2.2 A). This new reporter was named Target-INM-LBR.
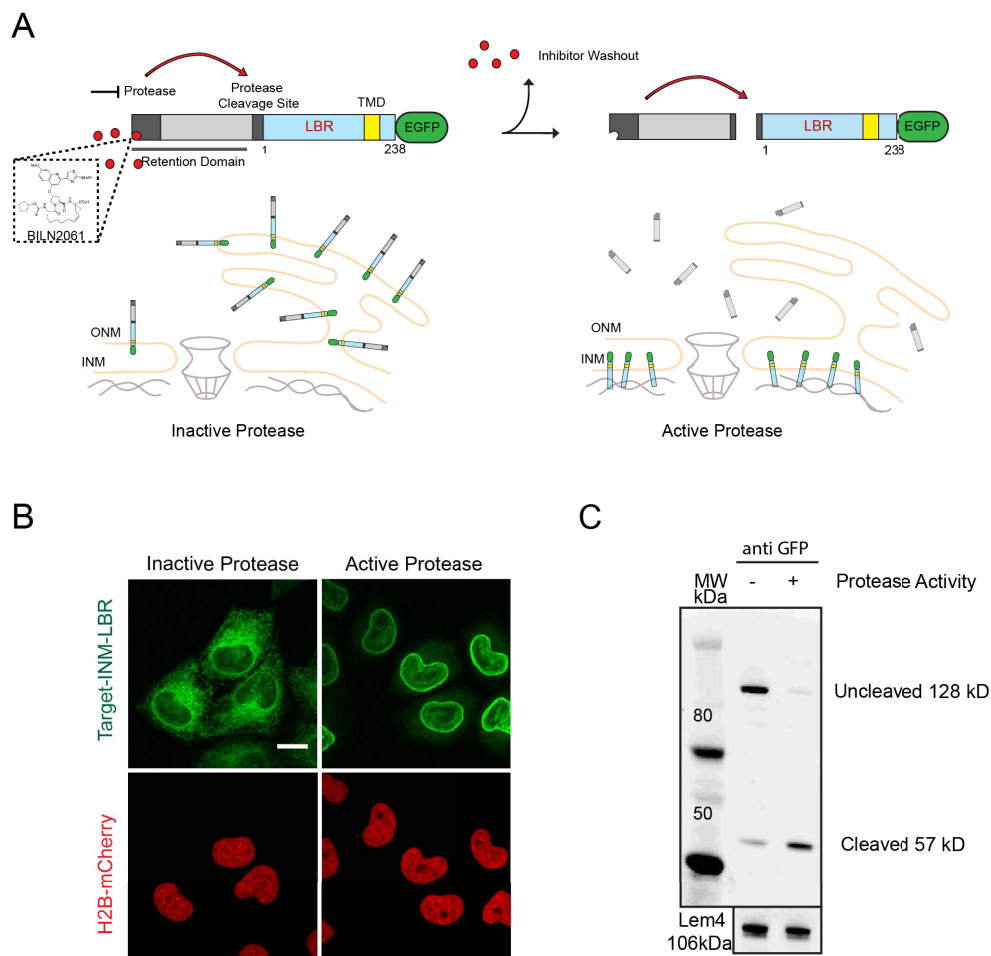
Figure 2.2 (A) Schematic representation of Target-INM-LBR reporter and its predicted subcellular localization before (left part of the panel) and after (right part of the panel) protease activation by inhibitor washout. In gray the retention domain with the NS3 protease and the protease cleavage site (dark gray) and CMPK domain (light gray). LBR 1-238 containing the N-terminal domain (light blue) and first transmembrane domain TMD (yellow) followed by EGFP. (B) Confocal images of HeLa cells stably expressing H2B-mCherry and Target-INM-LBR grown for 24h in the presence of (inactive protease) or without (active protease) the protease inhibitor. Bar, 10μm (C) WB analysis of cells grown for 24 hours in the presence (protease activity -) or absence (protease activity +) of the protease

inhibitor shows respectively the full-length and cleaved form of the reporter respectively,

A HeLa doxycycline (DOX) inducible system was used to express the Target-INM-LBR in combination with stable expression of the chromatin marker H2B-mCherry. This system allows for single site genomic integration of the Target-INM-LBR construct and expression by Doxycycline. Expression of the reporter was induced by adding Doxycycline (1μg/ml) to the culture medium in the presence or absence of the protease inhibitor BILN2061 (2μM) and cells were incubated for an additional 24h before imaging.   By monitoring the localization of the reporter by confocal microscopy, I confirmed that the reporter is localized in the ER when the protease and the NE when it is active (Figure 2.2 B). Western blot analysis shows that predominantly the full length protein is present when the protease is kept inactive whereas when it is active the reporter is efficiently cleaved (Figure 2.2 C).

2.1.3 Controlled induction of Target-INM targeting by inhibitor removal

The Target-INM reporter allows me to observe trafficking of INM proteins between the ER and INM in a single living cell. This can be achieved by acutely inducing the activity of the NS3 protease. The BILN2061 inhibitor can be washed out from the cells due to its cell permeability leading to the cleavage of the CMPK retention domain and synchronous targeting of the reporter to the INM. I therefore employed high resolution time-lapse confocal microscopy to image HeLa cells expressing the Target-INM-LBR before and after inhibitor washout. To ensure complete removal of the inhibitor the cells were repeatedly washed with normal fresh medium and then imaged for more than 1h after the inhibitor removal. After inhibitor washout the reporter accumulates over time at the NE while the ER fraction of the reporter is depleted during the translocation (Figure 2.3).
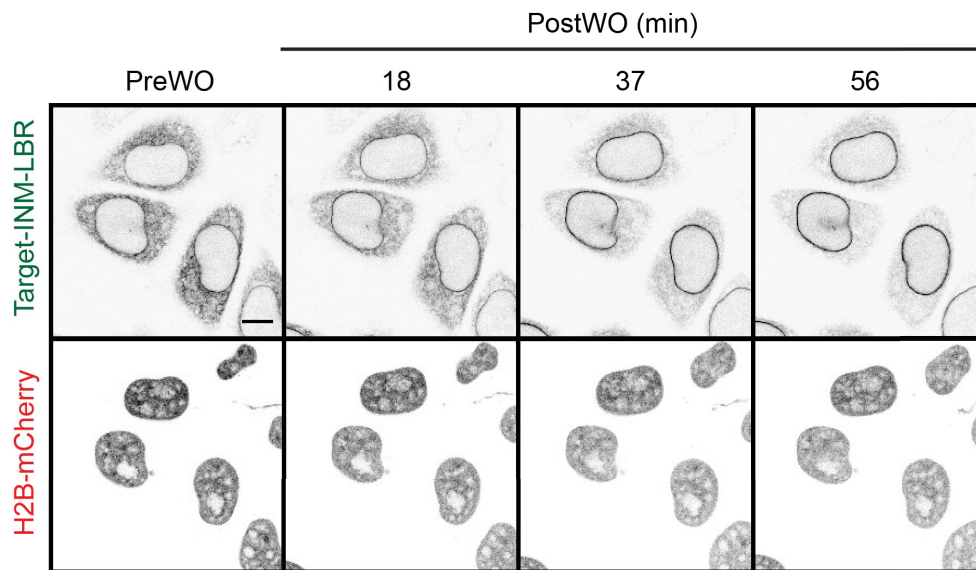
FIGURE 2.3 Acute inhibitor wash-out leads to Target-INM-LBR reporter translocation from the ER (preWO) to the NE (PostWO). Images are shown with inverted gray color. Bar, 10μm.

Due to the resolution limit of the confocal microscope is not possible to determine if the fluorescent NE signal is coming from the ONM or INM. It is therefore important to prove that the reporter is localized to the INM after translocation. The mobility of LBR-GFP at the INM is reduced due to its binding to nuclear substrates when compared to the mobility observed in the ER (Ellenberg et al., 1997; Oustlund et al., 1999). Therefore reduced mobility would be an indicator of successful INM targeting. To assess changes in mobility of the Target-INM reporter before and after relocation to the NE, I performed Fluorescence Recovery After Photobleaching (FRAP) experiments. A small region of ER or NE is bleached at full laser power intensity and the fluorescence recovery is followed over time. The mobility of the reporter in the ER is analyzed before inhibitor washout and compared to that of the NE after complete translocation of the reporter. ER fluorescence recovery is fast with a $t_{1/2}$ of about 10 sec, reaching a plateau around 60 sec when the recovery is almost complete, indicating that the proportion of the mobile fraction of the protein is more than 90%. After relocation to the NE the reporter shows reduced mobility compared to the ER (Figure 2.4 A). This observation suggests that the reporter is indeed targeted to the INM.

To independently check the INM localisation I expressed a dedicated reporter carrying a Myc-tag between the NS5a/b cleavage site and the N-terminus of the LBR (CMPK-NS5a/b-Myc-LBR1TM-GFP). In this case the protease activity was supplied by co-transfecting the cells with a construct expressing the NS3 protease. Following complete reporter relocation I then selectively permeabilized the plasma membrane by using a low concentration of the detergent digitonin, which leaves the nuclear membrane intact. Immunofluorescence after such partial digitonin permebilitation does not allow detection of nuclear epitopes that are instead accessible only with Triton X-100 permeabilization (Figure 2.4 B). After Triton X-100 permeabilization the nuclear rim is strongly stained with the anti-Myc antibody; in contrast after digitonin permebilitation ER but no nuclear rim signal is detected with the anti-Myc antibody while a green fluorescence nuclear rim from the GFP fluorescence is clearly visible (Figure 2.4 B). This data demonstrates that the large majority of the NE fraction of the reporter is translocated to the INM.
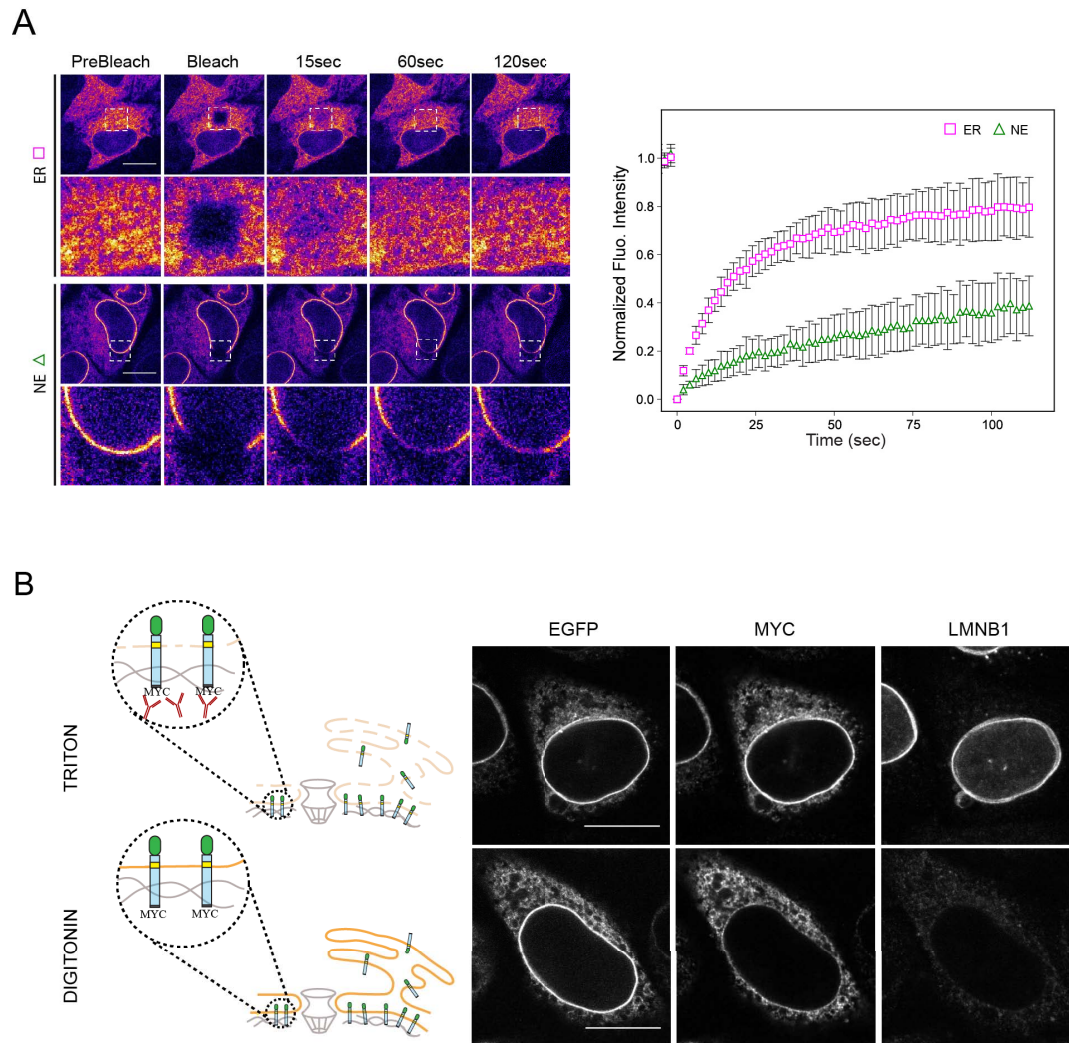
Figure 2.4 (A) FRAP analysis of reporter mobility in the ER and at the NE. ER or NE regions of the cell were bleached and imaged every 2sec for 2 minutes. Fluorescence recovery curves were normalized between 1 (prebleach value) and 0 (postbleach value) and plotted over time. Error bars are standard deviation of the mean. Scale Bars, 15μm. **(B)** IF after Triton/Digitonin permeabilization of cells expressing the modified reporter carrying a Myc tag at the LBR N-terminus. Antibody against LMNB1 (Lamin B) is used as a control for the accessibility of the antibodies to the INM after Digitonin or Triton X-100 permeabilization. From the images it is clear that Digitonin permeabilized cells do not display Lamin B stain. Scale Bars, 15μm.

2.1.4 Target-INM strategy can be applied to other INMPs

The Target-INM was successful in allowing me to followthe trafficking of the LBR indicating that this approach may work as general strategy to study other INMPs in living cells. I therefore applied the same strategy to other INMPs, namely the Lamin associated polypeptide 2 β (Lap2β), Torsin 1A Interacting Protein 1 (Tor1AIP1), Man1 and Sun1 that are representative members of the main INMPs subclasses. Lap2β, Tor1AIP1 and Man1 contain putative NLS signals. Based on the distance between their TMD domain and NLS sequences, Tor1AP1 and Man1 (Heh2 homologues) are predicted to be transported thorough the NPC according to the *central channel* model whereas Lap2β is believed to be targeted via the peripheral NPC channel.

Sun1 has a large nucleoplasmic domain compared with the other INMPs and the contribution of the SUN domain to the targeting process is unknown.

I cloned the NS3 protease, CMPK domain and the NS5 cleavage site at the N-terminus of the selected INMPs which carry the GFP at their C-terminus. All the INMPs are full length proteins except Man1 which was truncated after the first TM in order to consistently have the GFP in the ER lumen.

I generated HeLa inducible cell lines expressing the Target-INM variants and tested the localization of each reporter as a function of protease activity (Figure 2.4 A). All the reporters are localized in the ER when the protease is inactive and activation of the protease leads to relocation of the reporter to the INM. Western blot analysis shows that ER and INM localization corresponds to the presence of the full length or cleaved form of the reporter. (Figure 2.5 B).
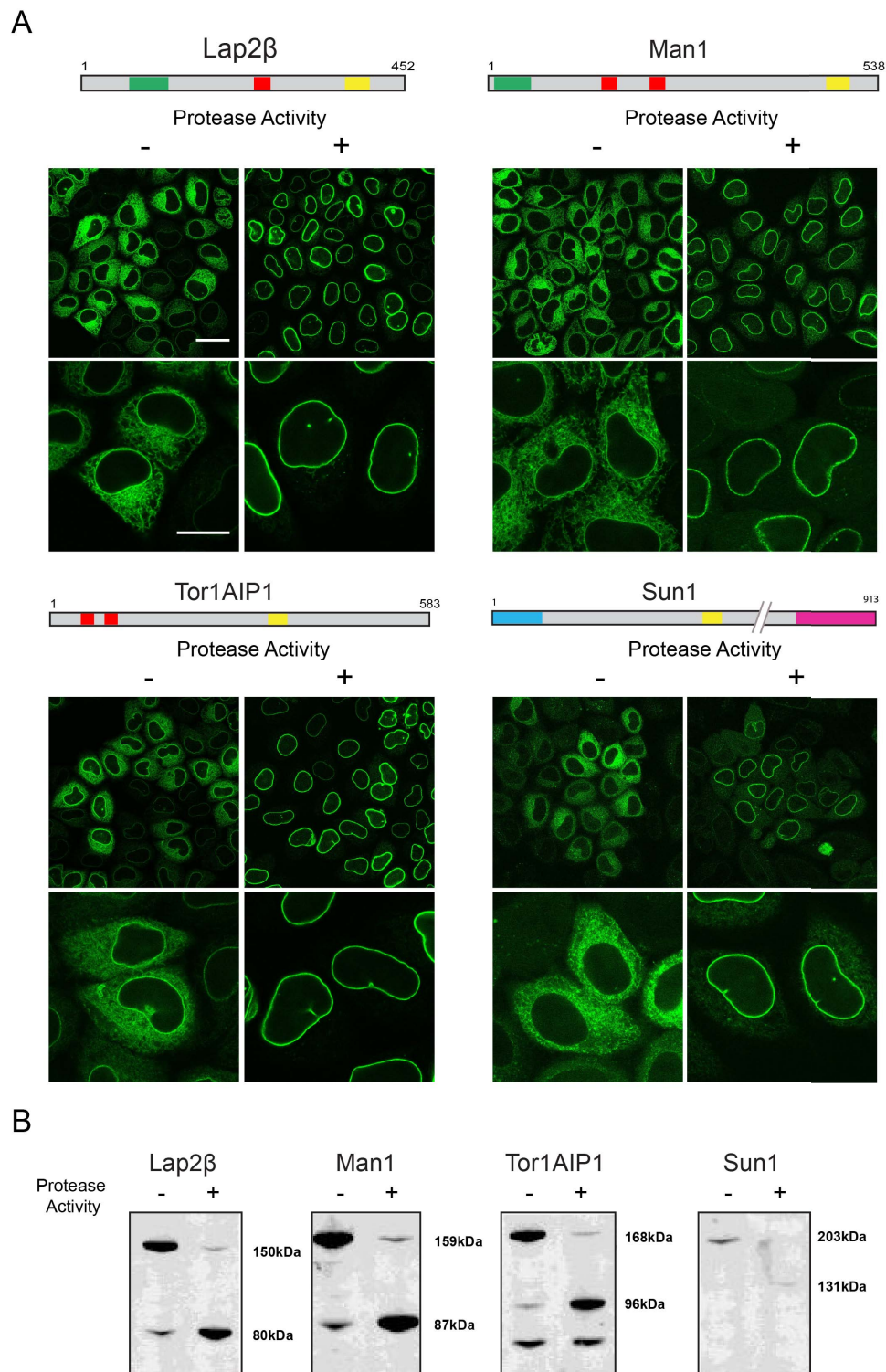
Figure 2.5 (A) Confocal images of HeLa cells stably expressing the Target-INM reporters grown for 24h in presence (inactive protease) or absence (active protease) of the protease inhibitor. Localization of the reporter depending on protease activity status is shown. The domain organization of each INMP is shown above the images. LEM domain (green), NLS sequences (red), Lamin binding domain (LMND) (blue), Sun domain (purple) TMD (yellow). (B) WB analysis of cells grown for 24 hours in the presence (protease activity -) or absence (protease activity +) of the protease inhibitor shows the full-length and cleaved form of the each reporter respectively.

2.2 A quantitative assay to study LBR targeting after siRNA gene knock down

The Target-INM reporters provide a simple and robust tool for the screening of candidates genes required for INM protein targeting by fluorescence microscopy-based. This can be done by monitoring the degree of reporter translocation from the ER to the INM upon knock down of a specific gene. In the first part of this chapter I discuss the development of a quantitative assay for siRNA screening using the LBR based Target-INM reporter and in the second part the results from the screennin of a panel of candidate genes is reported.

2.2.1 General screening pipeline and implementation

The assay combines long term gene knock down with time-lapse confocal microscopy of the previously established Target-INM-LBR cell line. Gene knock down was achieved by reverse transfection of siRNA using siRNA spotted microarrays (Erfle et al., 2007). For the screening assay, the Target-INM cell line was seeded on the siRNA microarray and 24 hours later the expression of the reporter was induced by doxycycline in the presence of the protease inhibitor. After 48 hours knock-down (KD), I washed out the protease inhibitor and started live cell confocal time-lapse imaging (Figure 2.6 A). Time-lapse imaging was carried out for 2.5 h in order to fully record the dynamics of reporter translocation. In order to achieve sufficient time sampling of the translocation dynamics the number of different genes targeted were limited to five, each of which was targeted by two distinct siRNAs in duplicate together with the on chip Control siRNA. This setup allows me to record a total of 30 siRNA knockdown time-lapse movie in the same wash-out experiment (Figure 2.6 B).

The recorded movies contain cells in different cell cycle stages and cell cycle transition from interphase to mitosis can occur during the time frame of image acquisition. Since I want to study INM protein trafficking in interphase an automatic method to isolate cells that persist in interphase for the whole time of acquisition is

A

B
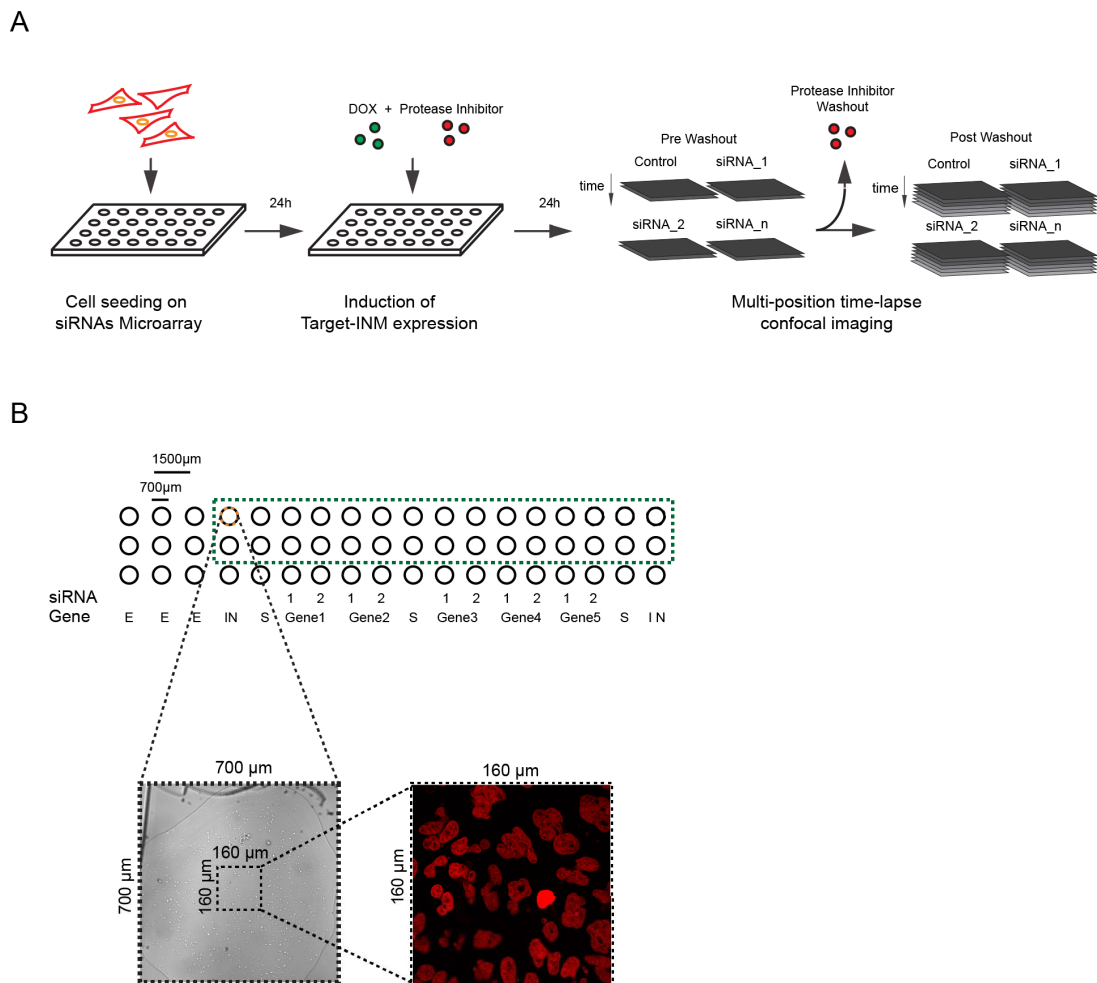
FIGURE 2.6 Schematic representation of the screening workflow. Each siRNA microarray was generated by siRNA spotting as described in Erfle et al. (2007). Cells were seeded on the siRNA microarray and after 24h Target-INM-LBR expression is induced by adding Doxycycline (1μg/ml) together with the protease inhibitor BILN2061 (2μM) to the culture medium. Imaging is started after additional 24h, i.e. 48h of siRNA treatment. Each siRNA position is imaged for two time points before inhibitor wash-out and then up to of 2.5 hrs after the activation of the protease with a time resolution of 9 min (B) Example of one siRNA spotted microarray. Each microarray includes scrambled siRNA (Control siRNA) (S), siRNAs against INCENP (IN), siRNAs against 5 different genes (targeted by two distinct siRNA) and empty positions (E) where only the transfection mix is present. Each siRNA spot measures 700μ x 700μ as shown in the transmission image inset before cell seeding. A field of view of 160μ x 160μ is imaged inside the siRNA spot. Since siRNAs spots are not visible after cell seeding I use the INCENP siRNAs placed at the microarray boundaries as positional fiducials. The INCENP siRNA gives rise to a distinguishable nuclear phenotype that allows the alignment of the microarray slide inside the microscope. The green dashed rectangle indicates the siRNA spots that are imaged for a total of 30 siRNA knockdown time-lapse movies in the same wash-out experiment.

needed. I therefore used CellCognition (http://www.cellcognition.org) to segment and track cells based on the nuclear marker H2b-mCherry (Held et al 2010, Walter et al., 2010). Additionally CellCognition allowed me to classify cell cycle stages (mitotic vs. interphase) based on chromatin features and to select cell trajectories that persist in interphase for the entire time-lapse movie (Figure 2.7 A).

The single cell trajectory for Control siRNA showed a clear increase in NE signal and corresponding decay in ER signal over time (Figure 2.7 B). To quantify INM protein targeting I implemented a method that accurately detects the NE and ER regions and records fluorescence intensity at these locations (Figure 2.7 C and Material and Methods). This method was applied along the complete cell trajectory leading to traces for the NE and ER intensities over time. The NE and ER intensities were normalized to one to the average of the first two pre-wash out time points and plotted over time as the fold change in intensity from the initial intensities values as shown in Figure 2.7 D.

For each cell trajectory I computed the *NE Increase (fold change),* a parameter that scores the maximal reporter accumulation after washout of the inhibitor. *NE Increase (fold change)* is defined as the average of the three highest consecutive NE values during the time course. This parameter is a reliable and reproducible indicator of reporter accumulation in a single replicate where typically the reporter reaches a maximal accumulation at the INM 40-50 min after activation of the protease (Figure 2.7 E).

In conclusion this pipeline allowed me to collect thousands of cell trajectories for Control siRNA and siRNA KDs for each of which I computed a single parameter (*the NE Increase (fold change)*) that represents the degree of reporter translocation. By comparing this parameter for Control siRNA and a specific siRNA, I will explain in the next section how genes that affect reporter translocation are identified.
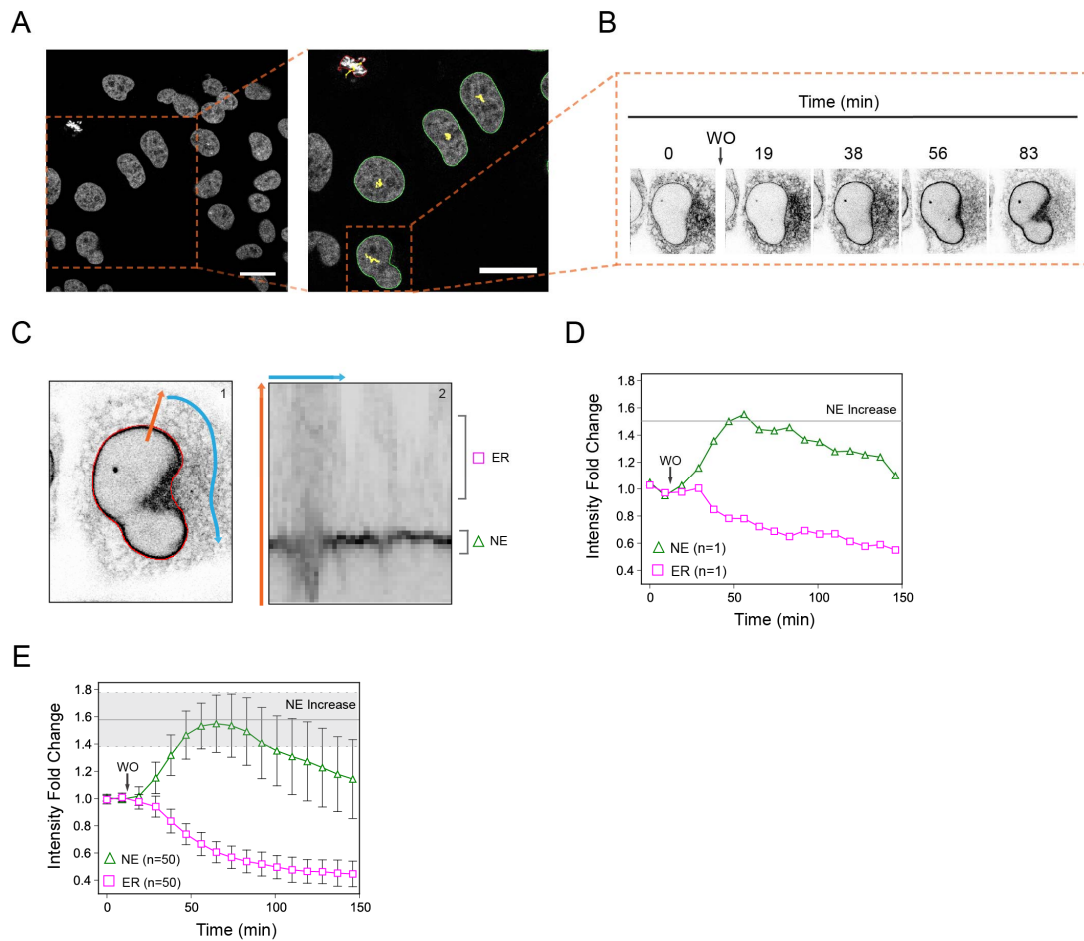
FIGURE 2.7 (A) Representative field of view acquired in the screening setup showing the H2B-mCherry signal. The zoomed inset shows the segmentation, tracking, and cell classification of interphase (green) and mitotic (red) cells by the CellCognition software. (B) Example of a single interphase cell trajectory. The images show translocation of the reporter to the INM after inhibitor washout. (C) Image analysis workflow. (1, left panel) The boundary of the segmented H2B-mCherry signal (red line) seeds a domain in the nucleus to ER direction (orange arrow) around the surface of the nucleus (blue arrow). (2, right panel) This domain is unfolded along the blue arrow and the regions for measuring nuclear envelope (NE, green triangle) and ER intensities (magenta rectangle) are determined (Material and Methods). (D) Quantification of a single cell trajectory. The plot shows the intensity fold change of the NE and ER normalized to the average of the first two pre-wash out time points. Gray line is the *NE increase (fold change)* defined as the average of the three highest consecutive NE values. (E) Quantification of Control siRNA NE and ER fold changes in a single replicate of the screening (mean ± s.d.). The gray line is the replicate average *NE increase (fold change)* (the region within the standard deviation is indicated by the gray area).

2.2.2 Identification of genes implicated in LBR targeting process

The molecular machinery for INM targeting is so far largely unknown. With the screening assay I can target by siRNA different genes and score in a robust manner how they affect INM targeting. In particular the current knowledge on the genes required for LBR targeting is limited; depletion of the nucleoporin Nup53 seems to affect LBR targeting (Zuleger et al., 2011) and the truncated membrane associated form of importin-α (KPNA-4-16) has been suggested to be able to bind the INM-SM present in LBR to facilitate its targeting (Braunagel et al., 2007). As previously mentioned the time resolution needed to record the full reporter translocation dynamic limits the number of genes I can simultaneously target by siRNA in the same microarray to five. I therefore started with a candidate gene list that is likely to be involved in the targeting process. This list includes around 100 genes that can be divided into the following groups: 1) nucleoporins, 2) validated INMPs 3) nuclear binding partners of INMPs, 4) ER remodeling proteins, and 5) nucleocytoplasmic transport factors (Material and Methods – Table 3.1) Systematic knock down of different nucleocytoplasmic transport factors should help to clarify if an *active transport* is required for LBR targeting, wheras targeting of INMP nuclear binding proteins will help to dissect the contribution of the *retention* at the INM.

In the screen I imaged a total of 73 siRNA microarrays including 3 or 4 replicates for each siRNA; this comes to over 2000 time lapse movies of reporter translocation in Control and KDs conditions. I used the pipeline described previously to derive *NE Increase (fold change)* values for Controls siRNA and siRNAs. Control siRNA *NE Increase (fold change)* across all the microarrays imaged show a normal shape distribution with the average value of 1.58 (Figure 2.9 A). I then tested if each siRNA significantly deviates from the Control siRNA in the same microarray (Material and Methods). A siRNA was considered to have reproducible effect when it significantly deviates from Control siRNAs in at least 2 of the 3-4 microarray replicates. All siRNAs were ranked based on the magnitude of their average deviation from Control siRNA (Figure 2.8, significant siRNA are shown in blue, Table 2.1). As a result the majority of significant siRNAs negatively affects *NE increase (fold change)* compared to Control siRNA. Interestingly a smaller number of siRNAs also increase the translocation of the reporter at the INM.
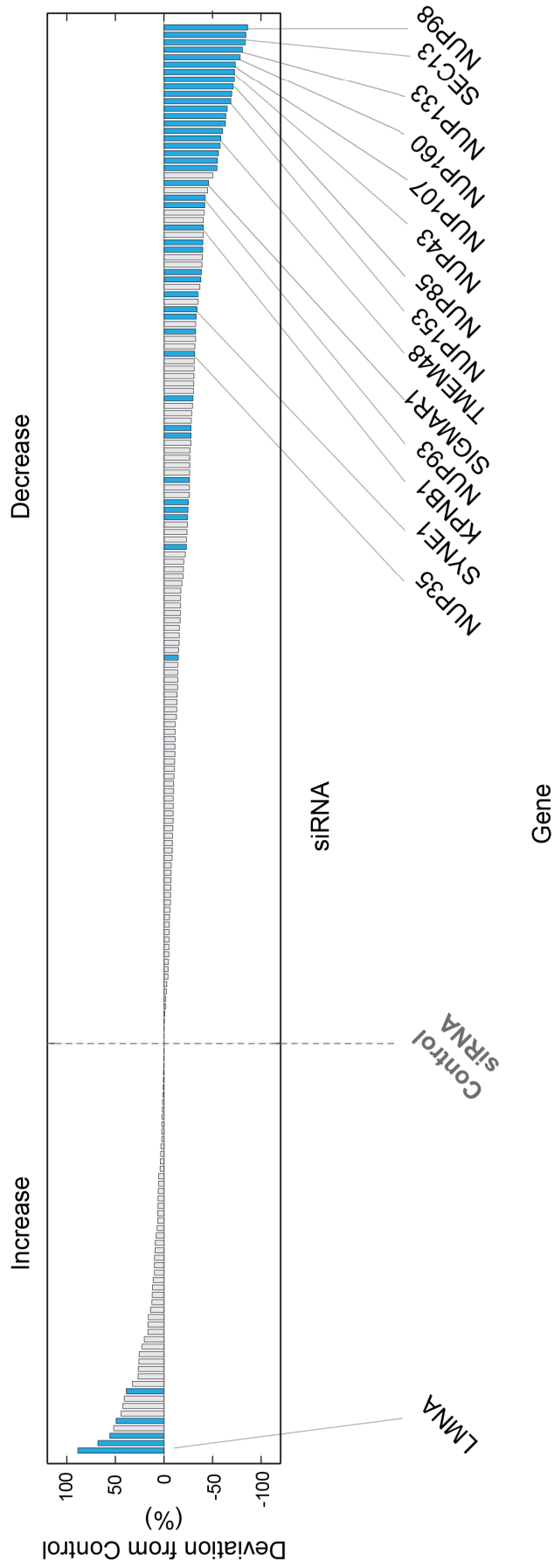
FIGURE 2.8 Ranking of siRNAs based on the average deviation of the *NE increase (fold change)* from Control siRNA. Blue bars indicate siRNAs which deviate from Control siRNA with statistical significance in at least two replicates (t-test *p*-value < 0.01, see Table 2.1). siRNAs on the left of Control siRNA show an increase whereas those on the right a decrease of *NE increase (fold change)* with respect to Control siRNA. Labels indicate genes for which both siRNAs show a reproducible effect. The lines point to the siRNA that shows a stronger effect.

To check if reporter expression is strongly affected by KDs I calculated for each siRNA the deviation of ER intensity pre-wash out *(ER Intensity PreWO)* from the Control siRNA. Although siRNA KDs do not cause a biased decrease in reporter expression, the reporter expression can change significantly after siRNA KD (mean deviation of ER *Intensity PreWO = 0.01 +/- 0.20 SD)* (see Table 2.1). Importantly the NE increase (fold change) scored for each siRNA does not correlate with the reporter expression before the wash out. (Figure 2.9 B).
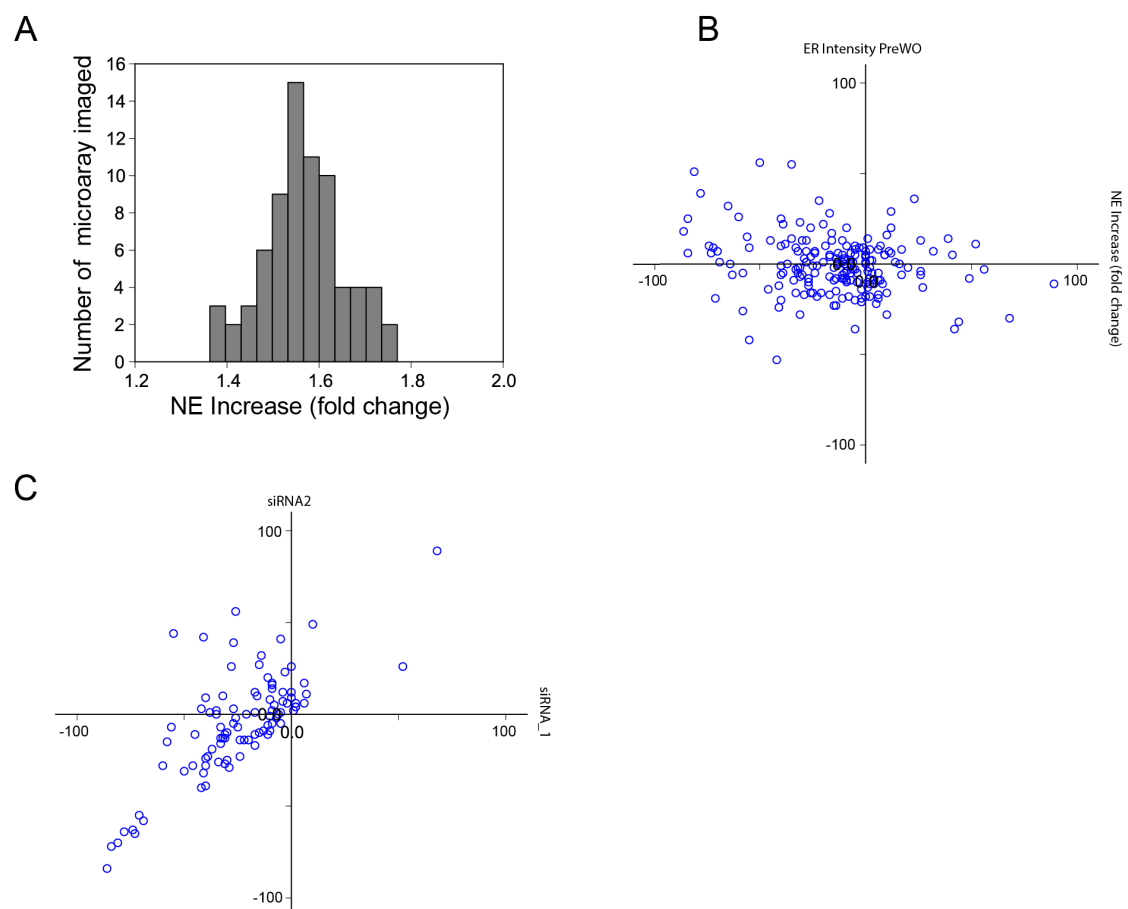
Figure 2.9 (A) Distribution of *NE increase (fold change)* of Control siRNA across all the microarrays imaged. Average = 1.58 +/- 0.08 SD (B) The scatter plot shows correlation for each siRNA between the deviation of *NE increase (fold change)* (x axis) and the deviation of ER Intensity PreWO (y axis) from Control siRNA. (C) Scatter plot showing the deviation of *NE increase (fold change)* from Control siRNA for the two siRNAs targeting the same gene.

To consider a gene as a hit two independent siRNAs targeting the same gene have to show statistically significant reproducible effects (Figure 2.8 A, listed names). Overall independent siRNA targeting of the same gene cause a similar magnitude of deviation of NE increase (fold change) from Control siRNA indicating robust reproducibility of the phenotype (Figure 2.9 C).

The vast majority of gene hits affecting INMPs are nucleoporins, all of which cause a decrease in *NE increase (fold change)*. Consistently almost all components of the NUP107-160 complex show a 50% to 80% decrease in *NE increase (fold change)* compared to Control siRNA. Additionally NUP153 and NUP93 KDs show a similar milder effect. Two of the gene hits code for NE proteins. I detected mild reduction of reporter translocation after depletion of the outer nuclear membrane protein Nesprin-1 (SYNE1), whereas LMNA depletion reproducibly increased the reporter accumulation at the NE. In LMNA KD cells the *NE increase (fold change)* was 80% higher than Control siRNA (Figure 2.8 and Figure 2.10 A). Although in the screening I targeted the complete set of importins none of them seems to have a major effect in the targeting process, except for KPNB1 KD having a mild but reproducible effect in reporter in the reduction of translocation (Figure 2.8).

Visual examination of single cell trajectories of gene KDs that have a reduced *NE increase (fold change)* reveals two possible reasons for this effect. In the first case, which represents the large majority of the genes, the reporter does not show any significant accumulation at the INM before and after WO suggesting that transport and/or retention at the INM is impaired. For example, in SEC13 KD cells the reporter only slightly accumulates at the INM over time reaching an approximately 10% increase compared to the preWO steady state level (Figure 2.10 B). In the second case, the reporter localizes at the INM throughout the experiment. A representative example of this phenotype is NUP93 KD (Figure 2.10 C). After depletion of NUP93 the full length form of the reporter has fully translocated to the INM already prior to inhibitor wash out. Therefore in this case the absence of the ER localized pool of the reporter suggests a loss of size selectivity of INM targeting.
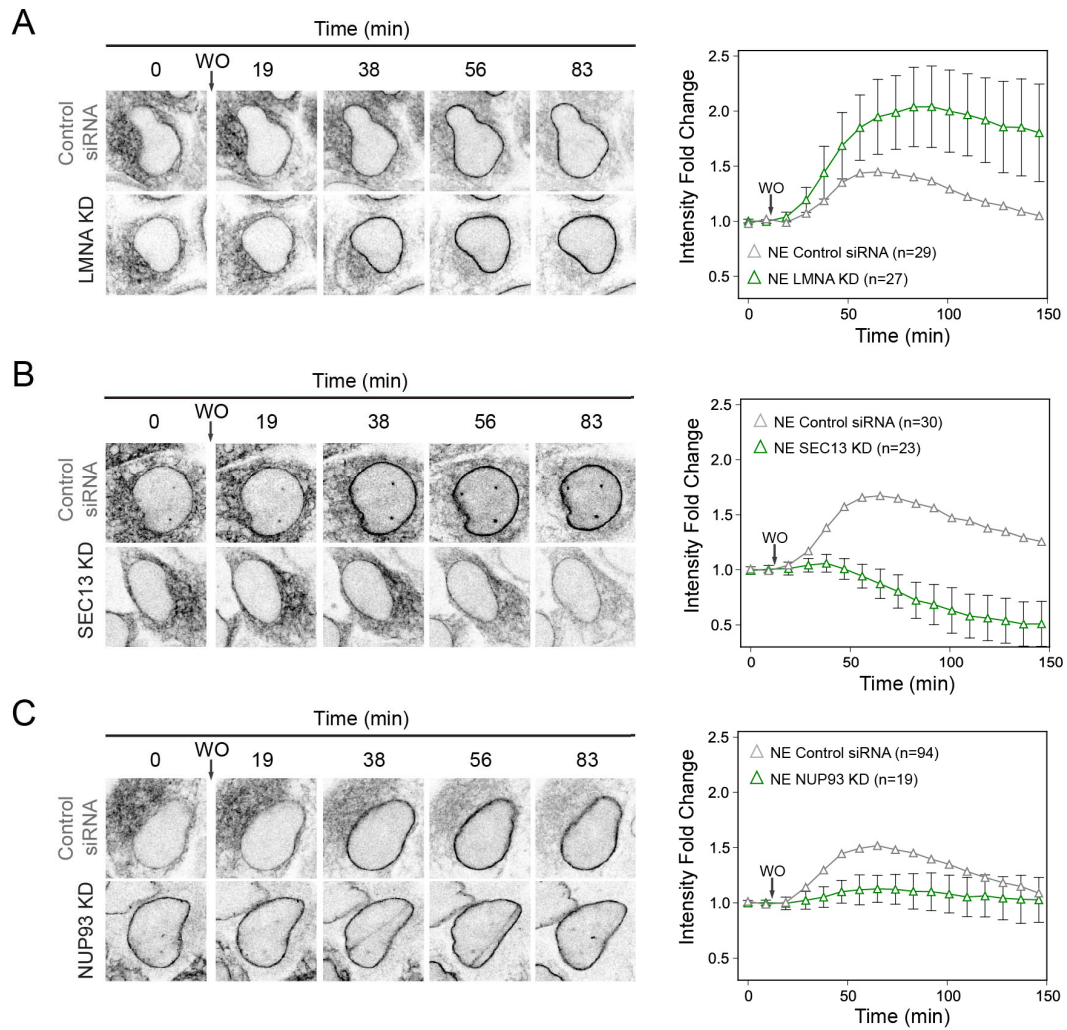
Figure 2.10 (A-C) Representative single cell trajectory images for the three main phenotypic classes: LMNA KD (A), SEC13 KD (B) and NUP93 KD (C) cells. The plots show NE fold change for the Control siRNA (grey triangle) and for the indicated gene KD (green triangle). The average data plot is from a single replicate of the screen. Error bars for the genes KD are standard deviation of mean.

2.3 A predictive mathematical model for INM proteins targeting

2.3.1 Model description

Although we used a simple single parameter score to identify genes implicated in INM protein targeting, the screening data contains detailed kinetic information for each hit. To exploit this information and gain insight into the mechanism underlying the RNAi phenotypes I generated, in collaboration with Antonio Politi (a postdoc in the lab), a mathematical compartmental model to parameterize the observed dynamics of reporter translocation. In this model we took into account the transport, binding at the INM, protease cleavage, production and degradation of the reporter during its relocation from the ER to INM after cleavage of the retention domain (Figure 2.11). The binding of the reporter to nuclear substrates (Lamins/chromatin proteins) causes a decrease in the export rate constant k_o and so a longer retention in the INM (Material and Methods). To describe phenotypes with an INM localization of the full length protein (Figure 2.10 C) we also include a reduced permeability for the uncleaved construct. By fitting the model to unperturbed Control siRNA dynamics the overall import and export rate of the reporter across the NPC can be determined. Furthermore, the model can help to give mechanistic insight for the previously identified gene hits, by distinguishing phenotypes that affect the import or retention of the reporter.
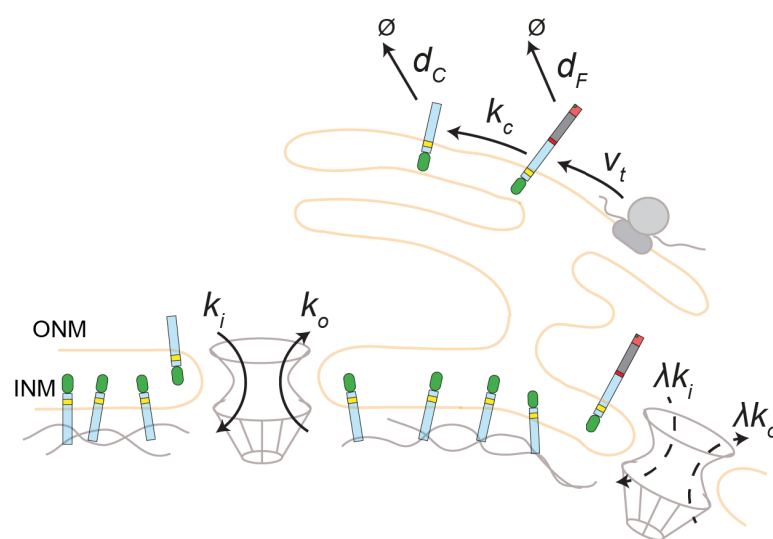
Figure 2.11 Schematic representation of the mathematical model. The model has two compartments, the ER and the INM, with the membrane area ratio $\alpha = A_{ER}/A_{NE}$. The model accounts for translation (v_t), degradation of the reporter construct (d_C and d_F), and the cleavage of the ER retention domain (k_c). The transport of the reporter is set by the import and export rate constants (k_i and k_o, respectively). The uncleaved protein can be transported with reduced rates set by λ

2.3.2 Parameters estimation for Control siRNA

I first determined the set of rate constants characterizing the reporter targeting for control siRNA. Some of the rates can be determined experimentally in order to constrain the fitting of the model to NE and ER kinetics.

The ER retention domain cleavage rate (k_c) was determined by Western blot analysis of cell lysates collected at different time points after inhibitor washout (Figure 2.12 A) The full length (uncleaved) reporter species was quantified and plotted over time. Fitting of the relative intensity value of the uncleaved reporter leads to a rate constant of $k_c = 2.05$ h^{-1} (Figure 2.12 B).

To compute the ER to NE membrane area ratio α, I used 3D images of distribution CMPK-LBR1TM-mEGFP, that is uniformly distributed in the ER-NE membranes. I then measured fluorescence intensity in the segmented ER and in a region around the chromatin that includes only the NE. Since this construct codes for a membrane anchor protein the ratio between the ER and NE intensities directly reflects the relative surface area between these two compartments with $\alpha = A_{ER}/A_{NE} = 7$ (see Material and Methods).

In the model, the translocation dynamic does not depend on the exact value of the translation rate (v_t) but can be influenced by variations in the rate constant.

I then tested the effect of an acute reduction of translation rate on maximal reporter accumulation at the INM. To completely block protein synthesis ($v_t = 0$) cells were incubated before wash out for 30min in presence of different concentration (10, 50, 100 µg/ml) of Cyclohexemide (CHX); protease inhibitor was then washed-out with medium containing CHX and the NE Increase (fold increase) was computed for each condition (Figure 2.12 C). Maximal accumulation of the reporter is reduced by around 50% after the complete block of protease synthesis at 50 µg/ml of CHX. In the screen set up such an acute drop in the translation rate just prior to wash out is unlikely and moreover I did not found a correlation between initial ER intensity, which is proportional to the translation rate and maximal reporter accumulation (NE Intensity (fold change) (Figure 2.12 D). I therefore assumed that the reporter synthesis rate is stable over the time frame of translocation and a constant fixed value of v_t can be used.

The remaining rate constants were estimated by fitting the model to NE and ER kinetics after WO and the pre-WO NE to ER intensity ratio (Figure 2.12 E and Material and Methods).

The derived degradation rates for the full length and the cleaved reporter (d_F and d_C) are respectively $d_F = 0.53$ [0.08], $d_C = 1.54$ [0.23] (median [inter quartile range]). This indicates that the full length protein is more stable (~ 3 fold longer turnover time) than the cleaved reporter and therefore the total reporter concentration in the cells should decrease after wash out. Quantification by microscopy shows that total reporter concentration indeed decreases after the wash out with a rate that is in agreement with the one predicted by the model (Figure 2.12 F). The difference in protein stability between the full length and the cleaved reporter also accounts for the transient peak in intensity at the NE seen during the translocation (Figure 2.12 E). In the end I could determine Control siRNA import and export rates ($k_i = 9.4$ [1.26], and $k_o = 1.88$ [0.61] in units h^{-1}). We found that the transport through the nuclear pore is in the order of minutes for the cleaved form and negligible for the uncleaved. The transport from the ER to the INM takes $t_{1/2} = \log(2)/k_i = 4$-5 min, whereas the inverse process, returning to the ER from the INM, is considerably slower due to binding in the INM with $t_{1/2} = \log(2)/k_o = 19$-25 min.
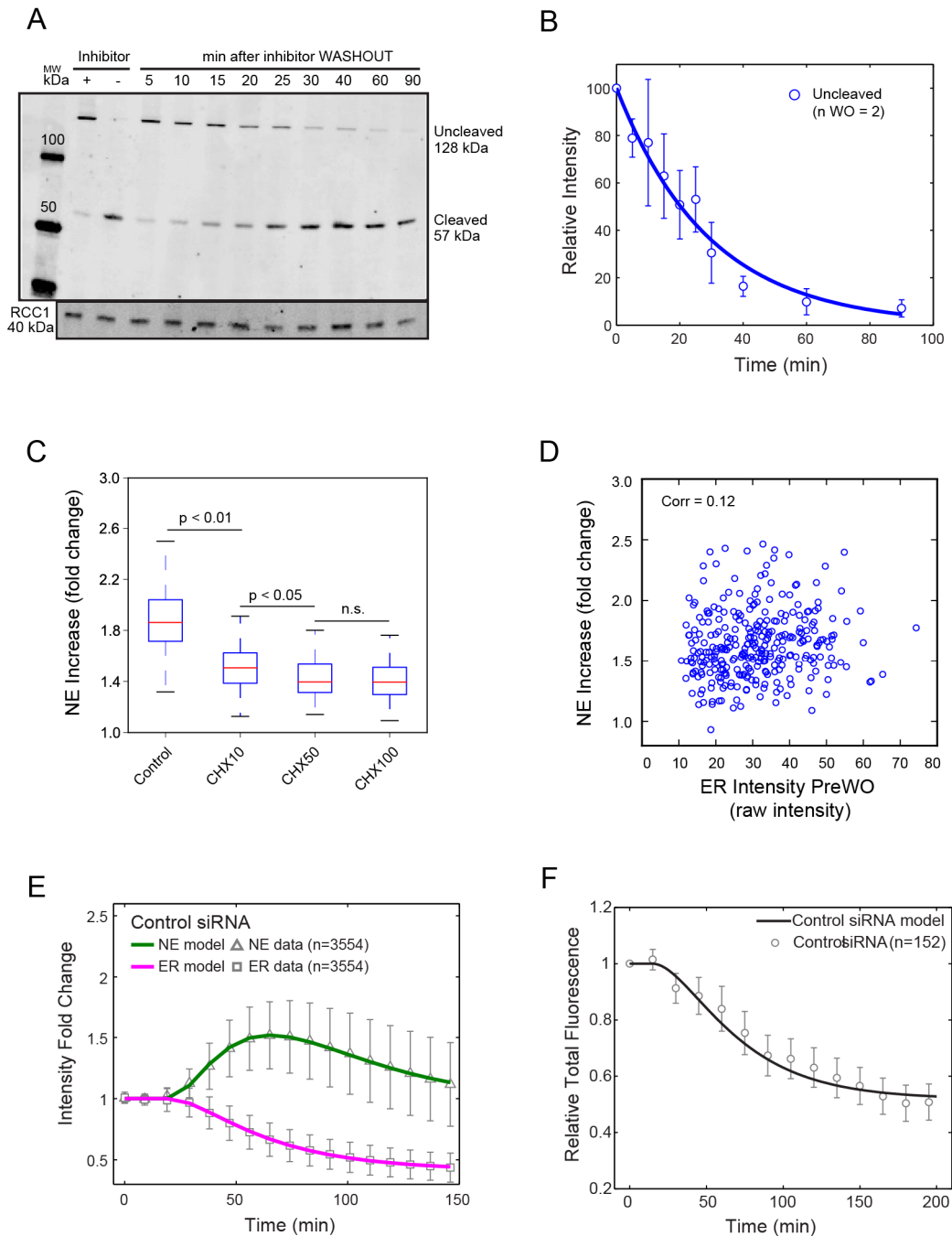
Figure 2.12 (A-B) WB analysis of protease cleavage kinetics. Cells lysates were collected at different time points after inhibitor wash out and blotted with anti-GFP antibody. The quantified intensity of the uncleaved reporter bands over time were plotted as relative intensity to the time point 0 (inhibitor +). Data were fitted with an exponential decay function and the cleavage rate $k_c = 2.05$ h^{-1} was determined. (C) NE increase (fold change) in Control cells and cells treated with different concentration (µg/ml) of Cyclohexemine (CHX). p values are derived from the t-test (D) Scatter plot showing no correlation between expression level of the reporter (ER intensity preWO) and the *NE increase (fold change)* (E) The reference parameter set is obtained by fitting the model (solid lines) to all cell trajectories for Control siRNA (symbols) in the screening. Obtained parameters are $d_F = 0.53$ [0.08], $d_C = 1.54$ [0.23], $k_i = 9.4$ [1.26], and $k_o = 1.88$ [0.61] in units h^{-1}, and $\lambda = 0$ (median [inter quartile range]).(F) Total Target-INM GFP fluorescence after washout in Control siRNA. Model curves are computed from Eq. 9-10 (Material and Methods) using parameters obtained from the fit to the single cell NE and ER kinetics, with $d_F = 0.53$ h^{-1}, $d_C = 1.54$ h^{-1} (control siRNA)

2.3.3 Determination of best model for a predictable phenotype

To simulate targeting phenotypes we systematically fitted different combinations and number of parameters to the NE and ER kinetics after WO. The parameter combination accounting for a phenotype with the smallest number of parameters that differ from control is then selected (Material and Methods). To validate this approach I generated a new reporter named Target-INM-Δ60LBR, in which the first 60aa of LBR are removed (Figure 2.13 A). Since this domain contains the binding regions for different nuclear substrates (laminB, histones and DNA binding domains)(Ye and Wormann, 1994), I predicted that the Target-INM-Δ60LBR would have a reduced INM accumulation. Indeed Target-INM-Δ60LBR is largely localized in the ER membrane when the protease is active. Moreover kinetic analysis shows that Target-INM-Δ60LBR only slightly accumulates at the INM (Figure 2.13 C). Different parameter combinations were then fitted to NE and ER kinetics and the best fitted was selected as illustrated in Figure 2.13 B. The model reliably reproduces the observed phenotype with an 8.7 fold increase in export rate (Figure 2.13 B). Thus our model correctly predicts the Target-INM-Δ60LBR phenotype as a reduced INM retention compared to the Target-INM-LBR reporter.
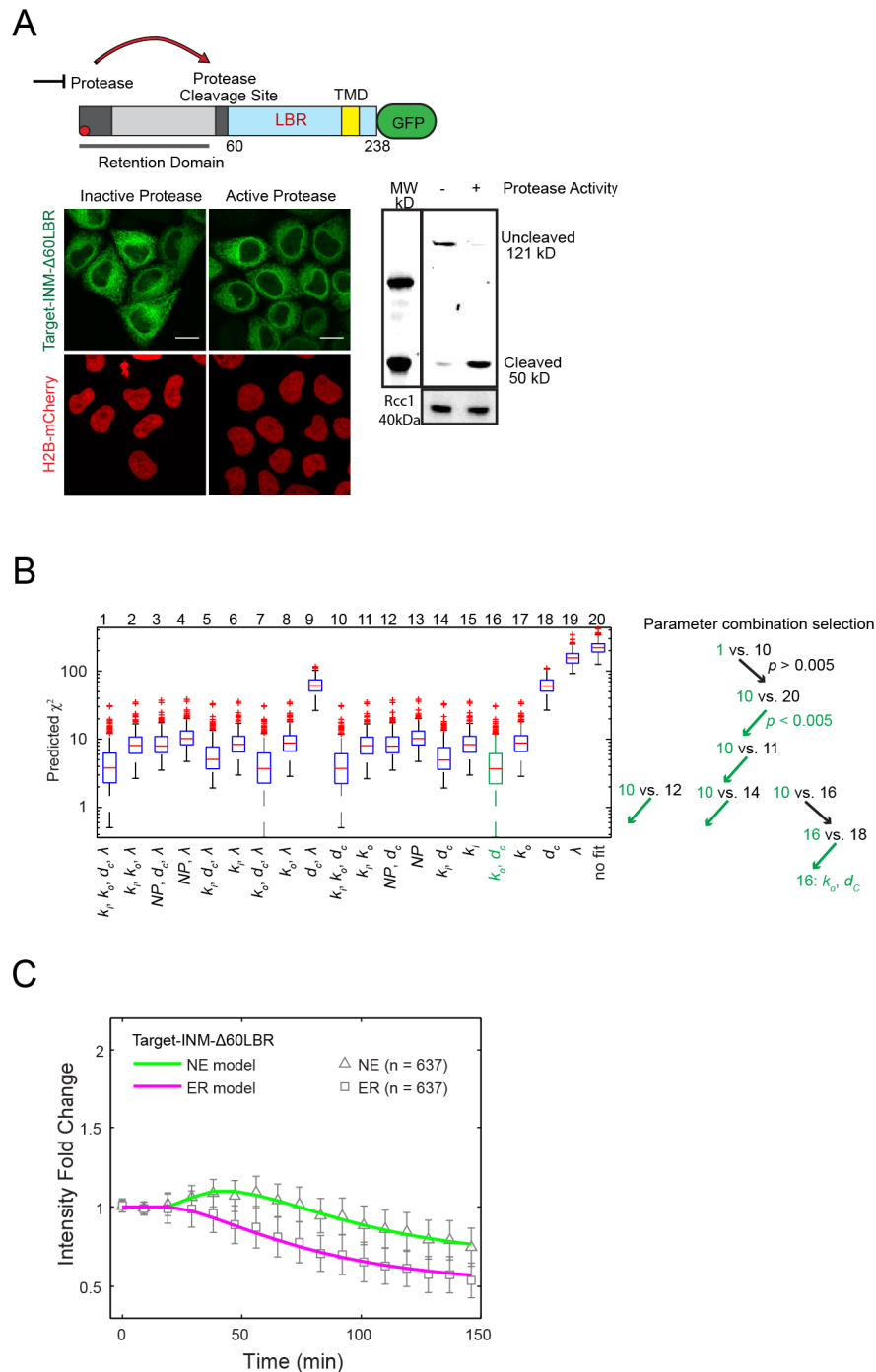
Figure 2.13 (A) Schematic representation of TARGET-INM-Δ60LBR reporter and its localization assessed by imaging of HeLa cells stably expressing H2B-mCherry grown for 24h in the presence (inactive protease) or absence (active protease) of the protease inhibitor. WB analysis of cells grown for 24 hours in presence (protease activity -) or in the absence (protease activity +) of the protease inhibitor shows respectively the full-length and cleaved form of the reporter. (B) Selection of parameter combinations using crossvalidation. Through resampling without replacing I createed a large number (here 300) of data sets from the original Target-INM-Δ60LBR data set. Different parameter combinations for *NP* (i.e. change k_i and k_o but leave k_i / k_o = const.), k_i, k_o, d_C, and λ are fitted to half of the resampled data. The predicted χ^2 for the other half is calculated (shown in the graph). Parameter not included in the fit are chosen equal to the Target-INM reference parameter set (Figure 2.12). Kolmogorov-Smirnov tests (*p* < 0.005) are used to test whether predicted traces using a

larger set of parameters are significantly better than traces that use a smaller set (right panel). See also Material and Methods. (C) To reproduce Target-INM-Δ60LBR traces (data points) with the model (solid lines) it is sufficient to assume a large increase in the export rate constant with k_o = 16.41 [1.54] h^{-1} compared to 1.88 [0.61] h^{-1} for Target-INM. We also found that the best fit is obtained when also d_C is slightly decreased, d_C = 1.28 [0.05] h^{-1} compared to 1.54 [0.23] h^{-1} for Target-INM. Parameter values are given in median [interquartile range].

2.3.4 The model clusters genes hit into 3 distinct classes

After having validated the approach for the selection of the parameters with Target-INM-Δ60LBR, the model was applied to the gene hits list (Figure 2.14). Genes were clustered according to the type of parameters that differ from Control siRNA and this leads to 3 distinct classes (Figure 2.15). In the first cluster **a**, containing 12/15 of the genes, a concomitant and equal decrease in both import and export rate is observed. For some genes in this cluster the model predicts a decreased stability of the cleaved reporter. For genes in the second cluster **b,** import and the export change independently; in particular the KPNB1 and LMNA KDs phenotype can be reproduced by an increase and respectively decrease of the export leaving the import unchanged. Finally, for cluster **c**, containing all the siRNAs for NUP93, the model predicts an increase in pore permeability for the uncleaved reporter and thus a decrease in the size-selectivity of the nuclear pore. This accounts for the pre-WO accumulation of the reporter and the reduced targeting after WO (Figure 2.10 C).
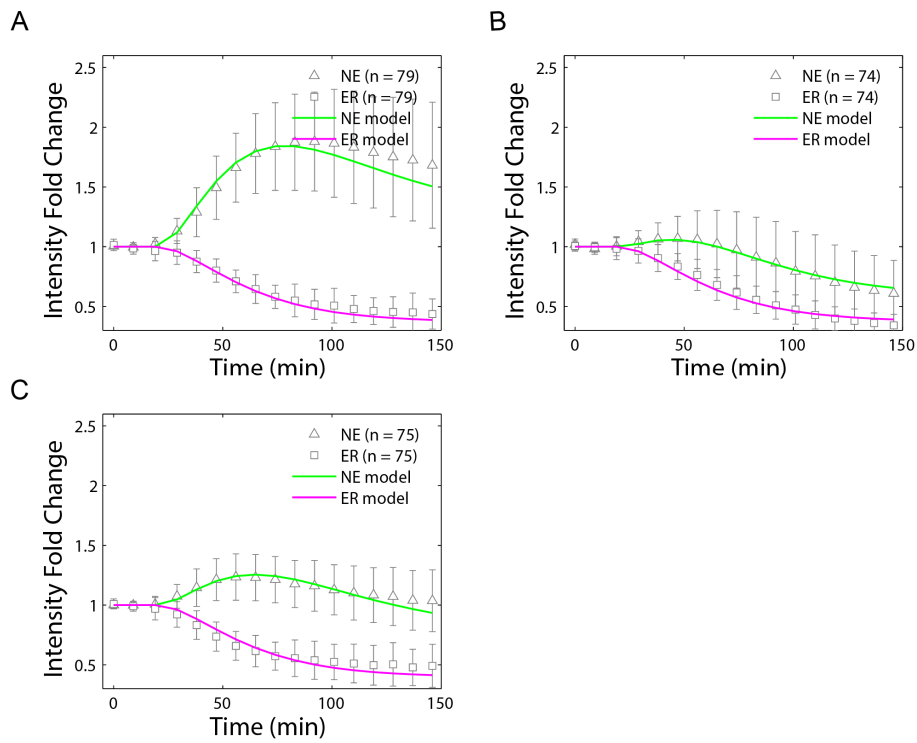
Figure 2.14 Example fits for (A) LMNA KD (d_F = 0.53 [0.08], d_C = 1.54 [0.23], k_i = 9.4 [1.26], ko = 0.24 [0.21] h⁻¹); (B) SEC13 KD (d_F = 0.53 [0.08], d_C = 2.35 [0.13], ki = 3.27 [0.45], ko = 0.65 [0.09] in units h⁻¹) and (C) NUP93 (d_F = 0.53 [0.08], d_C = 2.35 [0.13], ki = 3.27 [0.45], ko = 0.96 [2.04] in units h⁻¹) and and λ 0.0535 [0.0068]. Parameteres are median [inter quartile range].
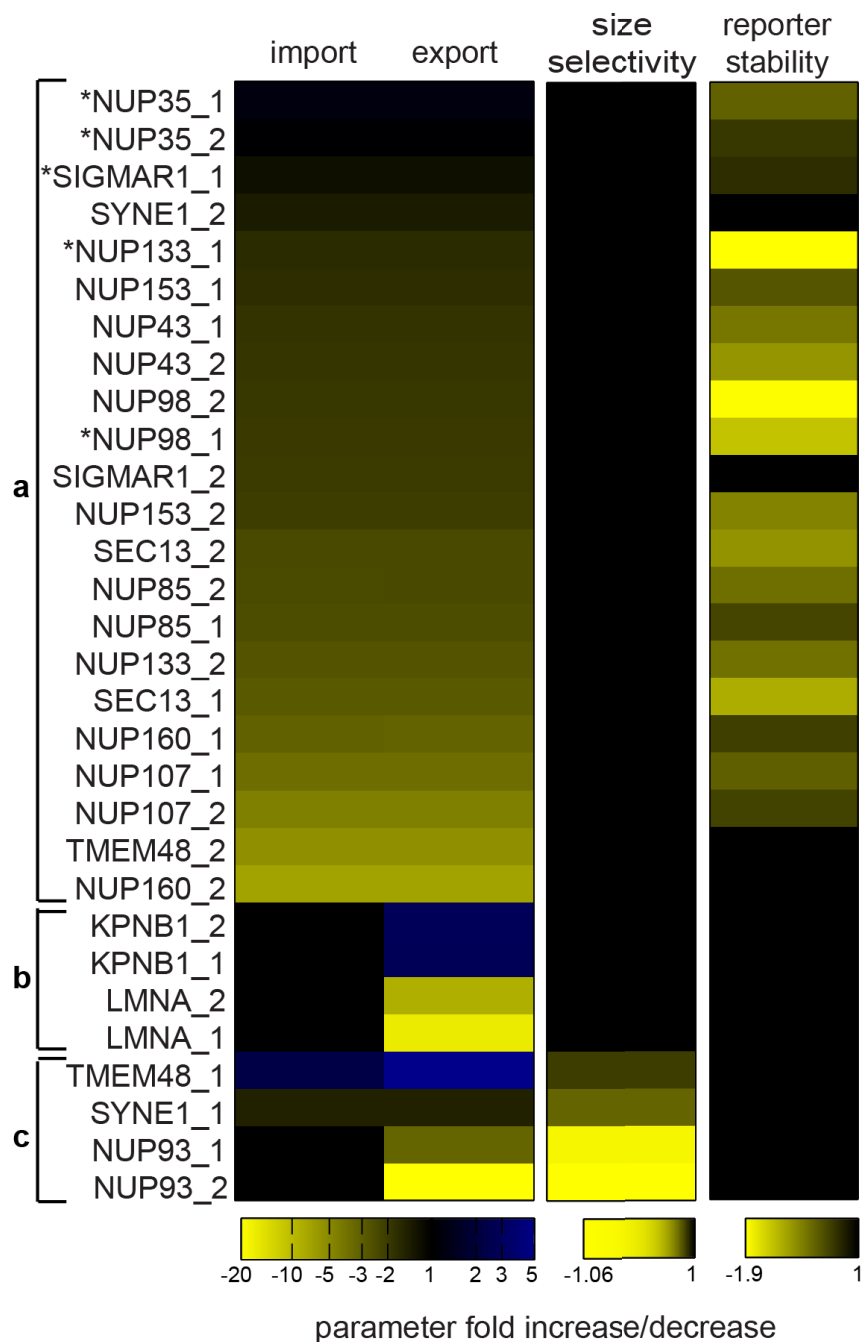
Figure 2.15 Parameter fold changes with respect to the Control siRNA set for each of the 2 siRNAs targeting the 15 hit genes. The reporter stability is defined by $1/d_C$, the size selectivity is 1- λ. Genes classes; **a**) changes in import/export **b**) change in import or export independently **c**) change in size selectivity For the siRNAs marked by an asterisk a fit to the data could also be obtained by varying the turnover time of only the cleaved form.

For SEC13 KD the model predicts both a change in transport rate and a decrease in reporter stability of the cleaved form (Figure 2.15). I tested the prediction by measuring the total protein amount over time after wash out. In agreement with the model a significant decrease in the total protein amount after WO compared to Control siRNA (Figure 2.16 A) is detected. When the same quantification is done in cells that are kept in presence of the protease inhibitor (no wash out) for up to 2.5 hrs., total protein concentration does not significantly deviate from Control siRNA indicating that in SEC13 KD cells the translation rate is constant over this time (Figure 2.16 B). Additionally I tested if protease cleavage occurs normally in these cells. Cell lysates were collected from cells grown in the presence or absence of protease inhibitor for 24 hours and after inhibitor wash out (time points 30min and 60min). Western blot shows that 1) after 48 hrs. of KD the reporter expression is still robust and 2) that reporter cleavage occurs quantitatively also in these cells (Figure 2.16 C). The Efficiency of SEC13 KD was confirmed by Western blot against the endogenous protein (Figure 2.16 D).

Genes clustered in the **b** class do not show any change in reporter stability compared to Controls. As predicted I confirmed that the total protein of LMNA KD cells concentration does not differ from the Control cells (Figure 2.16 E).
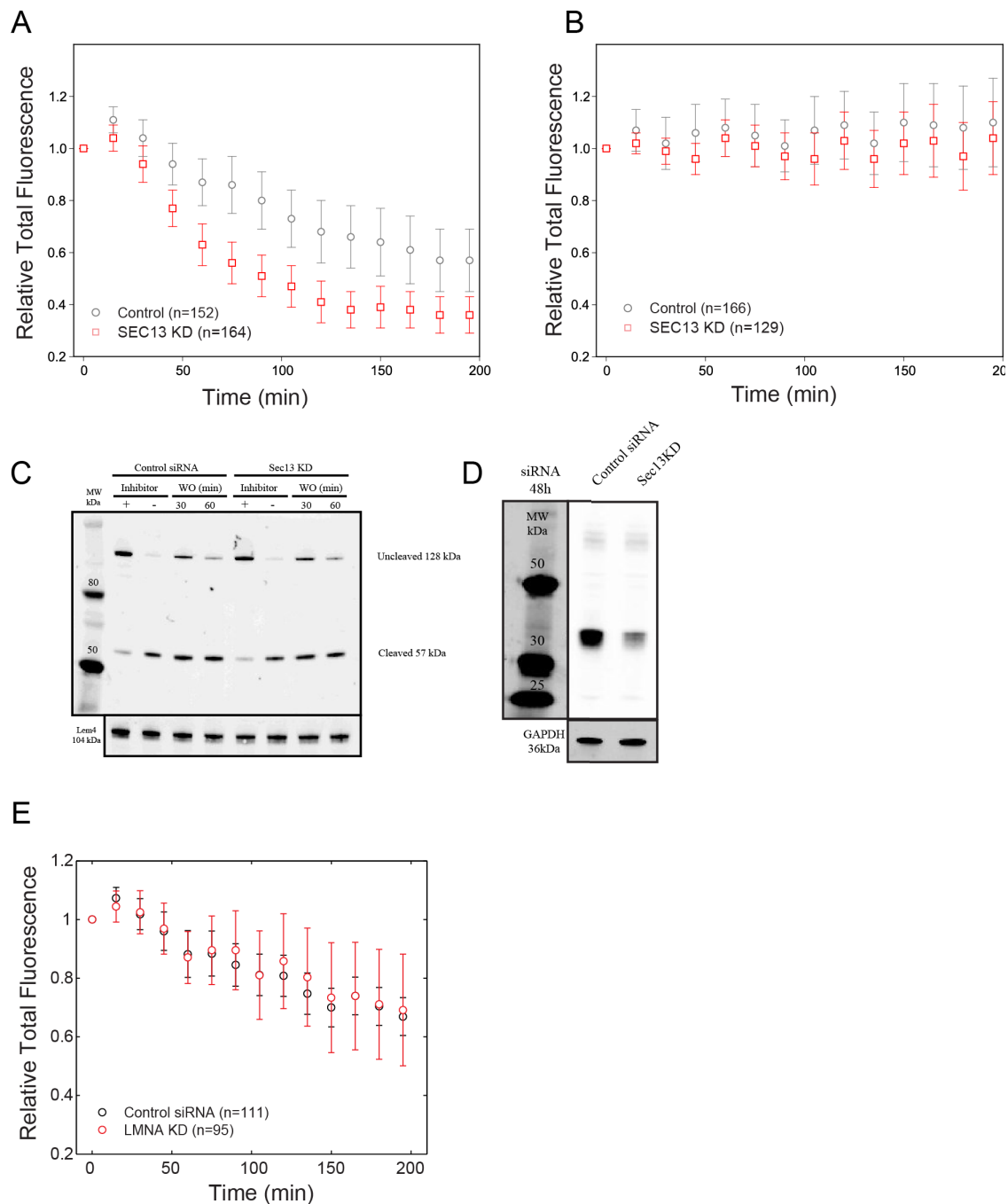
Figure 2.16 Total reporter concentration in Control siRNA (black circle) and Sec13 KD (red circle) plotted over time after inhibitor washout (A) or without washout (B) measured by microscopy. Bars are standard errors of means. (C) WB analysis of Control and Sec13 KD cells in presence and absence of inhibitor and after inhibitor wash out (30 and 60 min). Blot was done against GFP protein. (D) SEC13 KD efficiency after 48 hrs. siRNA (E) Total reporter concentration in Control siRNA (black circle) and LMNA KD (red circle) plotted over time after inhibitor washout. Bars are standard errors of means.

2.4 Validation of model prediction

2.4.1 NPCs densities partially account for reduction of targeting

For the majority of the hits (**a** and **b** in Figure 2.15) the model predicts that the import and export rate constants varies by the same amounts. Both the import and export rates are proportional to the number of pores and pore permeability (Material and Methods Eq. 1-2). Thus a simultaneous decrease of import and export could be due to a decrease in pore numbers. We tested this prediction for four nucleoporins (NUP98, SEC13, NUP107 and NUP153) belonging to four distinct NPC complexes and quantified NPC density after 48 hours KD of each nucleoporin. Super-resolution images of nuclei stained with mab414 antibody allowed us to count single NPC (Figure 2.17). From this we computed the NPC density in the KD and Control siRNA. We found that all four nucleoporin KDs lead to a reduction of NPC density ranging from 25% (NUP153 KD) to 60% (SEC13 KD) relative to Control siRNA (Figure 2.17). The good agreement between experimentally derived and model predicted NPC density for SEC13 KD and NUP98 KD indicates that these two phenotypes can be accounted for a reduced NPC density. Interestingly, for NUP107 KD and NUP153 KD the model predicted a larger reduction in NPC density than observed experimentally. This indicates that additional mechanisms, such as decreased permeability or non-functional pores, may contribute to the observed phenotypes.
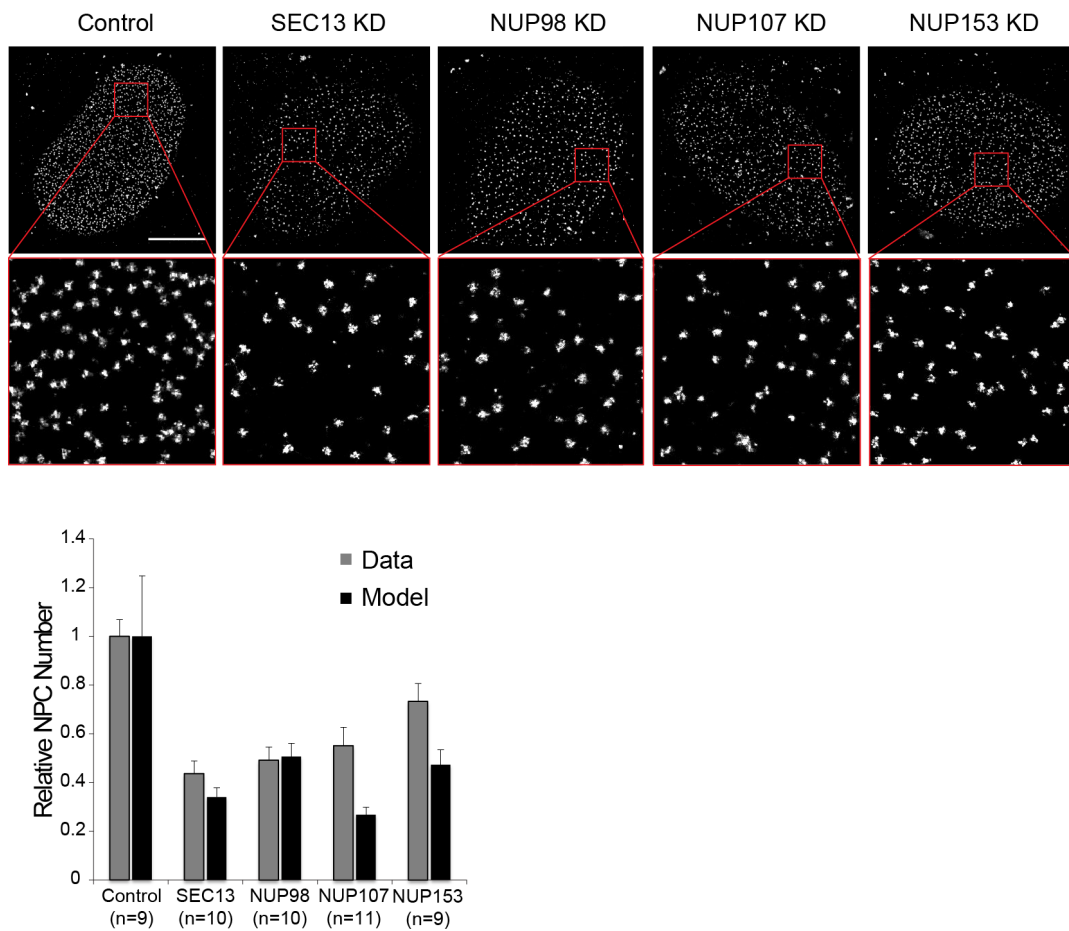
Figure 2.17 Super-resolved images of Control siRNA, SEC13KD, NUP98KD, NUP107KD and NUP153KD nuclei stained with anti mab414 antibody. Scale bar 10μm. In the inset single NPCs are visible. Lower panel: Density of the NPCs derived from experimental data (grey bars) or predicted by the model (black) normalized to 1 relative to Control siRNA. Raw NPC densities are for Control siRNA (9.55 +/- 0.65 NPC/μm^2), SEC13KD (4.17 +/- 0.49 NPC/μm^2), NUP98KD (4.70 +/- 0.51 NPC/μm^2), NUP107KD (5.26 +/- 0.71 NPC/μm^2), NUP153KD (7.00 +/- 0.70 NPC/μm^2)

2.4.2 The LMNA KD phenotype is explained by increased retention in the NE

For LMNA KD the model predicted a decreased export rate constant. This will cause an increased retention and higher accumulation of the reporter in the nucleus. Alternatively, if the increased accumulation would be due to an increased import we would expect decreased retention (Material and Methods). To test this prediction we performed fluorescence recovery after photobleaching (FRAP) experiments in Control siRNA and LMNA KDs cells where we bleached part of the NE 90min after inhibitor wash out (Figure 2.18 A B). Qualitatively FRAP curves for LMNA KD (red squares) show a slower recovery than for Control siRNA (gray circles) indicating a stronger retention in the nucleus (Figure 2.18). We computed characteristic times of recovery by fitting a two exponential function to the data (solid lines and inset). The estimated ratio of characteristic times (1.54) is in agreement with the ratio estimated from the model (1.44). The predicted and experimentally observed increased retention in the nucleus can have two reasons: (i) an asymmetric impairment of the passage through the NPC, (ii) stronger binding to nuclear proteins in the INM. As an asymmetric change in NPC permeability is thermodynamically unlikely, we propose that the phenotype seen for LMNA KD is caused by an increased binding of the reporter to nuclear proteins .

This could be explained by an increase availability of binding sites for LBR at the INM; since LBR interacts with Lamin B at the INM I tested if after depletion of A-type lamins a compensatory effect would lead to overexpression of Lamin B. However WB analysis of cells treated for 48 hours with siRNA against LMNA shows no change in Lamin B expression (Figure 2.18 B). As well Lamin B concentration at the NE is not increased due to LMNA KD cells compared to Control siRNA as shown by immunofluorescence (Figure 2.18 C)

74
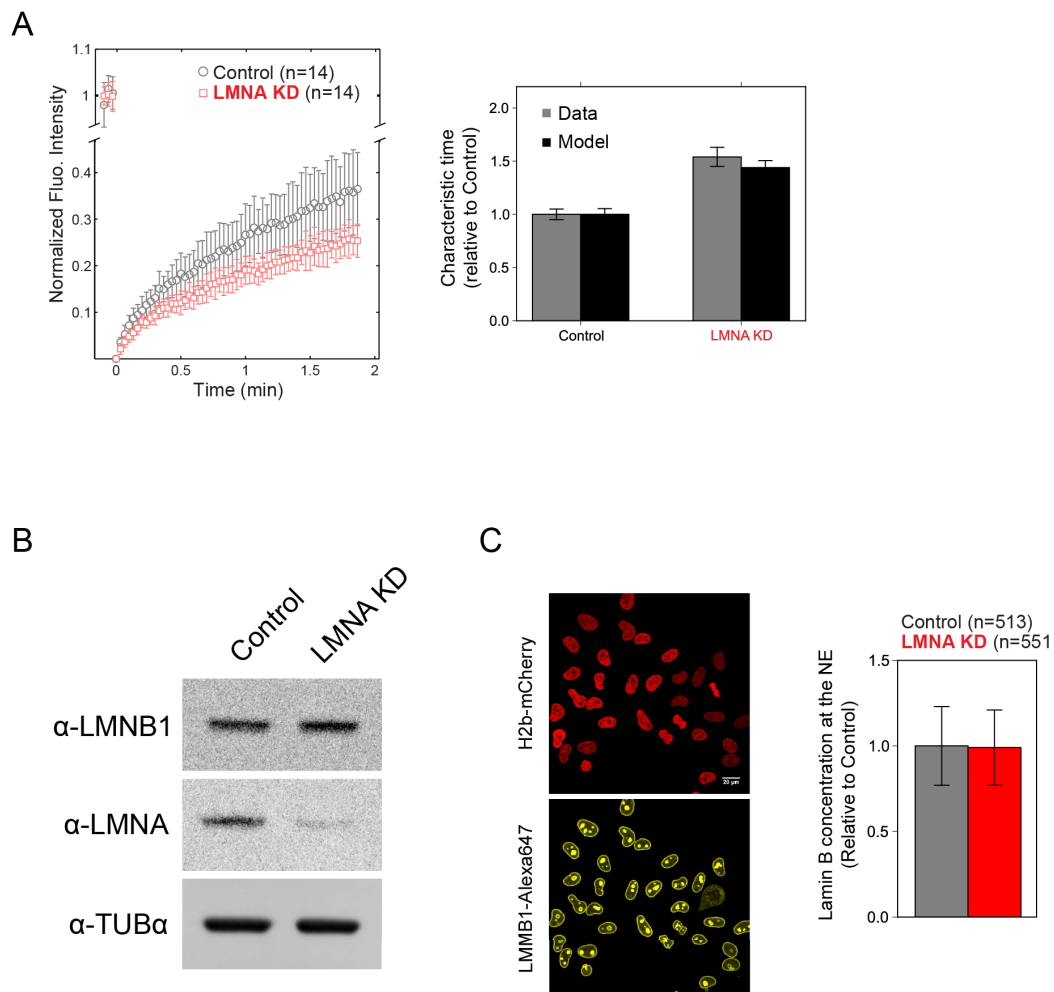
Figure 2.18 A) NE FRAP recovery curves of Control siRNA (gray) and LMNA KD (red). Data are normalized between 1 (prebleach value) and 0 (post bleach value) and plotted over time. Solid lines are a fit of the double exponential $FRAP(t) = A\exp(-k_1 t) + (1-A)\exp(-k_2 t)$ to the data. The characteristic time is computed from $A/k_1 + (1-A)/k_2$ and shown in the inset for Control and LMNA KD (mean ± s.d., $n = 3$ independent experiments). B) WB analysis of Lamin B1 expression after depletion of Lamin A C) *left panel*: HeLa cells stably expressing H2b-mCherry stained with anti-LaminB1. Lamin B1 concentration at the NE is calculated by measuring fluorescence intensity a in a region around the chromatin signal and plotted as normalized value to the Control siRNA (right panel).

2.4.3 NUP93 KD cells also lose size selectivity for soluble dextrans

Depletion of NUP93 leads to a distinctive phenotype in which the full length form of the reporter has already translocated to the INM before inhibitor washout. Among the other nucleoporins NUP93 is the only one for which the model predicts a decreased size-selectivity of the NPC without affecting the other processes. We therefore asked if the decrease in size-selectivity is restricted to membrane protein or if soluble macromolecules are also affected. The NPC represents a barrier for soluble protein larger than 50 kDa whereas protein smaller than this size are free to enter the nucleus. To assess the NPC permeability barrier after 48 hours of NUP93 KD, we microinjected the cell cytoplasm with two size dextran (70kDa and 160kDa) to mimics the behavior of soluble proteins. With a decrease in NPC size-selectivity we would expect a larger fraction of the dextran being to be able to enter the nucleus in the NUP93 KD than in Control cells. We therefore quantified the total amount of dextran in the nucleus compared to the whole cell for both Control and KDs cells. In this experiment using cells that express the reporter in the presence of the inhibitor allowed us to score at the same time the permeability for membrane protein and for soluble dextran (Figure 2.19 A). We could detect a significant increase of about 50% in the nuclear accumulation of the 70kDa dextran in knock down cells relative to Control but only a mild, not significant, increase in nuclear accumulation of the 160kDa dextran (Figure 2.19 B) This evidence indicates that NUP93 depletion affects the size-selectivity of the NPC permeability barrier for both membrane and soluble proteins.

A
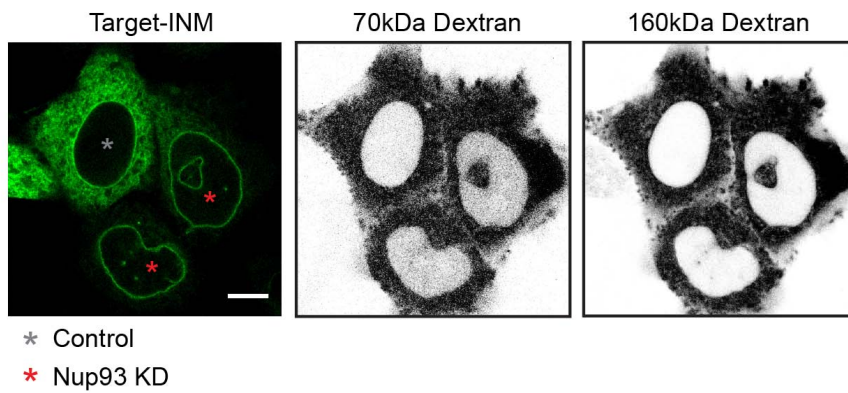
* Control
* Nup93 KD

B
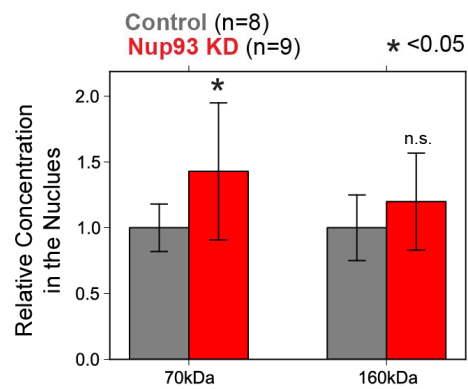
Figure 2.19 (A) NE permeability assay. Representative images showing respectively reporter, 160kDa and 70kDa dextran localization in internal Control (gray asterisk) or NUP93 KD cells (red asterisk). (B) The bar plot shows dextran nuclear concentration relative to the Control siRNA.

The NUP93 forms a complex with other nucleoporins namely NUP188, NUP205 and NUP155. It has previously shown that depletion of Nup188 from *in vitro* reconstituted *X. Laevis* nuclei leads to mislocalization of ER resident proteins into the NE and results in enlarged size nuclei (Theerthagiri et al., 2010). A very similar phenotype to NUP93 KD has been reporter also in mammalian cells for Nup188 KD (Antonin et al., 2011). In my screen, I could not observe any "NUP93 like" phenotype after Nup188 depletion and as well for the other NUP93 subcomplex member NUP155; on the contrary examination of single cell trajectories show that in NUP205 KD the full length form of the reporter has already translocated to the INM before inhibitor washout. However this phenotype can be reproduce only with one siRNA targeting NUP205 and is linked with a decrease translocation after the wash out (Figure 2.20).
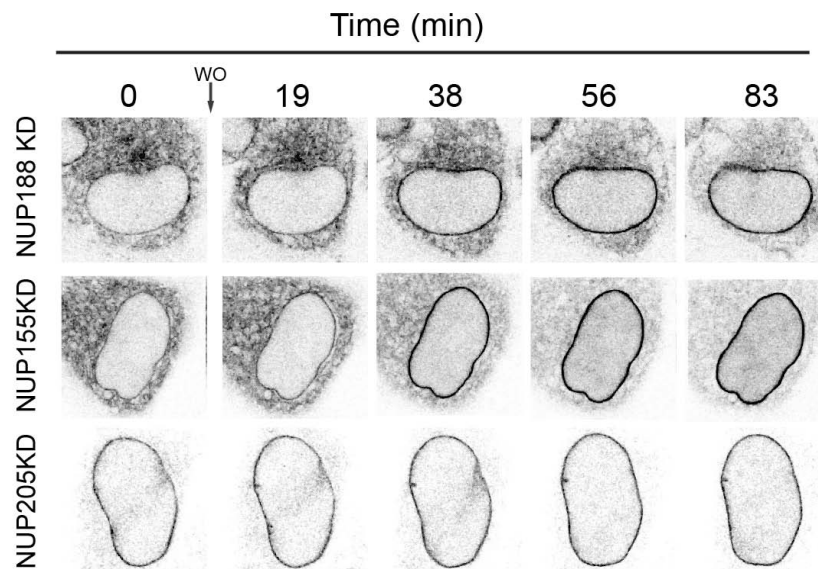
Figure 2.20 Representative single cell trajectories images other Nup93 complex component: Nup188 KD, Nup155 KD and NUP205 KD cells.

78

Table 2.1 Ranking of each siRNA based on the average deviation of *NE Increase (fold change)* from Control siRNA. For each siRNA the siRNA Ambion identifier, the Gene Symbol, the number of average replicates, the deviation of *NE Increase (fold change)* and the ER Intensity PreWO from Control siRNA is reported. siRNA that show a statistical reproducible effect in at least 2 of the scored replicates are marked in blue.

siRNAID-Gene Symbol	n. of Replicates	DEVIATION from Control siRNA	
		NE Increase (fold change)	ER Intensity PreWO
s9782–NUP98	4	-86.28	17.71
s9783–NUP98	4	-84.32	6.36
s12663–SEC13	4	-83.72	25.40
s31401–NUP133	4	-80.83	51.04
s23466–NUP160	4	-78.47	38.50
s32727–NUP107	4	-73.57	10.48
s51377–NUP43	4	-72.68	5.78
s12664–SEC13	4	-72.50	8.58
s36612–NUP85	4	-71.30	-19.21
s31402–NUP133	4	-69.77	6.84
s19376–NUP153	3	-68.87	1.27
s51375–NUP43	4	-65.08	32.29
s23465–NUP160	4	-63.64	-0.05
s32728–NUP107	4	-63.12	-6.46
s35441–NUP37	4	-60.33	26.13
s31303–TMEM48	4	-58.49	-25.97
s19374–NUP153	3	-57.80	-5.47
s37878–SEH1L	4	-56.09	14.97
s36610–NUP85	4	-55.04	8.96
s23177–NUP205	4	-54.56	-41.83
s18985--NupL1	4	-50.30	55.93
s20088–SIGMAR1	4	-45.84	-13.52
s7927--KPNA4	4	-44.88	12.53
s18655–NUP93	4	-42.42	-52.86
s23965–NUP188	4	-41.93	130.09
s7929--KPNA5	2	-41.33	-23.92
s37271--REEP4	3	-40.59	-12.39
s7917–KPNB1	3	-40.44	25.43
s27911--REEP2	3	-40.36	-1.23
s11773–RANBP2	3	-39.92	10.37
s18654–NUP93	4	-39.81	-20.24
s46245--C14orf49	4	-39.59	-6.49
s28724--NUP54	4	-39.08	-5.09
s7919–KPNB1	3	-38.57	21.87
s47158–TMEM201	4	-37.89	11.01
s35169--REEP1	3	-36.96	0.38
s26210–TOR1B	3	-34.98	13.83
s24159--LEMD3	4	-34.98	54.57
s23608–SYNE1	3	-34.01	-9.09
s224849–NUP214	3	-33.10	-16.21
s195252--C9orf167	3	-32.58	9.29
s14233–TMPO	4	-32.56	-3.25
s7930--KPNA5	3	-32.49	-2.34
s7924--KPNA3	4	-31.78	7.34
s24249–NUP62	4	-31.58	-4.96

siRNAID-Gene Symbol	n. of Replicates	DEVIATION from Control siRNA	
		NE Increase (fold change)	ER Intensity PreWO
s18984--NupL1	4	-31.21	-28.45
s24241--KPNA6	3	-31.09	-6.88
s11680--RAB5A	4	-30.81	23.42
s15607--AAAS	3	-30.61	-1.94
s23883--CBX5	3	-30.49	-5.87
s1NUP35--NUP35	4	-29.81	12.93
s21139--NUP50	3	-29.33	-17.34
s21138--NUP50	3	-28.58	2.59
s35439--NUP37	4	-28.08	1.37
s27913--REEP2	3	-27.93	6.88
s20086--SIGMAR1	4	-27.85	0.84
s18874--BCLAF1	4	-27.83	13.34
s34576--TOR3A	3	-26.75	-8.41
s7922--KPNA2	4	-26.58	-11.66
s24242--KPNA6	3	-26.55	-9.68
s23125--ANKLE2	4	-26.53	-7.68
s23609--SYNE1	4	-26.18	19.62
s24466--SUN2	4	-26.15	3.67
s23630--SUN1	4	-26.05	-15.52
s2NUP35--NUP35	4	-25.06	-16.34
s31301--IPO9	3	-24.62	-0.96
s46246--C14orf49	4	-24.29	-5.16
s20162--RTN3	3	-24.14	5.74
s33322--KLHL14	3	-23.82	6.92
s20161--RTN3	3	-23.16	-0.61
s28725--NUP54	4	-23.08	-17.65
s8401--SMAD3	4	-21.87	35.25
s23331--NUP210	4	-20.52	-15.89
s224003--LBR	4	-20.06	22.28
s7935--IPO5	3	-19.96	0.86
s227344--REEP1	3	-18.52	10.42
s226034--SUN3	4	-17.36	-16.89
s20636--IPO8	4	-17.00	28.46
s8398--SMAD2	4	-16.97	-6.67
s8397--SMAD2	4	-16.86	4.78
s32766--RTN4	3	-16.62	3.88
s19144--POM121	4	-15.93	12.70
s195251--C9orf167	3	-15.73	17.43
s46436--C19orf46	4	-15.49	-8.67
s40756--YTHDC1	4	-14.98	-1.85
s31302--TMEM48	4	-14.78	-22.63
s33323--KLHL14	3	-14.25	-14.55
s7936--IPO5	3	-14.25	-8.44
s8402--SMAD3	3	-14.18	-23.37
s26882--TNPO2	4	-14.15	3.49
s7923--KPNA3	4	-13.47	5.60
s11678--RAB5A	4	-13.37	-0.21
s23838--ATP1B4	4	-13.20	132.99
s15548--NUP214	3	-12.78	1.17
s32767--RTN4	3	-11.42	5.50

siRNAID-Gene Symbol	n. of Replicates	DEVIATION from Control siRNA	
		NE Increase (fold change)	ER Intensity PreWO
s7928--KPNA4	4	-11.42	1.04
s48070--LEMD2	4	-11.41	-8.38
s48071--LEMD2	4	-11.33	-19.45
s15608--AAAS	3	-11.25	13.33
s35704--TMEM43	4	-11.00	-6.26
s47938--REEP3	3	-10.74	-8.05
s18609--IPO13	4	-10.26	1.92
s23885--CBX5	4	-10.01	3.06
s40757--YTHDC1	4	-9.93	-4.60
s16105--RAE1	2	-9.56	-7.63
s39476--LMNB2	4	-9.54	0.40
s25668--AKAP8L	4	-9.42	-9.14
s7934--TNPO1	3	-9.41	19.74
s18608--IPO13	4	-9.09	10.17
s23839--ATP1B4	4	-8.75	-3.85
s4404--TOR1A	4	-8.70	-9.77
s24031--TNPO3	4	-8.56	-1.10
s9779--NUP88	3	-8.38	-17.62
s37879--SEH1L	4	-7.43	-8.65
s31300--IPO9	3	-7.29	-5.42
s14235--TMPO	4	-7.28	0.21
s7424--INCENP	5	-7.14	5.57
s6414--H2AFZ	4	-6.80	1.53
s46465--TOR1AIP2	4	-6.63	-1.27
s47939--REEP3	3	-6.08	1.49
s25081--TOR1AIP1	4	-5.72	-2.60
s23124--ANKLE2	4	-5.45	-20.48
s5809--GLE1	3	-5.42	-2.92
s22250--NRM	4	-5.28	5.08
s36154--IPO4	3	-5.04	7.92
s24030--TNPO3	3	-4.93	10.35
s5808--GLE1	3	-4.71	-36.31
s26230--TOR2A	3	-4.29	-5.12
s225840--EMD	4	-4.19	-9.85
s20640--IPO7	4	-2.85	9.30
s23629--SUN1	4	-2.44	-19.36
s14353--TPR	3	-1.93	-14.26
s46466--TOR1AIP2	4	-1.72	-21.28
s39477--LMNB2	4	-0.66	8.86
s7915--KPNA1	4	-0.43	4.50
s24158--LEMD3	4	-0.26	-17.82
s12379--RTN1	3	-0.05	6.67
Control_siRNA	73	0.00	0.00
s25079--TOR1AIP1	4	0.28	5.26
s16808--BANF1	4	0.38	0.56
s23333--NUP210	4	0.40	3.67
s20635--IPO8	4	0.53	-4.25
s8646--MECP2	4	0.60	-10.00
s22251--NRM	4	0.83	13.78
s47157--TMEM201	4	1.06	-12.57

siRNAID-Gene Symbol	n. of Replicates	DEVIATION from Control siRNA	
		NE Increase (fold change)	ER Intensity PreWO
s26212--TOR1B	3	1.50	-17.55
s15455--REEP5	3	1.68	-1.53
s25667--AKAP8L	4	1.88	1.59
s8644--MECP2	4	2.15	-8.42
s27652--IPO11	4	2.29	7.74
s23329--SYNE2	4	2.33	-10.89
s7920--KPNA2	4	3.10	1.77
s23966--NUP188	4	3.39	-4.74
s15456--REEP5	3	3.97	-9.20
s27654--IPO11	4	4.12	-11.02
s9780--NUP88	3	5.45	-21.82
s8224--LMNB1	3	5.52	-17.26
s41035--REEP6	3	5.92	-8.53
s14354--TPR	3	6.13	-18.76
s23328--SYNE2	4	6.29	-5.44
s8226--LMNB1	4	6.50	7.76
s4647--EMD	4	6.53	-8.55
s21879--NUPL2	3	7.05	9.62
s16107--RAE1	3	8.08	-11.00
s223979--KPNA1	4	9.02	4.54
s11774--RANBP2	3	9.16	4.77
sPOM121--POM121	4	9.70	-28.50
s24247--NUP62	4	9.83	-16.00
s18514--NUP155	4	9.88	16.33
s21878--NUPL2	3	11.04	7.22
s26228--TOR2A	3	11.89	5.90
s48826--SUN3	4	12.09	29.01
s12378--RTN1	3	12.50	20.32
s6415--H2AFZ	4	13.93	0.92
s7933--TNPO1	3	16.13	0.47
s4402--TOR1A	4	16.54	7.54
s41034--REEP6	3	16.70	-5.56
s35705--TMEM43	4	20.41	-1.57
s20638--IPO7	4	22.59	35.76
s10167--PCYT1A	3	25.54	-6.20
s18873--BCLAF1	3	25.87	12.88
s16807--BANF1	4	26.49	-3.87
s46437--C19orf46	4	26.78	-12.64
s223838--TNPO2	4	32.38	7.45
s34577--TOR3A	3	38.75	14.11
s36155--IPO4	2	40.78	4.61
s37270--REEP4	1	42.29	-35.83
s23175--NUP205	3	44.19	-32.08
s18512--NUP155	4	49.28	-8.03
s10166--PCYT1A	3	51.85	11.00
s24465--SUN2	4	55.77	-2.70
s8221--LMNA	4	68.09	-29.61
s8222--LMNA	4	88.75	-10.60

3 Material and Methods

3.1 Materials

Instruments

Heating Block Eppendorf Thermomixer comfort
Magnetic stirrer Heidolph MR 3001
Thermo cycler GeneAmp PCR System 9700 Applied Biosystems
Centrifuges Eppendorf Centrifuge 5417R
Heraeus Megafuge 1.0 R
Heraeus Labofuge 400
MC 6 Centifuge, Sarstedt
Water baths GFL
Spectrophotometers NanoDrop 8000, ThermoScientific
Ultrospec 2100 Pro, Amersham Biosciences
Cell culture incubator Heraeus Hera cell
Laminar flow hood Safe 2020 ThermoScientific
UV lamps Benchtop UV Transilluminator, UVP
Vacuum Concentrators Speed-Vac Concentrator, Bachofer
miVac Quattro Concentrator, GeneVac, Ltd.
Pipettes P2, P10, P20, P200, P1000 Gilson Pipetman
Pipetus-Akku, Hirschmann
Midi Plus, BioHit
pH meter 240 pH/Temp meter, Beckman
Spin coater KL-SCV-10, Lot Oriel
Vacuum pump ME1, Vaccubrand
Shakers Rollodrum TC-7, New Brunswick Scientific
Sartorius Certomat RM
VersArray_ChipWriterProSystem ,Bio-Rad
Odyssey Scanner, LICOR

Microscopes

Leica SR GSD
Zeiss LSM780

Software

LAS AF v2.6.1.7314, Leica Microsystems
Zen up to v2012, Carl Zeiss Microscopy
Matlab up to vR2012b, The Mathworks
Python up to 3.3.2,
Image J up to v1.46h, NIH, USA
Adobe Illustrator CS3, Adobe
Clone Manager 9 Professional Edition, Sci-Ed Software

3.2 Molecular Biology

Agarose gel electrophoresis of nucleid acids

Gels for nucleid acid separation were made from 0,8% or 1,5% (w/v) agarose dissolved in TBE buffer with 0,3 µg/ml ethidium bromide (stock solution 10mg/ml from Invitrogen). Separation was performed at 120 Volt in 1x TBE

TBE: 89mM Tris, 89mM boric acid, 2mM EDTA

DNA loading buffer: 30% v/v glycerol and 0,1 % w/v bromophenole blue in TBE

DNA ladder: GeneRuler 1kb DNA ladder, (Thermo Fisher Scientific)

Gel extraction of DNA

Bands of DNA fragments were cut from agarose gels. The DNA was purified from the agarose gel using the NucleoSpin Gel and PCR Clean-up kit (Macherey-Nagel GmbH) according to the manufacturer's instructions. The DNA was eluted in 15 or 20 µL of water.purify using NucleoSpin Extract II (Macherey-Nagel).

DNA restriction digestion

Restriction enzymes are from NEB (Ipswisch, MA, USA). Restriction digestions of DNA were perfomed in 15 µl or 50 µl reaction volume in the buffer suggested by the provider of the restriction enzyme. When recommended 0.1mg/ml BSA was added for stabilization of the enzyme. 1-2 units of enzymes per 1µg was used and the reaction was carried out at recommended temperature for 1-2 hours. Restriction reactions were loaded on agarose gels.

Polymerase Chain Reaction

PCR was performed in 50µl reaction volume with 10-50 ng DNA. The concentration of each dNTPs was 0,2mM and 0,2mM of each primer was used in the reaction. Amplification was catalysed by 1 U of Phusion® High-Fidelity DNA Polymerase (NEB) in the provided buffer. 30 cycle were run with denaturating step at 94°C for

45s, anneling for 30-60s and elongation 1 min for 1000 nucleotides of products at 68°C. Every PCR round was preceded by 3 min at 94°C for complete denaturation and followed by 10 min at 68°C. The anneling temperature was chosen as the melting temperature of the primer with the lower melting temperature. The melting temperature of the primers is derived from the formula $T_m=4(G+C)+2(A+T)$, cycling was performed in a PT C-200 thermocycler (MJ research, Inc). PCR products were analysed on agarose gel and the purified from the gel by NucleoSpin Extract II (Macherey-Nagel, Germany)

Annealing of oligos and PCR with anneled oligo

Oligos were dissolved in TE buffer (10 mM Tris-HCl, pH 7,5, 1 mM EDTA pH8.0) to 0.5 OD_{260}. 1OD_{260} was then mixed with 7.5 µl of NEB restriction enzyme buffer 2 and the filled to 75µl of dd H_2O. The reaction was incubated on a heating block at 85°C for 5 minutes. Afterwards the block was switched off and the reaction was allowed to cool to room temperature. The annealed oligos were diluted in TE buffer (10mM Tris-HCl, 1mM EDTA, pH 8.0) to 1:500 and 2 µL were added to the ligation reaction.

Table 4.1 Oligonucleotides Oligonucleotides were synthesized by Sigma. Numbers refer to the internal filing number of the laboratory

Primer #	Sequence
758AB	ATGGATCCGATGCCGGAGTTCCTAG
759AB	ATACCGGTAAGTTGGATATTTTAGTATC
945AB	CGAAGAACAGAAGCTGATCTCAGAGGAGGACCTGTGCAG
946AB	GATCCTGCACAGGTCCTCCTCTGAGATCAGCTTCTGTTCTTCGAT
1073AB	AATGCTAGCATGACGGCCTACTCCCAACAG
1074AB	AATAAGCTTAGACCGCATAGTGGTTTCC
1170AB	AATGGATCCTTAGGCAAAGGAAAGGTGG
1171AB	AATACCGGTGGATCTTTCTGTTTAC
1076AB	AATGGATCCTCATGGACTTTTCTCGGC
1077AB	AATTCCGGACCCAACTGGATGGGCTCTC
1078AB	AATAGATCTCGGACGAGAAAATGGCGGC
1079AB	AATTCCGGAGCAAGCTGTGCCAATCGATC
1436AB	AATTAGATCTAGCATGACGGCCTACTCCCAACAG
1437AB	AATTTTTAAAATTACTTGTACAGCTCGTCCATGC
1455AB	AATTGGATCCAGATGGCGGGCGACG
1457AB	AATTCCCGGGTCTACCTCAGGAGTACTAAAGAAC

Ligation of DNA

Ligation reactions were made in a volume of 15-20 µl using a range of 50-75 ng of vector and a ratio of 1:3 or 1:5 vector to insert. T4 ligase (NEB) was used to catalyze the reaction in the buffer recommended by the provider for 2 h at RT or at 16C ON.

Coltivation of competent *E.Coli* cells

Two *E.Coli* strains were used: E.Coli XL1-blue, subcloning grade (Strategene) and 5-alpha High Efficiency (NEB). Both were growing in LB medium 1% (w/v) Bacto trypton, 1 % (w/v) NaCl, 0,5 % (w/v) yeast extract, pH 7.0 or in agar plats with LB-medium with 1.5 % (w/v) agar, 100µg/ml ampicillin or 30µg/ml kanamycin.

Transfomation of competent *E.coli* cells

Amplification of plasmid was performed in 5-alpha High Efficiency (NEB). 5 ng of plasmid DNA of 3 µl of ligation reaction was used for trasformation as follow: 30 min incubation of *E.Coli* cells with DNA in ice, heat shock for 30 sec at 42°C, 5 min incubation in ice. After addition of 200 µl of SOC medium the *E.Coli* cells were incubated for 2 h at 37 in shaking machine. *E.Coli* cells were plated either in ampicillin or kanaycin plated and growed ON at 37°C.

Plasmid purification

Small scale plasmid preparations were purified by a ON cultures in 4 ml of LB medium by using as decribed in the protocol and diluted in 20 µl of ddH$_2$0. Large plasmid preparations were purified from ON cultures in 50ml of LB. For large-scale preparation of DNA for mammalian cell transfection, 50 ml of LB broth supplemented with the appropriate antibiotics was inoculated with 10 µl of the small scale culture and grown overnight on an orbital shaker. The pellets were collected by 15 min centrifugation at 4000 rpm at 4°C. DNA was isolated using Nucleo Bond Kit (Macherey-Nagel) according to the manufacturer's instruction. The purified DNA was

suspended in water to 1 µg/ µl final concentration. The DNA concentration was estimated either by agarose gel electrophoresis or using the NanoDrop spectrophotometer.

Sequencing

Sanger sequencing of the DNA constructs was carried out using the Single Read Sequencing service of GATC Biotech AG or Value Read service of Eurofins MWG Operon. Whenever possible, the sequencing was done using standard primers provided by either of the companies. Otherwise the sequencing primers were ordered from Sigma.

Recombinant Plasmid

pNS3-cMPK-2longNS5A/B-LBR1TM-EGFP (#1261):
NS3 protease (without cofactor 4a) was amplified by PCR from pNS3/4Asc-mCherry (#768) with primer #1073AB and #1074AB. The product was inserted into pcMPK-2longNS5A/B-LBR1TM-EGFP (#883) digested NheI and HindIII.

pNS3-cMPK-longNS5A/B-LBR1TM-EGFP (#1275):
NS3 was removed from by PCR from pNS3-pcMPK-2longNS5A/B-LBR1TM-EGFP (#1261) and inserted into pcMPK-longNS5A/B-LBR1TM-EGFP (#770) digested NheI and HindIII.

pNS3-cMPK-longNS5A/B-LBR1TM-mEGFP (#1276):
Digest pNS3-pcMPK-longNS5A/B-LBR1TM-EGFP (#1275) with NheI and AgeI and inserted in pmEGFP-N1 (V#94)

pcMPK-2longNS5A/B-Δ60LBR1TM-EGFP (#1291):

Δ60LBR1TM was amplified with PCR from pcMPK-2longNS5A/B-LBR1TM-EGFP (#883) with primer #1170AB and #1171AB. The product was inserted with BamHI and AgeI into pcMPK-2longNS5A/B-LBR1TM-EGFP (#883)

pNS3-cMPK-longNS5A/B-Δ60LBR1TM-EGFP (#1292):

Δ60LBR1TM was removed after cutting with BamHI and AgeI from pcMPK-2longNS5A/B-Δ60LBR1TM-EGFP (#1291) and inserted into NS3-cMPK-longNS5A/B-LBR1TM-EGFP BamHI and AgeI (#1275).

pNS3-cMPK-longNS5A/B-LBR1TM-mEGFP/pcDNA5_FRT_TO (#1293):

NS3-cMPK-longNS5A/B-LBR1TM-mEGFP was amplified by PCR from (#1276) with primer #1436AB and #1437AB and the product digested with BglII and DraI. The digested product was inserted into pcDNA5_FRT_TO (V#261) digested with BamH1 and EcoRV.

pNS3-cMPK-longNS5A/B-Δ60LBR1TM-mEGFP/pcDNA5_FRT_TO (#1294):

Δ60LBR1TM was extracted by digesting pNS3-cMPK-longNS5A/B-Δ60LBR1TM-EGFP (#1292) with BamHI and AgeI. The digested product was inserted into pNS3-cMPK-longNS5A/B-LBR1TM-mEGFP/pcDNA5_FRT_TO (#1293) digested with BamHI and AgeI.

pNS3-cMPK-longNS5A/B-Sun1-mEGFP/pcDNA5_FRT_TO (#1295):

mmSun1 was amplified by PCR from pEGFP-mmSUN1 (#757) with primer #1076AB and #1077AB and the product digested with BamH1 and BspEI. The digested product was inserted into pNS3-cMPK-longNS5A/B-LBR1TM-mEGFP/pcDNA5_FRT_TO (#1293) digested with BamHI and AgeI.

pNS3-cMPK-longNS5A/B-hMan-mEGFP/pcDNA5_FRT_TO (#1296):

hMan1 (1-538) was amplified by PCR from pSVK-Flag-Man1 (#944) with primer #1078AB and #1079AB and the product digested with BglII and BspEI. The digested product was inserted into pNS3-cMPK-longNS5A/B-LBR1TM-mEGFP/pcDNA5_FRT_TO (#1293) digested with BamHI and AgeI.

pNS3-cMPK-longNS5A/B-Tor1AIP1-mEGFP/pcDNA5_FRT_TO (#1297):

Tor1AIP1 (1-538) was amplified by PCR from pTOR1AIP1-FLAP (#1003) with primer #1455AB and #1457AB and the product digested with BamHI and XmaI. The digested product was inserted into pNS3-cMPK-longNS5A/B-LBR1TM-mEGFP/pcDNA5_FRT_TO (#1293) digested with BamHI and AgeI.

pNS3-cMPK-longNS5A/B-Lap2b-mEGFP/pcDNA5_FRT_TO (#1298):

rLap2b was amplified by PCR from pEYFP-LAP2b (#24) with primer #758AB and #759AB and the product digested with BamHI and AgeI. The digested product was inserted into pNS3-cMPK-longNS5A/B-LBR1TM-mEGFP/pcDNA5_FRT_TO (#1293) digested with BamHI and AgeI.

pcMPK-longNS5A/B-MYC-LBR1TM-EGFP (#1299):

Myc tag generated by oligo anneling (#945AB, #946AB) and inserted into construct pcMPK-2longNS5A/B-LBR1TM-EGFP with BamHI and PvuI

Table 4.2: Expression plasmids. Internal data base numbers are given.

Gene	Plasmid Name	Plasmid #	Note
hH2B	pH2B-mCherry-IRES-Puro2b	#616	(unpublished, Made by Phil Rogers)
rLap2b	pEYFP-LAP2b	#24	(Beaudouin et al., 2002)
hMan	pSVK3-FLAG-MAN1	#944	(gift from Worman lab)
hTo1Aip1	pTOR1AIP1-FLAP	#1003	(unpublished, C. Chapuis)
hLBR	pCMPK-longHCVNS5AB-LBR1TM-EGFP	#770	(unpublished, E. Dultz)
hLBR	pCMPK-2longHCVNS5AB-LBR1TM-EGFP	#883	(unpublished, M. Isokane)
hLBR	pNS3-cMPK-2longNS5A/B-LBR1TM-EGFP	#1261	(unpublished, A. Boni)
hLBR	pNS3-cMPK-longNS5A/B-LBR1TM-EGFP	#1275	(unpublished, A. Boni)
hLBR	pNS3-cMPK-longNS5A/B-LBR1TM-mEGFP	#1276	(unpublished, A. Boni)
hLBR	pcMPK-2longNS5A/B-Δ60LBR1TM-EGFP	#1291	(unpublished, A. Boni)

hLBR	pNS3-cMPK-longNS5A/B-Δ60LBR1TM-EGFP	#1292	(unpublished, A. Boni)
hLBR	pNS3-cMPK-longNS5A/B-LBR1TM-mEGFP/pcDNA5_FRT_TO	#1293	(unpublished, A. Boni)
hLBR	pNS3-cMPK-longNS5A/B-Δ60LBR1TM-mEGFP/pcDNA5_FRT_TO	#1294	(unpublished, A. Boni)
hLBR	pcMPK-longNS5A/B-MYC-LBR1TM-EGFP	#1299	(unpublished, A. Boni)
mmSun1	pNS3-cMPK-longNS5A/B-Sun1-mEGFP/pcDNA5_FRT_TO	#1295	(unpublished, A. Boni)
hMan1	pNS3-cMPK-longNS5A/B-hMan-mEGFP/pcDNA5_FRT_TO	#1296	(unpublished, A. Boni)
hTor1AIP1	pNS3-cMPK-longNS5A/B-Tor1AIP1-mEGFP/pcDNA5_FRT_TO	#1297	(unpublished, A. Boni)
rLap2b	pNS3-cMPK-longNS5A/B-Lap2b-mEGFP/pcDNA5_FRT_TO	#1298	(unpublished, A. Boni)
NS3/4Asc	pNS3/4Asc-mCherry	#768	(unpublished, E. Dultz)
Flp	pOG44	#V75	Invitrogen
FRT	pcDNA5_FRT_TO	#V261	Invitrogen

3.3 Sample Preparation

Cell lines and cell culture

Hela R19 FlpIn TREx cells used in the screen were a generous gift of Gromeier lab, Duke University Medical Center, Durham, North Carolina USA. described in Kaiser et al., 2008. Cells were grown in complete DMEM cell culture medium prepared by mixing High-Glucose Dulbecco's Modified Eagle Medium (D-Glucose (+), L-Glutamine (+), Sodium Pyruvate (-) with 10% fetal bovine serum (FBS, PAA Laboratories, GmBH), 1mM Sodium Pyruvate, 1x MEM nonessential amino acids, 2mM L-Glutamine, and 100 U/ml Pen-Strep mix (all from Gibco Life Technologies). The medium was filtered through 0.22 μm Steritop filter (Millipore). The cells were grown on 10 cm BD Falcon tissue culture dishes (BD Biosciences) in 5% CO_2 in a

humidified Hera cell incubator. For passaging, the cells were washed with PBS (EMBL Media Kitchen) and incubated with 1x Tripsin-EDTA solution for 2-5 minutes. The cells were grown for up to 35 passages. All cell culture manipulation was performed under a laminar flow hood.

Transfection of plasmid DNA

Transfections of HeLa cells with plasmid DNA were carried out with different trasfection reagents: Lipofectamine 20000 (Invitrogen) and JetPRIME™ (Polyplus Transfection) following the protocol provided by the manufacturer. For co-transfections with several plasmid the DNA amount was divided among those. The transfection mixes were done in OPTIMEM for Lipofectamine or in the provided solution for JetPRIME. The mixes were replaced with fresh medium after 4h for JetPRIME or after 24h for Lipofectamine.

Generation of cell lines expressing Target-INM reporters

H2B-mCherry (#616) was transfected into Hela R19 FlpIn TREx with JetPrime (Polyplus-transfection) according to the protocol of the manufacturer. A clone stably expressing H2b-mCherry was isolated by selection with 0.5 μg/ml Puromycin (Calbiochem). Each Target-INM reporters (#1293, #1294, #1295, #1296, #1297, #1298) construct was transfected together with the pOG44-Flp recombinase (V#75). Cells were kept under selection with 10 μg/mL Blasticidin (InvivoGen) and 200 μg/mL HygromycinB (Invitrogen) till resistant clones were isolated.

Table 4.3: Mammalian cell lines. Internal data base numbers for plasmids and cell lines are given.

Gene	Plasmid Name	Cell type	Plasmid #	Cell Line #	Note
		Hela R19 FlpIn TREx		#720	(Kaiser et al., 2008)
H2B	pH2B-mCherry-IRES-Puro2b	Hela R19 FlpIn TREx	#616	#805	(unpublished, A. Boni)
H2B/hLBR	pNS3-cMPK-longNS5A/B-LBR1TM-mEGFP/pcDNA5_FRT_TO	Hela R19 FlpIn TREx	#1293	#811	(unpublished, A. Boni)

H2B/hLBR	pNS3-cMPK-longNS5A/B-Δ60LBR1TM-mEGFP/pcDNA5_FRT_TO	Hela R19 FlpIn TREx	#1294	#812	(unpublished, A. Boni)
H2B/mmSun1	pNS3-cMPK-longNS5A/B-Sun1-mEGFP/pcDNA5_FRT_TO	Hela R19 FlpIn TREx	#1295	#826	(unpublished, A. Boni)
H2B/hMan1	pNS3-cMPK-longNS5A/B-hMan-mEGFP/pcDNA5_FRT_TO	Hela R19 FlpIn TREx	#1296	#823	(unpublished, A. Boni)
H2B/hTor1AIP1	pNS3-cMPK-longNS5A/B-Tor1AIP1-mEGFP/pcDNA5_FRT_TO	Hela R19 FlpIn TREx	#1297	#825	(unpublished, A. Boni)
H2B/rLap2b	pNS3-cMPK-longNS5A/B-Lap2b-mEGFP/pcDNA5_FRT_TO	Hela R19 FlpIn TREx	#1298	#824	(unpublished, A. Boni)

Production of siRNA microarrays and coated 8-well LabTEK.

HeLa cells were transfected with siRNAs by solid-phase transfection on siRNA microarray. The siRNA microarrays were spotted in batches using the following protocol from Erfle et al., 2008. 3 μl OptiMEM containing 400 mM sucrose were mixed with 1.75 μl Lipofectamine 2000, 1.75 μl H2O and 5 μl 3 μM siRNA oligo followed by incubation for 20 min at RT. After incubation the mixture was supplemented with 7.25 μl of a sterile 0.2% (w/v) gelatine water solution. 16 μl of mixture was transfer in each well of a 384-wells plate. Microarrays were spotted using VersArray_ChipWriterProSystem (Bio-Rad). The microarrays were stored in sealed boxes with drying pearls for further use. The siRNA microarrays were spotted with the specific siRNA (see Table 4.1) and a scrambled siRNA XWneg9 used as a control siRNA

For a coated 8-well LabTEK after addition of gelatin the 16 μl of this coating solution were diluted and thoroughly mixed in 800 μl H2O resulting in 15 nM total siRNA concentration. 100 μl of this final coating mixture were transferred to a well of an 8-well Lab-Tek and the solution was evaporated for 45 min at 37° C using a SpeedVac Concentrator from Thermo Scientific (Wilmington, US). The siRNA coated 8-well Lab-Teks were either used directly or stored at RT in a sealed box containing dry pearls for up to one year.

Western blot on Hela cells extracts

Hela cells were rinsed three times in PBS and resuspended in ice-cold lysis buffer (50 mM Tris-HCl pH 7.5, 150 mM NaCl, 1% Triton X-100 and protease inhibitor cocktail (Roche) and incubated for 30 minutes at 4°C in a rotor. The lysates were centrifuged for 15 min at 14000 at 4°C. The resulting supernatants were used as total cell lysates and load in NuPAGE® precast gel (Invitrogen). Western blot was carried out according to the protocol for The Odyssey® Infrared Imaging System (LICOR). The following antibodies were used for Western Blotting: anti-GFP (mouse, clones 7.1/13.1, Roche); anti Rcc1 (rabbit, Mattaj Lab, EMBL, Heidelberg); anti Lem4 (rabbit, Mattaj Lab, EMBL, Heidelberg); anti-LMNA (ab26300 Abcam); anti-LMNB1 (ab16048 Abcam) Secondary antibodies: anti-mouse Alexa680 (Molecular Probes), anti-rabbit Alexa680 (Molecular probes), anti-mouse IRDye800CW (LI-COR) 1:10000, anti-rabbit IRDye800CW (LI-COR) 1:10000. Blots were scanned in an Odyssey fluorescence imaging system (LI-COR).

Dextrans Microinjection

Cells were grown overnight in a 2 well LabTEK. The day after, cells were liquid transfected with NUP93 siRNA and incubated for additional 48 hrs. Microinjection was performed under a Zeiss LSM 780 confocal microscope with a 63x PlanApochromat oil objective, NA 1.4 (Carl Zeiss) equipped with a microinjection system (Eppendorf). Cells were microinjected with a mix of 160kDa Dextran-TRIC (Sigma) and 70kDa Dextran-Cy5 (Molecular Probes) in water. After 10 min equilibration cells were imaged. Dextran intensities in the nuclear and cytoplasm were measured.

NPC staining with antibodies

Cells were grown for 48 hrs. in a siRNA 'ready-to-transfect' 8-well LabTEK. The cells were then rinsed twice with PBS and stained using one of the protocols described below. Washing consisted in a series of 3 5 minute incubations in PBS,
Cells were pre-fixed with 2% PFA, PBS for 20 seconds. This step helps to keep the cells attached to the cover slip in the subsequent extraction and washing steps. The

cells were then extracted with 0.2 % Triton X-100, PBS for 3 minutes, rinsed once with PBS and fixed with 2% PFA, for 15 minutes. Extraction of the cells with a detergent before fixation washes out the soluble cytoplasmic pool of nucleoporins and thus reduces background. Subsequently, the samples were washed three times with PBS and blocked with 5% NGS, PBS for 1 hour. The incubation with primary antibody mab414 1:2500 (Covance), diluted in 5% NGS, PBS, was carried out for 1 hour at RT or overnight at 4°C. Next, the samples were washed and incubated with the appropriate secondary antibody1:1000 anti-mouse Fab Alexa Fluor 647 (Invitrogen) for 1 hour at RT. This was followed by a final round of washing.

Immunofluorescence on Triton-X100/Digitonin permeabilized cells

Cells were grown in a 8-well LabTEK For IF Cells were washed three times with transport buffer (TB) (20 mM HEPES pH 7.3, 110 mM potassium acetate, 5 mM sodium acetate, 2 mMmagnesium acetate, 1 mM EDTA). For digitonin permeabilization cells were incubated with TB containing 33µg/ml digitonin for 5min on ice, washed three times in TB and then fixed in 2% PFA in TB for 10min at RT; for Triton-X100 permeabilitation cells were incubated for 5 min at RT with 0.2% Triton X-100, washed three times and then fixed in 2% PFA in TB for 10min at RT. After fixation the cells were washed again three time in TB and blocked with 2% BSA ON at 4°C. Primary and secondary antibodies were diluted in BSA and used for 1h incubation at RT (dilution indicated below). Between the two incubations the cells were washed three times with TB 5 min

3.4 Imaging

Confocal microscopy

For the screening assay, the Target-INM-LBR cell line was seeded on the siRNA microarray; 24 hours later the expression of the reporter was induced with 1 µg/mL Doxycycline (Sigma) in presence of 2 µM BILN2061 NS3 protease inhibitor (Boehringer Ingelheim). After additionally 24 hours we washed out the protease

inhibitor and started live cell confocal time-lapse imaging time-lapse microscopy. Each siRNA microarray was acquired with the ZEN 2010 Software on a Zeiss LSM 780 confocal microscope with a 63x PlanApochromat oil objective, NA 1.4 (Carl Zeiss). Each siRNA spot was imaged every 9 minutes before inhibitor wash out (two time points) and up to a 2.5 hrs after wash out. For total cell fluorescence imaging ZEN 2010 Software on a Zeiss LSM 780 confocal microscope with a 20x PlanApochromat dry objective, NA 0.8 (Carl Zeiss) was used; each position was imaged every 15min. All live-cell imaging was performed at 37°C using CO_2-independent medium without phenol red (Invitrogen) containing 20% fetal bovine serum, 2 mM l-glutamine, and 100 mg/ml penicillin and streptomycin.

Super-resolution microscopy

Super-resolution imagin was performed on a Leica SR GSD microscope, equipped with Leica HCX PL APO 100x, NA 1.47 Oil CORR TIRF PIFOC objective. The image was acquired on an Andor iXon3 897 EMCCD camera. The lateral drift was minimized by the Suppressed Motion (SuMo) stage. The system was equilibrated for about 2 hours after switching on. Imaging was performed in epifluorescence mode. In order to bring the fluorophores into dark states, the sample was first illuminated with the excitation light at the maximum laser power, until single fluorophore blinking behavior was observed. For AF 647 this typically required less than 30 s. Next, a long series was acquired at intermediate laser power, at a rate of 100 frames per second. Typically up to 50,000 frames were acquired for images of NPCs.

3.5 Image analysis

Image analysis

H2B-mCherry signal was used to monitor cell cycle stage of single cells. For this purpose nuclei were detected in the H2B-mCherry channel and classified with CellCognition (Held et al., 2010; Walter et al., 2010) in two morphological classes: Interphase and Mitotic. Cells were tracked with a constrained nearest-neighbor

tracking procedure, and cell trajectories that persist in interphase for the duration of the time-lapse were extracted. To reduce the effect of classification errors classification results were corrected with Hidden Markov Models (Held et al., 2010; Walter et al., 2010). Target-INM reporter fluorescence intensity along each single cell trajectory was quantified in the ER and NE with an in house developed routine implemented in MatLab. H2b-mCherry signal is used to trace the border of the nucleus and along which the NE is unfolded. The NE is divided in multiple segments with a fixed step length extending from the nucleus into the cytoplasm. Average intensity of the Target-INM reporter is then calculated along each segment length (Figure 4.1 1-2). The first derivative of segment average intensity in the direction from nucleus to cytoplasm is then computed; the derivative maxima (d_{max}) defines the nucleus to cytoplasm transition where the NE is positioned (Figure 4.1 2). Segments with d_{max} below a fixed intensity threshold are removed from the analysis. For the remaining segments the position of d_{max} (Y_{max}) is used as coordinate for deriving the following parameters:

- NE_{max} = highest intensity pixel in region $[Y_{max}, Y_{max} + 4]$ (Figure 4.1 4)
- NE_{mean} = mean intensity in region $[Y_{max}, Y_{max} + 4]$ (Figure 4.1 4)
- $Nucleus_{mean}$ = mean intensity of pixels in $[Y_{max} - 6, Y_{max} -2]$

The ratio between $Nucleus_{mean}$ / NE_{mean} of a segment must be below 0.6 otherwise the segment is removed from the analysis. The NE intensity is computed by averaging NE_{max} of all remaining segments. For calculating the ER intensity I accept as valid all the segments; I then compute a moving average of pixels with window size equals to 1/4 of the total segments and with step size equals to one segment in the region $[Y_{max} + 8, Y_{max} + 25]$. Among all the computed averages the highest one was selected as single value for the ER (Figure 4.1 5).
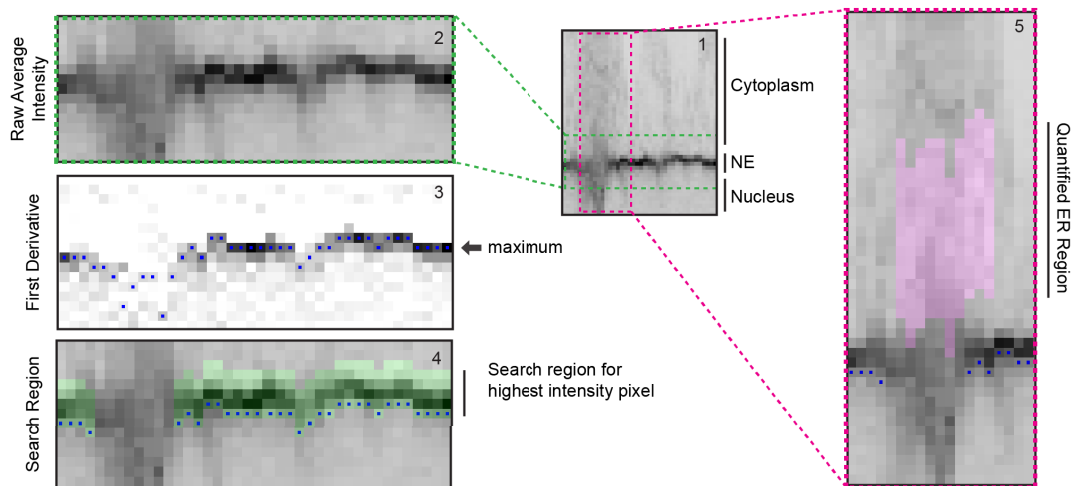
Figure 4.1 (1) Raw average intensity along the nuclear surface as calculated in Figure 2.7 C In (2) a zoomed region of the raw average profile is shown. The first derivative of the raw average intensity (2) is calculated and shown in (3) (negative values are left white). The blue dots represent the first derivate maxima. (4) The computed derivate maxima is used as positional information for the search region (highlighted in green) for the brightest pixel of the NE. The search region does not include NE regions that do not fulfill the selection criteria. In (5) a zoomed inset of the ER shows the region where the ER intensity was measured (magenta region).

For the total Target-INM fluorescence measurements I use the H2b-mCherry signal and CellCognition to automatically select and track nuclei that persist in interphase for the 2.5 h of the imaging after wash out. The ER is detected by thresholding the Target-INM GFP signal and single cells are separated by marker based watershed segmentation, using the nuclei as markers. For this I used an in house written scripts in FIJI (Schindelin et al. 2012) and MatLab. The GFP intensity for each cell is then averaged in space at every time point and the ratio computed with respect to the first pre-washout time point.

Segmentation of NE and ER region

A fully automated 3D computational pipeline has been implemented in Matlab to segment nucleus and ER region from H2B-mCherry and Target-INM-LBR channels, respectively. Fluorescent signal from confocal microscopes undergoes intensity decay with the increase of distance from the cover slip surface. The loss of intensity is

modelled as an exponential function of distance from the surface (Kervrann et al., 2004). This function is used to compute a correction factor in order to compensate the intensity decay in different slices. Intensity corrected anisotropic stacks are interpolated to have an isotropic resolution that provides greater flexibility in 3D image analysis. 3D Gaussian filter is applied on the interpolated stacks to reduce the effects of noise. To segment the nucleus a global threshold is determined by analyzing the histogram constructed from all the pixels within the stack. This threshold is adapted to each of the slices by combining a second threshold (local) determined from individual slices (Hériché et al., 2014). By combining local and global thresholds within a stack it avoids over-segmentation and under-segmentation significantly. ER regions are also segmented by combining two thresholds in the same way. To separate ER region of individual cells a marker based watershed algorithm has been applied. In this process segmented nuclei are used as markers where the watershed method is applied on the distance transformed image of the segmented ER region. The NE membrane region is detected from the segmented nucleus volume with a fixed width. Integrated intensity of Target-INM-LBR in the ER and NE regions are computed.
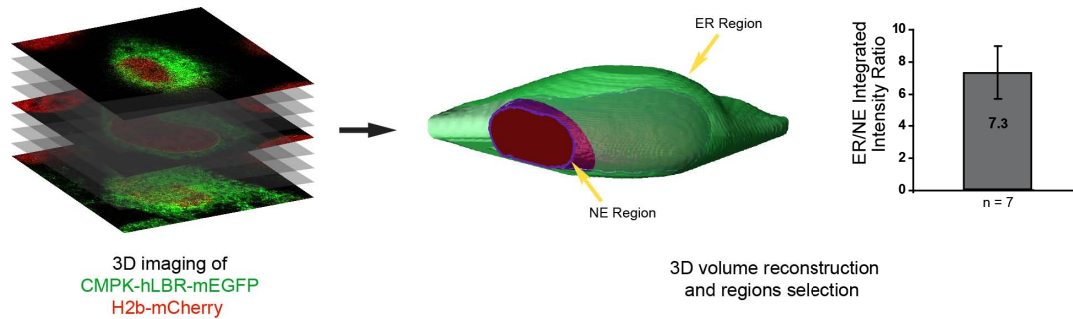
Figure 4.2 3D imaging of CMPK-hLBR-mEGFP and H2B-mCherry transfected cells. Representation of segmented ER (green), chromatin (red) and NE region (blue). Plot shows ER and NE integrated intensity ratio.

NPC counting in super-resolution imaging

Single molecules in the super-resolved movies were localized with a centroid fit of the Leica SR GSD Wizard. The lists of localization events were then saved in a binary format and imported into Matlab. For correction of lateral drift a MatLab routine developed previously in our lab. Lateral drift in the images was corrected using the correlation method (described in Szymborska et al., 2013). The pixel size in super-resolved images has be chosen to be 10 nm pixel. NPC counting was done using an in house custom written MatLab routine. Briefly super-resolved (SR) images were median filtered and single NPC clusters were detected. A peak detection algorithm was applied on the SR raw images and the number of peaks inside each NPC cluster was counted. To define a NPC as fully assembled a minimum number of three peaks were required. NPC clusters that fulfill this requirement were counted and an average NPC density was computed.

Data analysis

For each siRNA microarray NE and ER intensities data of single cell trajectory data were analyzed using an in house written Python pipeline. A fixed intensity threshold was applied to remove low reporter expressing cells. For each remaining cell raw NE and ER intensity values were normalized to the average of the two pre-wash out intensity values. The *NE increase (fold change)* was defined as the average of the three highest normalized values after wash out. An average *NE increase (fold change)* is derived for Control siRNA and gene siRNA by combining respectively cells from six Control siRNA and two siRNA spots. Deviation of each siRNA from the Control siRNA *NE increase (fold change)* was computed and tested for statistical significance with Student´s *t* test (p < 0.01). For making value comparable between replicates, a percentage *NE increase (fold change)* deviation from Control siRNA was calculated and a combined average deviation for the siRNA replicates derived.

ER Intensity PreWO is the average of ER intensity before wash-out. An average *ER Intensity PreWO* is derived for Control siRNA and gene siRNA by combining respectively cells from six Control siRNA and two siRNA spots. Deviation of each siRNA from the Control siRNA *ER Intensity PreWO* was computed. For making value comparable between replicates, a percentage *ER Intensity PreWO* deviation

from Control siRNA was calculated and a combined average deviation for the siRNA replicates derived.

3.6 Mathematical modelling

Mathematical description

The diffusion of the reporter in the ER is fast compared to the translocation time, for instance the reporter requires 5-15 sec to diffuse to the NE ($t_{1/2}$ FRAP = 20 sec Figure 2.4 , D = 0.03-0.1 µm^2/sec, Zuleger et al. 2011) whereas protein cleavage and translocation time are in the order of 10 of minutes. Accordingly, during translocation gradients of the reporter radially away from the nucleus was not observed. Therefore, in the ER and INM fast diffusion and homogeneous distribution of the reporter was assumeed. Translocation occurs through nuclear pores evenly distributed on the NE, therefore the reporter density in the INM can also be considered to be spatially homogeneous. Finally fast binding of the reporter to nuclear proteins was assumed and that in this bound state the reporter can't translocate through the pore. Under these assumption effective transport rates that are proportional to the number of pores N, permeabilities for import and export (P_i and P_o, respectively), and the degree of binding to nuclear proteins

$$k_i = NP_i \qquad\qquad \text{(Eq. 1)}$$

$$k_o = NP_o/\beta \qquad\qquad \text{(Eq. 2)}$$

The parameter β = 1+Kb L, where Kb is the binding constant to nuclear proteins and L their concentration, quantifies the binding of the reporter to INM proteins and increases with increased retention. For a pure diffusive transport P_i = P_o = P. In this case, in order to vary the number of pores and/or permeability compared to the control data set k_i and k_o were changed and the ratio left equal to the ratio obtained for control. The total density was defined for full length and cleaved protein in ER and ONM, computed with respect to the ER area, by $F = F_{ER} + F_{ONM}/\alpha$ and $C = C_{ER} + C_{ONM}/\alpha$, respectively. The subscripts indicate the localization of the reporter. The parameter

$\alpha = A_{ER}/A_{INM}$ gives the area ratio of the membranes. The system of ordinary differential equations (o.d.e.) reads

$$\frac{dF}{dt} = v_t \frac{(\alpha+1)}{\alpha} - \left(k_c + d_F + \frac{\lambda k_i}{1+\alpha}\right) F + \frac{\lambda k_o}{\alpha} F_{INM} \qquad \text{(Eq. 3)}$$

$$\frac{dC}{dt} = k_c F - \left(d_C + \frac{k_i}{1+\alpha}\right) C + \frac{k_o}{\alpha} C_{INM} \qquad \text{(Eq. 4)}$$

$$\frac{dC_{INM}}{dt} = k_c F_{INM} + \frac{\alpha k_i}{1+\alpha} C - (d_C + k_o) C_{INM} \qquad \text{(Eq. 5)}$$

$$\frac{dF_{INM}}{dt} = \frac{\alpha \lambda k_i}{1+\alpha} F - (d_F + k_c + \lambda k_o) F_{INM} \qquad \text{(Eq. 6)}$$

The parameter $1-\lambda$ characterizes the size selectivity barrier of the pore, a value of 0 indicates that the full-length protein can equally translocate through the pore as the smaller cleaved protein. The experimentally observables quantities in the ER and nuclear envelope (NE) are a linear combination of these variables

$$ER = (F + C) \frac{\alpha}{1+\alpha} \qquad \text{(Eq. 7)}$$

$$NE = (F + C) \frac{\alpha}{1+\alpha} + C_{IN} + F_{IN} \qquad \text{(Eq. 8)}$$

These quantities, normalized to their initial steady-state values (at $t = 0$), are used to fit experimental data. The total reporter density, computed with respect to ER area is given by

$$\frac{dF_{tot}}{dt} = v_t \frac{(\alpha+1)}{\alpha} - (k_c + d_F) F_{tot} \qquad \text{(Eq. 9)}$$

$$\frac{dC_{tot}}{dt} = k_c F_{tot} - d_C C_{tot} \qquad \text{(Eq. 10)}$$

The system of o.d.e.'s is solved analytically for $k_c = 0$, t < 20 min and $k_c = 2.05$ h^{-1} for t ≥ 20 min.

Derivation of the mathematical model

The model given by Eqs. 3-6 is a simplified version of a more detailed model that includes the three compartments (the ER, the ONM and the INM). The model considers the surface density of uncleaved/cleaved reporter in the different compartments and the reversible binding of the reporter to inner nuclear proteins, e.g. lamin B. The equations describing the time changes of the uncleaved reporter read

$$\frac{dF_{ER}}{dt} = v_t - (k_c + d_F)F_{ER} + k_t(F_{ONM} - F_{ER}) \qquad \text{(Eq. 11)}$$

$$\frac{dF_{ONM}}{dt} = v_t - (k_c + d_F)F_{ONM} - k_t\alpha(F_{ONM} - F_{ER}) \qquad \text{(Eq. 12)}$$
$$+\lambda\,(\kappa_o\,f_{INM} - k_i\,F_{ONM})$$

$$\frac{df_{INM}}{dt} = -(k_c + d_F)f_{INM} - \lambda\,(\kappa_o\,f_{INM} - k_i\,F_{ONM}) \qquad \text{(Eq. 13)}$$
$$-k_b f_{INM}L + k_u f_L$$

$$\frac{df_L}{dt} = k_b f_{INM}L - (k_u + d_F)f_L \qquad \text{(Eq. 14)}$$

The rate constant k_t describes diffusion between ER and ONM. f_{INM} and f_L are, respectively, the free and bound to nuclear proteins reporter density. Binding and unbinding of the reporter to proteins in the INM occur with rate constants k_b and k_u, respectively. Binding sites are assummed to be in excess compared to the reporter so that their concentration $L = const.$ Similarly for the cleaved reporter one obtains

$$\frac{dC_{ER}}{dt} = k_c F_{ER} - d_C C_{ER} + k_t(C_{ONM} - C_{ER}) \qquad \text{(Eq. 15)}$$

$$\frac{dC_{ONM}}{dt} = k_c F_{ONM} - d_C C_{ONM} - k_t\alpha(C_{ONM} - C_{ER}) + \qquad \text{(Eq. 16)}$$
$$\kappa_o\,c_{INM} - k_i\,C_{ONM}$$

$$\frac{dc_{INM}}{dt} = k_c f_{INM} - (\kappa_o + d_C)c_{INM} + k_i\,C_{ONM} - k_b c_{INM}L + k_u c_L \qquad \text{(Eq. 17)}$$

$$\frac{dc_L}{dt} = k_b c_{INM}L - (k_u + d_C)c_L \qquad \text{(Eq. 18)}$$

The rate constant κ_o is the export rate constant of the free protein. If the exchange between ER and ONM is fast compared to the translocation ($k_t \gg 1$), so that $F_{ONM} \approx F_{ER}$ and $C_{ONM} \approx C_{ER}$, the parameters C can defined derived as $C = C_{ER} + C_{ONM}/\alpha$ and $F = F_{ER} + F_{ONM}/\alpha$ and obtained

$$\frac{dF}{dt} = v_t \frac{(1+\alpha)}{\alpha} - \left(k_c + d_F + \frac{\lambda k_i}{\alpha+1}\right) F + \frac{\lambda \kappa_o}{\alpha} f_{INM} \qquad \text{(Eq. 19)}$$

$$\frac{dC}{dt} = k_c F - \left(d_C + \frac{k_i}{\alpha+1}\right) C + \frac{\kappa_o}{\alpha} c_{INM} \qquad \text{(Eq. 20)}$$

Finally, if the binding of the reporter to inner nuclear proteins is close to equilibrium, that is $c_L \approx \frac{k_b L}{k_u} c_{INM} = K_b c_{INM}$, and defining the total densities in the INM $C_{INM} = c_{INM} + c_L$ and $F_{INM} = f_{INM} + f_L$, model given in the main text is derived. The effective export rate constant is then given by $k_o = \frac{\kappa_o}{1+K_b} = \frac{\kappa_o}{\beta}$ and is reduced by the increased binding of the reporter in the INM.

Parameter estimation

For parameter estimation the mean squared distance was minimized as:

$$\chi^2 = \sum_i \left[\left(\frac{NE(t_i) - NE_{exp}(t_i)}{\sigma_{NE}(t_i)}\right)^2 + \left(\frac{ER(t_i) - ER_{exp}(t_i)}{\sigma_{ER}(t_i)}\right)^2 \right] + 25 \left(\frac{ER(0)/NE(0) - ER_{exp}(0)/NE_{exp}(0)}{\sigma_{ER/NE}(0)}\right)^2$$

(Eq. 21)

where the NE and ER values are normalized by their initial densities. The first three time points (pre-wash out and point just after wash out) are omitted from the distance measure. A value of 25 multiplying the initial ER/NE ratio was chosen in order to increase the weight of this measure so that it reflects the 14 time points used in the fit for NE and ER. To estimate the variance of the parameters bootstrapping was used and the fitting repeated for 100 resampled data sets. These sets are obtained from the original data sets by resampling with replacing and contain the same number of cells as the original data set.

To find a minimal set of parameters different from control reproducing the siRNA KD, 20 parameter combinations using crossvalidation were compared. Not fitted parameters are taken as the control values.

1. Using resampling without replacing two data sets each containing half of the cells were generated

2. In the crossvalidation step the 20 parameter combinations investigated here were fit to one half of the data and the predicted χ^2 for the other half was computed.

3. this procedure was repeated 100 times and pairs of parameter combinations compared with a Kolmogorov-Smirnov $p < 0.005$.

The smallest parameter combination was chosen if the statistical test is not significant. In case sets with equal number of parameters are not statistically different:

- If sets changing NP (leaving the ratio of k_i and k_o unchanged), k_i, or k_o, are not statistically different, sets changing NP was selected. The rationale is that, for a pure diffusive transport, a change in number of pores and/or permeability after knock down is more likely than an unidirectional change of one of the rates.

- If sets changing k_i or k_o are not statistically different the sets with the best mean predicted χ^2 was taken.

Estimating transport rates per NPC

The maximal transport rate through a single membrane pore of radius $R = 60$ nm and length $L = 40$ nm (Maimon et al. 2012) is derived from Fick's first law

$$f_{\max} = \frac{D\pi R \Delta C N_A}{L}(1 - r/R)^2$$

(Eq. 22)

Where D is the membrane diffusion of the reporter, r the hydrodynamic radius of the cytoplasmic moiety, and ΔC the concentration difference between INM and ONM. The last term describes steric hindrance of entry into the channel (Mohr et al. 2009). For the transport rate estimated from our kinetic model:

$$f_{\exp} = \frac{\alpha}{1+\alpha}\frac{k_i C A_{NM} N_A}{N} = \frac{\alpha}{1+\alpha}\frac{k_i C N_A}{\rho_{NPC}}$$

(Eq. 23)

Where ρ_{NPC} is the density of nuclear pores, here estimated to be ~ 9 NPC/μm^2. At washout the density in INM is ~ 0 therefore $\Delta C = C$. the ratio of these two rates which is independent of concentrations can be then computed

$$\frac{f_{\max}}{f_{\exp}} = \frac{1+\alpha}{\alpha}\frac{D R \pi \rho_{NPC}}{k_i L}(1 - r/R)^2$$

(Eq. 24).

To compare the absolute transport rates obtained here to previous reported rates for diffusible proteins at a standard cytoplasmic concentration of 1 μM the concentration needs to be converted to a surface density. In the cell line used in this study the area ratio of ER and nuclear membrane was estimated from fluorescent images

$\alpha = \dfrac{A_{ER}}{A_{NM}} = 7$, a nuclear membrane area of 1200 μm^2, and a cytoplasmic volume (including ER and organelles) of 4650 μm^3. This yields a surface area ER density of ~ 2 μm^2/μm^3. From this, it can be computed, assuming evenly distributed ER, that a 1 μM cytoplasmic concentration correspond to a ER surface density in the ER of 5*10^{-22} mol/μm^2.

Fitting of FRAP experiments

For FRAP experiments, in the limiting case were the entire nucleus is homogenously bleached, lateral diffusion can be neglected and a characteristic time for the fluorescence recovery can be computed

$$\tau = \dfrac{\int_0^\infty NE(\infty) - NE(t)\, dt}{NE(\infty) - NE(0)} = \dfrac{k_o + k_i + (\alpha + 1)d_C}{d_C((\alpha + 1)k_o + k_i + (1 + \alpha)d_C)} \qquad \text{(Eq. 25)}$$

Here $\lambda = 0$ was taken. The computed characteristic time overestimates the characteristic FRAP time after local bleaching; in this case lateral diffusion of fluorescent molecules from the side of the bleached area will speed up recovery. Nevertheless, Eq. 25 can be used to qualitatively estimate the effect of parameter changes on the recovery time. For instance, both import, export and degradation contribute to the residence time. As observed in experiment a decrease in k_o from our reference parameter set causes an increase in τ. Equation 25 has been used to compute the ratio of characteristic times for LMNA KD to Control siRNA.

Table 4.4 List of siRNAs sequences

Gene Symbol	siRNA ID	Sense siRNA Sequence	Antisense siRNA Sequence
XWNeg9	Custom	UACGACCGGUCUAUCGUAGtt	CUACGAUAGACCGGUCGUAtt
INCENP	s7424	AGUCCUUUAUUAAGCGCAAtt	UUGCGCUUAAUAAAGGACUtc
Nup35	Custom	UGCCCAGUUCUUACCUGGAtt	UCCAGGUAAGAACUGGGCAtt
Nup35	Custom	CCUCUUGUUGGAGUUACAUtt	AUGUAACUCCAACAAGAGGac
Nup188	s23966	GGAGCUGAUUCAUGCGAUAtt	UAUCGCAUGAAUCAGCUCCaa
Nup188	s23965	GGAAACCUCUUGAUGAACAtt	UGUUCAUCAAGAGGUUUCCgt
Pom121	s19144	GCCCAUCCAUCCUAUCUUUtt	AAAGAUAGGAUGGAUGGGCgt
Pom121	Custom	CAGUGGCAGUGGACAUUCAtt	UGAAUGUCCACUGCCACUGcu
Nup205	s23177	GGAACGAGAUGAUAUGAUUtt	AAUCAUAUCAUCUCGUUCCtc
Nup205	s23175	GGAGCAAGAUGGAUUGAUUtt	AAUCAAUCCAUCUUGCUCCtt
Nup93	s18654	GGAAUGAUACCAUACCGAAtt	UUCGGUAUGGUAUCAUUCCag
Nup93	s18655	CCGCUUCACAGGUAGUUAAtt	UUAACUACCUGUGAAGCGGca
Nup155	s18512	GGCAUCUACUUGUGAGUAAtt	UUACUCACAAGUAGAUGCCtc
Nup155	s18514	GGAUCCAACUUCAGAUACAtt	UGUAUCUGAAGUUGGAUCCta
Nup62	s24249	GGAGAGCCUGAUCAACAAAtt	UUUGUUGAUCAGGCUCUCCag
Nup62	s24247	GGGCUUCAGCUUAAAGGCAtt	UGCCUUUAAGCUGAAGCCCtg
Nup54	s28724	CGAUUCAGGGUGAACUAAAtt	UUUAGUUCACCCUGAAUCGta
Nup54	s28725	CUGCUGGUGUUGAUCCUAUtt	AUAGGAUCAACACCAGCAGga
NupL1	s18984	CAAGACCAGAGGAUAGUAAtt	UUACUAUCCUCUGGUCUUGtt
NupL1	s18985	GCCUUGGUGGUAUAGAUUUtt	AAAUCUAUACCACCAAGGCct
Nup210	s23331	CCGUGACGGUUUACUAUGAtt	UCAUAGUAAACCGUCACGGat
Nup210	s23333	GGUGCUUCUAGGUUACCCAtt	UGGGUAACCUAGAAGCACCtt
TMEM48	s31302	GGAUUAGCACUGCUAUGAAtt	UUCAUAGCAGUGCUAAUCCaa
TMEM48	s31303	GGAGGAUAGUUGCAAGUAUtt	AUACUUGCAACUAUCCUCCag
NUP133	s31401	CUGUAGAAGUCACUCAAUAtt	UAUUGAGUGACUUCUACAGta
NUP133	s31402	GCCUAUCUGUAUAACGAAAtt	UUUCGUUAUACAGAUAGGCag
NUP160	s23465	GGCAAGUUGUUCUCCGUAAtt	UUACGGAGAACAACUUGCCac
NUP160	s23466	GUUUCGAAAUUUACAACAAtt	UUGUUGUAAAUUUCGAAACtc
NUP107	s32727	GAUACGAGAGAGCAAUUUAtt	UAAAUUGCUCUCUCGUAUCta
NUP107	s32728	GUAGAUUGGUUAGAGAGUAtt	UACUCUCUAACCAAUCUACca
NUP85	s36610	GACGAAGAGUUGACUGGAAtt	UUCCAGUCAACUCUUCGUCaa
NUP85	s36612	CCAUUGAUCUGCACUACUAtt	UAGUAGUGCAGAUCAAUGGgt
NUP98	s9783	GGAUUGUUUGGAACCAGUUtt	AACUGGUUCCAAACAAUCCtc
NUP98	s9782	GGAGUUAGCACUAACAUAAtt	UUAUGUUAGUGCUAACUCCag
SEH1L	s37878	CGACCAAAGAUGUGAGAAtt	AUUCUCACAUCUUUGGUCGct
SEH1L	s37879	CAGAUGGUAUAGUAAGAAtt	AUUCUUACUAUACCAUCUGcg
SEC13	s12663	ACAGGUCCGUCAAAAUCUUtt	AAGAUUUUGACGGACCUGUct
SEC13	s12664	GGACACGACUCCUCAGUGAtt	UCACUGAGGAGUCGUGUCCcg
NUP37	s35439	GGUGGUCCACAAUUAGUGAtt	UCACUAAUUGUGGACCACCtg
NUP37	s35441	GGAUAUUACUCGGUCCAGUtt	ACUGGACCGAGUAAUAUCCca
NUP43	s51375	CAUCCAACCCAGAACAUCUtt	AGAUGUUCUGGGUUGGAUGgg
NUP43	s51377	GCAUUAGUAACCAAGCUAAtt	UUAGCUUGGUUACUAAUGCta
TPR	s14353	GAGUCUGCGUUAUCGACAAtt	UUGUCGAUAACGCAGACUCtc
TPR	s14354	GAAGUUCAUACUAAGCGUAtt	UACGCUUAGUAUGAACUUCct
NUP50	s21139	CUGUUUUACAAGAAAGACAtt	UGUCUUUCUUGUAAAACAGtt
NUP50	s21138	GAAGGACUGUCGAAUGGAAtt	UUCCAUUCGACAGUCCUUCca
NUP153	s19376	CAGUCUAAACUACGAAAUAtt	UAUUUCGUAGUUUAGACUGtc

107

NUP153	s19374	CGAAAAUCUCUCUACCGAUtt	AUCGGUAGAGAGAUUUUCGgt
NUP214	s224849	GGAUCACUGUCCCAACAGAtt	UCUGUUGGGACAGUGAUCCga
NUP214	s15548	GGUUCAGCUUUGGGUCAAAtt	UUUGACCCAAAGCUGAACCct
GLE1	s5808	CGAGGAUGUUUUAGAAGAAtt	UUCUUCUAAAACAUCCUCGcg
GLE1	s5809	CCAAGUAAAGGAUUCCAAAtt	UUUGGAAUCCUUUACUUGGta
NUPL2	s21878	AGGUAAUAAUAGACGUGGAtt	UCCACGUCUAUUAUUACCUga
NUPL2	s21879	GAGCUUCAACUAACAGGAAtt	UUCCUGUUAGUUGAAGCUCca
NUP88	s9779	CCACUAACGUGAUAAUACUtt	AGUAUUAUCACGUUAGUGGgt
NUP88	s9780	GGGCUAACUUGGAUUCAUAtt	UAUGAAUCCAAGUUAGCCCaa
RANBP2	s11773	CCGUUUUGGUGAGUCAACAtt	UGUUGACUCACCAAAACGGaa
RANBP2	s11774	CCUGUAGAUUUGUCAACUAtt	UAGUUGACAAAUCUACAGGtt
AAAS	s15607	GGUACAGGAUGGUAAACCAtt	UGGUUUACCAUCCUGUACCct
AAAS	s15608	GCUGUUCACUGUAUUGGGAtt	UCCCAAUACAGUGAACAGCag
RAE1	s16105	AACCAUCCAUUGGAUCAAAtt	UUUGAUCCAAUGGAUGGUUtt
RAE1	s16107	GUAACCAAGCGAUACAGAUtt	AUCUGUAUCGCUUGGUUACtg
KPNB1	s7917	CCAGCAAGUUUUAUGCGAAtt	UUCGCAUAAAACUUGCUGGtg
KPNB1	s7919	CAGUGUAGUUGUUCGAGAUtt	AUCUCGAACAACUACACUGgg
TNPO1	s7933	GCCGUUGCAUCAUGGAUUAtt	UAAUCCAUGAUGCAACGGCat
TNPO1	s7934	GCAACAAGAGAGUACAAGAtt	UCUUGUACUCUCUUGUUGCtg
IPO5	s7935	GCAUCUCAGCAGUAGGGAAtt	UUCCCUACUGCUGAGAUGCag
IPO5	s7936	CCUCAUUUGUCCACAUAGAtt	UCUAUGUGGACAAAUGAGGtt
IPO4	s36154	GCCCUGACCAGGUUAUAGAtt	UCUAUAACCUGGUCAGGGCtg
IPO4	s36155	GCAUUUCGCUGUACAAGUUtt	AACUUGUACAGCGAAAUGCtt
IPO9	s31300	GGAUCCUCUCUAUCAGAUUtt	AAUCUGAUAGAGAGGAUCCtt
IPO9	s31301	CAUUCUUGCUACAAGUAAAtt	UUUACUUGUAGCAAGAAUGtc
IPO7	s20640	GGAAUCUGCUUACAGGUCAtt	UGACCUGUAAGCAGAUUCCct
IPO7	s20638	GACUGACAAGAGAGGUUAAtt	UUAACCUCUCUUGUCAGUCtt
IPO8	s20636	GCUCGGCUCUUUGAACGAUtt	AUCGUUCAAAGAGCCGAGCta
IPO8	s20635	CAUUCAACAUUCACGAAAAtt	UUUUCGUGAAUGUUGAAUGga
IPO11	s27654	GGUCGAGUUCUACUACAAAtt	UUUGUAGUAGAACUCGACCca
IPO11	s27652	CCACAAAUGUUUCAACCGAtt	UCGGUUGAAACAUUUGUGGac
TNPO2	s223838	AGAACAACGUGAAGGCACAtt	UGUGCCUUCACGUUGUUCUtg
TNPO2	s26882	CGUGCAGGAUAAACUCAAAtt	UUUGAGUUUAUCCUGCACGat
TNPO3	s24030	GGGACUCAUUGCUAACCCAtt	UGGGUUAGCAAUGAGUCCCgt
TNPO3	s24031	CCUUACGAAUUGGAGCUAAtt	UUAGCUCCAAUUCGUAAGGaa
IPO13	s18608	GGAUCAUCCUGAUAUUGUUtt	AACAAUAUCAGGAUGAUCCct
IPO13	s18609	UCGCUUAUCUCACCCUAUAtt	UAUAGGGUGAGAUAAGCGAgt
KPNA1	s7915	GAGCAGUUAUUCAAGCGGAtt	UCCGCUUGAAUAACUGCUCtt
KPNA1	s223979	GCGGAGAAAUGUUGCUACAtt	UGUAGCAACAUUUCUCCGCtt
KPNA2	s7920	GCAGAAUAGAGGUCAAUGUtt	ACAUUGACCUCUAUUCUGCga
KPNA2	s7922	GAGACUUGGUUAUUAAGUAtt	UACUUAAUAACCAAGUCUCgg
KPNA3	s7923	CAAUAGCUGAAAUAAUAGAtt	UCUAUUAUUUCAGCUAUUGtg
KPNA3	s7924	GGCAUUAACUAACAUAGCAtt	UGCUAUGUUAGUUAAUGCCca
KPNA4	s7927	CGAUGGACUAAGUAAUAUAtt	UAUAUUACUUAGUCCAUCGag
KPNA4	s7928	CAUUGUUACUGGAACUGAUtt	AUCAGUUCCAGUAACAAUGtt
KPNA5	s7929	CAAUAGAUCAAGUUAUACAtt	UGUAUAACUUGAUCUAUUGgt
KPNA5	s7930	GCAGAGUUUCGUACCAGAAtt	UUCUGGUACGAAACUCUGCtt
KPNA6	s24241	GCAGAGUUUCGUACAAGGAtt	UCCUUGUACGAAACUCUGCtt
KPNA6	s24242	GACUGACGAUGACACGGAAtt	UUCCGUGUCAUCGUCAGUCgt
TMPO	s14233	GAAUGGAAGUAAUGAUUCUtt	AGAAUCAUUACUUCCAUUCtg
TMPO	s14235	CCAGGAAGCUAUAUGAGAAtt	UUCUCAUAUAGCUUCCUGGtt
TOR1AIP1	s25079	GAACAAGUCUAGGCCUAAAtt	UUUAGGCCUAGACUUGUUCca

TOR1AIP1	s25081	GAUGUAGCCUUAGUCCUGAtt	UCAGGACUAAGGCUACAUCtt
LEMD3	s24158	GGGACUGACUUACCUAGGAtt	UCCUAGGUAAGUCAGUCCCag
LEMD3	s24159	GAAGGUAUAUUUAACACUUtt	AAGUGUUAAAUAUACCUUCat
UNC84A	s23629	GUGUUGAACUGGGCAAGCAtt	UGCUUGCCCAGUUCAACACgg
UNC84A	s23630	CAAUCAGUGCGGUUGGGUGAtt	UCACCAACCGCACUGAUUGtt
SUN2	s24466	GGAAAUCCAGCAACAUGAAtt	UUCAUGUUGCUGGAUUUCCtc
SUN2	s24465	CAACAGCACUAUCUCCAGUtt	ACUGGAGAUAGUGCUGUUGgg
SUN3	s48826	GCUUGCUACAAAGAUCAUAtt	UAUGAUCUUUGUAGCAAGCtt
SUN3	s226034	CCACCGUUCAAACAUUUGAtt	UCAAAUGUUUGAACGGUGGtt
LBR	s224003	GUACCACUGUAAGAAGAAAtt	UUUCUUCUUACAGUGGUACtc
LBR	s8100	GAAAUAGCAUCAGCAGAUAtt	UAUCUGCUGAUGCUAUUUCca
EMD	s4647	GCUUUACUCUACCAGAGCAtt	UGCUCUGGUAGAGUAAAGCgt
EMD	s225840	GACCUGUCCUAUUAUCCUAtt	UAGGAUAAUAGGACAGGUCca
ANKLE2	s23124	CGUCAAAGCCGGAUUGAAAtt	UUUCAAUCCGGCUUUGACGat
ANKLE2	s23125	GGCUUUACUGGAGCAAGGAtt	UCCUUGCUCCAGUAAAGCCtg
TMEM43	s35704	GUGUUUCAUAGAGAACUAAtt	UUAGUUCUCUAUGAAACACct
TMEM43	s35705	CAUUCGCCGUGGAGACUUUtt	AAAGUCUCCACGGCGAAUGat
LEMD2	s48071	GCACUGACCUGGAUACUGAtt	UCAGUAUCCAGGUCAGUGCgg
LEMD2	s48070	AGCUGGUAAUUUUGAGUGUtt	ACACUCAAAAUUACCAGCUtg
TMEM201	s47157	GCUGUGGAGUACUACAUCAtt	UGAUGUAGUACUCCACAGCcg
TMEM201	s47158	CAGUACUUGGAGCACCUGAtt	UCAGGUGCUCCAAGUACUGgg
LMNA	s8222	GAAGGAGGGUGACCUGAUAtt	UAUCAGGUCACCCUCCUUCtt
LMNA	s8221	CCAAAAAGCGCAAACUGGAtt	UCCAGUUUGCGCUUUUUGGtg
LMNB1	s8226	GAGAUUAACGAGACCAGAAtt	UUCUGGUCUCGUUAAUCUCct
LMNB1	s8224	GGACUUGGAGUUUCGCAAAtt	UUUGCGAAACUCCAAGUCCtc
LMNB2	s39476	AGUCCUCGGUGAUGCGUGAtt	UCACGCAUCACCGAGGACUtc
LMNB2	s39477	GAACAACUCGGACAAGGAUtt	AUCCUUGUCCGAGUUGUUCtt
NRM	s22251	CGGGCCCAGCUACAAAGAAtt	UUCUUUGUAGCUGGGCCCGga
NRM	s22250	CCUUCUCGUCUUUGACUAUtt	AUAGUCAAAGACGAGAAGGat
SIGMAR1	s20088	CUAUACUCUUCGCUCCUAUtt	AUAGGAGCGAAGAGUAUAGaa
SIGMAR1	s20086	AGAGACCCAUGGGAACAAAtt	UUUGUUCCCAUGGGUCUCUgt
SYNE1	s23608	GCAUAGUACCGAAACCCAAtt	UUGGGUUUCGGUACUAUGCag
SYNE1	s23609	CGAUUCCUGUAACUCGGAAtt	UUCCGAGUUACAGGAAUCGta
SYNE2	s23328	GAAGAAAAGGUGCAUGUUAtt	UAACAUGCACCUUUUCUUCag
SYNE2	s23329	CAGCUGAACUCUGAUAUCAtt	UGAUAUCAGAGUUCAGCUGtt
C14orf49	s46245	AGAUCACCGGAGAACUGGAtt	UCCAGUUCUCCGGUGAUCUtc
C14orf49	s46246	AGCUCAUCGUCUUCCCUCAtt	UGAGGGAAGACGAUGAGCUcc
C19orf46	s46437	GCACGUCACCAAAGACACUtt	AGUGUCUUUGGUGACGUGCta
C19orf46	s46436	GGAAGCCUCAGGACAAGAAtt	UUCUUGUCCUGAGGCUUCCgg
TOR1AIP2	s46465	CGGUCAAGCUGUUGGUUGAtt	UCAACCAACAGCUUGACCGtg
TOR1AIP2	s46466	GUAUUGUGAUCAUGAGAAUtt	AUUCUCAUGAUCACAAUACtt
CBX5	s23883	GGAGCACAAUACUUGGGAAtt	UUCCCAAGUAUUGUGCUCCtc
CBX5	s23885	ACCUGGUUCUUGCAAAAGAtt	UCUUUUGCAAGAACCAGGUca
MECP2	s8644	GGAAGCUCCUUGUCAAGAUtt	AUCUUGACAAGGAGCUUCCca
MECP2	s8646	GCUUCCCGAUUAACUGAAAtt	UUUCAGUUAAUCGGGAAGCtt
BANF1	s16807	AGUUUCUGGUGCUAAAGAAtt	UUCUUUAGCACCAGAAACUgg
BANF1	s16808	AGAUUGCUAUUGUCGUACUtt	AGUACGACAAUAGCAAUCUtt
AKAP8L	s25667	GGAACACUUUAAGUACGUAtt	UACGUACUUAAAGUGUUCCtt
AKAP8L	s25668	CCAUGGAUCACAACCGGAAtt	UUCCGGUUGUGAUCCAUGGtc
TOR1A	s4404	GAGCAGAAAGGAUCACAGAtt	UCUGUGAUCCUUUCUGCUCca
TOR1A	s4402	CCACAUGCUUCAAACAUCAtt	UGAUGUUUGAAGCAUGUGGaa
ATP1B4	s23838	GGCAAACUGACUCACGUUAtt	UAACGUGAGUCAGUUUGCCgt

109

ATP1B4	s23839	CAGACUCGAUGAUCCGGAUtt	AUCCGGAUCAUCGAGUCUGta
RAB5A	s11680	GCAAGCAAGUCCUAACAUUtt	AAUGUUAGGACUUGCUUGCct
RAB5A	s11678	GGAAGAGGAGUAGACCUUAtt	UAAGGUCUACUCCUCUUCCtc
BCLAF1	s18873	UAUCGUCGCGAUUACAGAAtt	UUCUGUAAUCGCGACGAUAat
BCLAF1	s18874	CAUUGAUCGCCGUAGAAAAtt	UUUUCUACGGCGAUCAAUGtc
YTHDC1	s40756	GGAAUUUCAUAACAUGGGAtt	UCCCAUGUUAUGAAAUUCCct
YTHDC1	s40757	CAGUAAAGAUCGGACGUGAtt	UCACGUCCGAUCUUUACUGgt
H2AFZ	s6414	CCGUAUUCAUCGACACCUAtt	UAGGUGUCGAUGAAUACGGcc
H2AFZ	s6415	GACUUAAAGGUAAAGCGUAtt	UACGCUUUACCUUUAAGUCtt
SMAD2	s8397	GGCUGUAAUCUGAAGAUCUtt	AGAUCUUCAGAUUACAGCCtg
SMAD2	s8398	GGAGUGCGCUUAUACUACAtt	UGUAGUAUAAGCGCACUCCtc
SMAD3	s8401	AGGUCUGCGUGAAUCCCUAtt	UAGGGAUUCACGCAGACCUcg
SMAD3	s8402	GUCUACCAGUUGACCCGAAtt	UUCGGGUCAACUGGUAGACag
RTN1	s12378	GGACUUGUGAGGACUCACAtt	UGUGAGUCCUCACAAGUCCca
RTN1	s12379	GGACCUGGUGGAUUCCUUAtt	UAAGGAAUCCACCAGGUCCtg
RTN4	s32766	GCCUCUUCUUAGUUGAUGAtt	UCAUCAACUAAGAAGAGGCgc
RTN4	s32767	GUGUUGAUGUGGGUAUUUAtt	UAAAUACCCACAUCAACACtg
RTN3	s20161	GGUGCUGUUUUUAACGGAAtt	UUCCGUUAAAAACAGCACCaa
RTN3	s20162	ACUCAUUAUUCGUCUCUUUtt	AAAGAGACGAAUAAUGAGUtt
REEP1	s227344	CAGGGUGCCUUAUCGGAGAtt	UCUCCGAUAAGGCACCCUGtc
REEP1	s35169	CCAUUCUAUUAUGAACUAAtt	UUAGUUCAUAAUAGAAUGGaa
REEP2	s27911	ACAAGGCCGUGAAGACAAAtt	UUUGUCUUCACGGCCUUGUag
REEP2	s27913	CGCAAGUUCGUGCACCCAAtt	UUGGGUGCACGAACUUGCGgt
REEP3	s47938	GGUAAACUUUGGACGGCAAtt	UUGCCGUCCAAAGUUUACCat
REEP3	s47939	CAGUAUGCAUGAUUUAAACtt	UGUUAAAUCAUGCAUACUGaa
REEP4	s37270	CAAGAACAUUCGUGAAUAUtt	AUAUUCACGAAUGUUCUUGgt
REEP4	s37271	GGAUUGUUUUUGCACUCUUtt	AAGAGUGCAAAAACAAUCCag
REEP5	s15455	CGCUCUUGGUGUCAUCGGAtt	UCCGAUGACACCAAGAGCGat
REEP5	s15456	AGAGAGUCCCAACAAAGAAtt	UUCUUUGUUGGGACUCUCUat
REEP6	s41034	GCUGUGCAAUCUCAUCGGAtt	UCCGAUGAGAUUGCACAGCag
REEP6	s41035	CGCAUAUGCCUCAAUCAAAtt	UUUGAUUGAGGCAUAUGCGgg
PCYT1A	s10167	GAAUUGUGCGGGAUUAUGAtt	UCAUAAUCCCGCACAAUUCgg
PCYT1A	s10166	CCAUGAUGAUAUUCCUUAUtt	AUAAGGAAUAUCAUCAUGGgc
TOR2A	s26228	GAACCUCACUGAGCCUUGAtt	UCAAGGCUCAGUGAGGUUCtg
TOR2A	s26230	CGGGACCAAUUACCGCAAAtt	UUUGCGGUAAUUGGUCCCGta
TOR3A	s34576	GGGAAGAAAUUACGAUGGAtt	UCCAUCGUAAUUUCUUCCCgg
TOR3A	s34577	UCAAUGAGGUGGUCCUAAAtt	UUUAGGACCACCUCAUUGAtt
TOR4A	s195251	UCCAAGUUCUCAACGCUAUtt	AUAGCGUUGAGAACUUGGAag
TOR4A	s195252	GGGUGUGUGUCCUACGCAAtt	UUGCGUAGGACACACACCCgg
TOR1B	s26210	GGAACAACAAAAAUCCCAAtt	UUGGGAUUUUUGUUGUUCCtg
TOR1B	s26212	GGAUCAUUGACGCAAUCAAtt	UUGAUUGCGUCAAUGAUCCcg
KLHL14	s33323	CGACGAUGAAAAGAAGACAtt	UGUCUUCUUUUCAUCGUCGta
KLHL14	s33322	GCUAUAACCUAGAAACGAAtt	UUCGUUUCUAGGUUAUAGCac

4 DISCUSSION

Despite the essential functions of INMPs in interphase, the INM represents the probably least understood destination compartment of cellular membrane trafficking. Compared to the nuclear import of soluble proteins, the mechanism of INM protein targeting in interphase to the nucleus has been poorly investigated. Progress in the field is currently limited by the absence of a general assessment of the molecular requirements for INM protein targeting, which could help to differentiate between the existence of different targeting pathways or a single unifying targeting mechanism.

I discuss here the development of an INM protein targeting reporter based on the on the Lamin B Receptor (LBR) that allows to assay the kinetics of the transport process to the INM quantitatively in living cells. I used this assay in a siRNA screen combined with automated high-resolution confocal time-lapse microscopy to dissect the molecular requirements of LBR targeting.

4.1 Target-INM: a new reporter for inner nuclear membrane protein targeting

I successfully established a novel reporter for studying INM protein targeting during interphase named Target-INM. This reporter allows to control the localization of an INM protein in the ER or INM by chemically inducible proteolytic cleavage of a retention domain in cis. Moreover synchronous trafficking of a wave of protease released INM proteins from the ER to the INM can be triggered after acute protease activation in live cells allowing for the first time a direct observation of the translocation kinetics in a non-steady state situation in live cells.

Different systems have been employed previously to study INM protein targeting. An inducible reporter for INM protein targeting has been generated by Ohba et al., 2004. This reporter was based on the rapamycin-mediated interaction between the FK506-binding protein (FKBP) and the 11kDa FKBP rapamycin binding domain (FRB). FRB was fused at the N-terminus of the transmembrane domain of LAP2beta; retention to the INM upon addition of rapamycin was induced by a FKBP-lamin fusion protein. Compared to this reporter the Target-INM presents several advantages. First, after cleavage of the retention domain only a very short artificial peptide remains at the N-terminus of the INM protein instead of the 100 amino acid sized FRB domain. Second the INM protein binds its endogenous nuclear interaction partners and thus relies on the physiological binding affinities to regulate its mobility/retention at the INM. A

more systematic analysis of targeting different INMPs tagged with GFP has been carried out previously by photobleaching experiments in steady state (Zuleger et al., 2011). A region of the NE was bleached and fluorescence recovery due to protein movement from the ER to the INM was followed over time. However in this experiment both lateral diffusion within the INM as well as from the ER to the ONM movement contributes to the observed fluorescence recovery, making it difficult to dissect the actual targeting kinetics. Because the Target-INM reporter is prevented from entering the INM and a large pool of protein accumulates in the ER, acute release of a wave of Target-INM allows to differentiate the rate of ER-ONM diffusion from translocation and since there is minimal retrograde flow initially, directly observe the kinetics of trafficking from the ER to the INM.

To demonstrate the generic applicability of the Target-INM strategy I generated four additional reporters based on the INM proteins Lap2β, Tor1AIP1, Man1 and Sun1. All these proteins can be trapped in the ER and targeted to the INM upon induction of the protease. In the case of the Tor1AIP1 cells show slightly enriched fluorescence in the nuclear rim already before protease induction (Figure 2.5). It is worth notice that most of the INMPs can be targeted to the INM during post mitotic NE reassembly; although the CMPK retention domain prevents targeting of the LBR both during interphase and post-mitotic targeting this block of postmitotic targeting may be only partially true in the case of other INMPs. The ability of the CMPK domain to abolish post-mitotic targeting of LBR is believed to occur by sterically preventing binding of the LBR N-terminus domain to its chromatin substrates during nuclear envelope reformation. The differences in the structural organization of nucleoplasmic domains of the other INM proteins as well as in the strength of their interactions to nuclear substrates may explain the subtle differences in the efficiency of the same cytoplasmic retention domain.

4.2 A quantitative assay to study kinetics of INM protein targeting

The Target-INM can be used to analyze the *kinetics* of targeting of different INMPs. I therefore established an assay in which INM targeting of the LBR based reported can be followed by confocal microscopy after acute activation of the protease. Quantification of NE and ER intensities changes over time reveals the kinetics of LBR targeting to the INM.

However the observed increase in NE intensity over time is the result of several distinct processes: the trafficking of the reporter to the INM, the cleavage kinetics of the protease, synthesis and degradation of the reporter. To account for the different rates of these processes and determine the rate of INM trafficking a mathematical model was developed and applied to the observed targeting kinetics.

Ideally the time required for the protease cleavage should be as short as possible and should not be a rate-limiting step in the targeting process. Cleavage of the retention domain starts immediately after protease activation but requires around 20-25 min for completion; comparison of protease cleavage by WB and kinetics of reporter targeting shows that cleavage of the retention domain by the protease is likely to partially limit reporter accumulation to the INM. Although the employed NS3 protease shows a fast kinetics at the NS5a/b cleavage site *in vitro* (6.2 -8.0 k_{cat} (min^{-1}) (Zhang et al., 1997), we observed a slower protease cleavage *in vivo.* In the future, it would be interesting to test a recently developed light-activatible NS3 protease (Zhou et al., 2012) which would abolish the necessity to complete the wash out of the reversible chemical inhibitor from the cells prior to the onset of cleavage.

Quantification of reporter accumulation at the INM shows that it reaches a transient peak around 40 min after induction of the protease followed by a slow decrease of NE intensity. In agreement with this observation the mathematical model predicts a reduced stability of the reporter after cleavage resulting in a 3-fold reduction in lifetime of the protein. It has previously reported that cleavage of NS3 protease on the NS5a\b cleavage site in an artificial construct can lead to increased degradation of the cleavage product (Sabariegos et al., 2009). Moreover a Target-INM reporter carrying an NS5a\b site in which critical amino acids for cleavage have been mutated showed no visible degradation after protease induction (data not shown) indicating that

protease activation does not generally affect protein stability in the cell.

On the approximately one hour time frame of reporter translocation, continuous synthesis of new full length reporter protein also has to be taken into account by the model, since whole cell reporter levels were reduced by around 50% when new protein synthesis was abolished by Cycloheximide (CHX) treatment.

Since both protease cleavage kinetics and degradation after cleavage may depend on sequence context of the cleavage site the reporter therefore requires careful control measurements of the non-trafficking related rates for the different Target-INM reporters, before it can be applied to compare different INM proteins. It is furthermore essential to use the developed mathematical model to derive import (k_i) and export rates (k_o) of the cleaved reporter across the NPC from the observed kinetics of NE intensity increase.

4.3 INM protein targeting is a slow process

By combining the experimental and the mathematical model approaches I could for the first time directly determine the exchange rate of INM protein targeting. Transport from the ER to the INM has a characteristic time of 4-5 min whereas export from the INM to the ER is slower due to binding at the INM with a characteristic time of 19-25 min for export. These values indicated that efficient LBR targeting relies on an only fivefold difference in exchange rates. These rates are in the same order of the ones computed in previous indirect estimates by FRAP (Zuleger et al. 2011).

The transport rate estimated from our kinetic model is 500 times slower than the one predicted for a membrane proteins moving by free diffusion through a membrane pore of the size of the NPC (for details see Material and Methods, Estimating transport rates per NPC). This indicates that passage across the NPC encounters a barrier to free diffusion and could be a limiting step in efficient delivery of LBR to the INM. In addition I could estimate absolute transport rate of 4.6 molecules/NPC/min for an effective reporter concentration of 1μM. Compared to the translocation rate obtained for a soluble freely diffusible GFP at 1μM, the absolute transport rate for the LBR reporter is 30 times slower. This is consistent with a 20-100 times faster diffusion of soluble GFP compared to integral membrane proteins (Ribbeck and Goerlich 2001,

Mohr et al. 2009) and indicates that membrane proteins encounter a similar impediment to free diffusion at the NPC.

In recent years single molecule tracking techniques allowed the directed visualization of individual molecules of both soluble cargo and mRNA during their motion across the NPC. This allowed a better characterization of the kinetics of nuclear import of soluble molecule in its different transport steps at the NPC (i.e. docking, passage and release of the cargo) (for review Tu and Musser, 2011). *In vivo* single molecule tracking employs photoactivatable or photoswitchable proteins that can switch between an ON and OFF states. The rate of switching is controlled in order to have in a limited volume only a single molecule in the ON state that can be tracked. To date a similar approach has not yet been undertaken for targeting of INM proteins. One prerequisite for single molecule tracking is the possibility to collect thousands of single events in order to obtain a robust statistic. The Target-INM reporter offers the advantage to induce a large number of transport events in a controlled time fashion. In future work it would be interesting to explore the possibility to use the Target-INM reporter tagged with photoactivatable or photoswitchable proteins to detect single molecule transport of an INM protein.

4.4 The first siRNA screen for INM protein trafficking

siRNA screens in mammalian cells have made important contributions to define the molecular machinery of different membrane trafficking pathways (e.g. Collinet at al., 2010, Simpson et al., 2012). To date no general assessment of the molecular requirements for INM protein targeting has been carried out, which should help to differentiate between the two prominent models of transport: the diffusion retention and the receptor mediated transport model. In the present work I applied for the first time a siRNA approach to study INM protein targeting taking advantage of the novel Target-INM reporter. I have used the reporter based on the LBR exhibiting both a (i) functional domains that bind to B type lamins and chromatin, consistent with a diffusion retention model, and (ii) three NLS, consistent with receptor mediated translocation. The possibility to acutely release the Target-INM reporter allowed me to study ER to INM exchange kinetics directly. I systematically knocked down 96 candidate genes and recorded the resulting kinetics of LBR targeting after gene

depletion. By applying the mathematical model to the observed kinetics I could reveal which proteins are required for normal targeting, what aspects of the LBR targeting process they affect and derive general insights on the mechanisms that normally govern targeting of an INM protein with mixed signals.

4.5 INM protein targeting is dependent on the number of NPCs

The predominant protein family that scored in the siRNA screen were nucleoporins, in particular the Nup107-160 complex. The mathematical model predicted that the mechanism underlying their depletion phenotype was a reduction of the number of NPCs. This is consistent with their previously demonstrated function in NPC assembly (e.g. NUP107, Nup98; Walther et al. 2003; Krull et al., 2004) and in two cases (SEC13 and NUP98) I could experimentally validate that the reduction of NPCs quantitatively explains the observed kinetic effect. Thus the targeting of INM proteins depends surprisingly sensitively on the number of available NPCs. NPC density in the HeLa cell line used in the current work was 9 NPCs/μm^2; It would be interesting to assess the targeting kinetic using the Target-INM in cell lines that have been reported to have a lower density of NPCs (e.g. normal rat kidney NRK ~6–7 NPCs/μm^2 as reported in Dultz et al., 2010).

For most of the nucleoporins phenotypes the model predicts a concomitant decrease in reporter stability associated with the reduced accumulation at the INM. Although a direct effect of nucleoporins in controlling reporter stability is difficult to envision, a secondary effect of nucleporin depletion in reporter expression is possible. The model assumes that reporter synthesis rate (v_t) is stable over the time frame of translocation; it is possible that knock down of Nups (e.g. Nup98 and Nup153, important for mRNA export Powers et al., 2007) could result in a acute decrease in reporter synthesis rate by depletion of the reporter mRNA in the cytoplasm. However reporter expression after 48 hours KDs of these Nups is not generally and consistently lower than the one of control siRNA suggesting that an acute drop in translation rate during the recorded translocation is unlikely. Indeed total reporter concentration in SEC13 KD cells does not change over 2.5 hrs frame when the protease is maintained inactive indicating that synthesis rate is stable.

4.6 INM protein targeting is limited by available nuclear retention sites

As soon as INM proteins reach the INM nucleus through the NPC, they can interact with nuclear binding partners. As the kinetic analysis has shown, efficient LBR INM accumulation relies on a fivefold reduced export rate compared to import due to binding at the INM. Interestingly, I observed an increased targeting of the reporter after knock down of lamin A which the model predicted to be due to an increased retention. Due to the abundance of nuclear lamina and chromatin it is often believed that nuclear binding sites are available in vast excess to INM protein ligands. Instead the increased retention we observed after knock down of lamin A, suggests that INM protein targeting is quite sensitive to the availability of nuclear binding sites.

It is possible that depletion of A-type lamins frees up B-type lamins as the cognate binding partners of the lamin B receptor based reporter. Another possibility is that INM proteins that bind preferentially Lamin A (e.g. emerin and Lap2) are cannot be targeted to the INM allowing more accumulation of LBR. These results suggest that the effective concentration of available binding sites at the INM is a major determinant for INM protein targeting in addition to the number of available pores.

4.7 The Nup93-based complexes function as size controllers of the NPC for membrane proteins

The screen revealed a third general insight, which is what controls the size selectivity of the NPC for membrane proteins. Nup93 is required to exclude the uncleaved reporter with the large retention domain in the ER, suggesting that Nup93 is part of the sizing mechanism of the NPC. It is has been shown that Nup93 can form two distinct complexes, either with Nup188 or Nup205 (Theerthagiri et al., 2010). In the screen NUP205 knock down showed a similar phenotype as NUP93 KD, albeit with only one siRNA, whereas neither of the two NUP188 siRNAs lead to loss of size selectivity against the uncleaved reporter. It is possible that incomplete depletion of Nup188 accounts for the lack of visible phenotype. Nevertheless Nup188 likely plays a similar role, since its depletion in mammalian cells allowed targeting of the INM protein Sun2 with an artificially enlarged nucleoplasmic domain that normally

excludes it from the nucleus (Antonin et al., 2011). Together these studies suggest that different Nup93-based complexes work together to establish the NPC's size selectivity for membrane proteins. In the future work it would be interesting to investigate if INM proteins with nucleoplasmic domains of different size are differentially affected when a particular Nup93-complex component is depleted. The already generated Target-INM variants offer a perfect tool to address this point.

4.8 Size selectivity for soluble proteins and membrane both involve Nup93 but are likely controlled by distinct mechanisms

Nup93 depletion also led to a moderate loss of size exclusion against medium sized soluble dextran indicating that the diffusion barrier for membrane and soluble macromolecules may have the same molecular basis. This double effect is in agreement with previous reports in *Caenorhabditis elegans* (Galy et al., 2003) and could be due to the loss of the central channel Nup62 after depletion of Nup93 observed in *Xenopus leavis* extracts (Sachdev et al., 2011). However, while both soluble and membrane protein size selectivity require Nup93, they are probably mechanistically distinct, since neither knock down of Nup62 nor of the other major soluble diffusion barrier determinant Nup98 impaired the size selectivity of the NPC for membrane protein in the screen. In this contest it would be important to directly assess the size exclusion for medium sized soluble cargo after depletion of Nup62 and Nup98. Conversely depletion of Nup188 did not impair the soluble protein diffusion barrier (Theerthagiri et al., 2010). Taken together, Nup93 is possibly required for two distinct size control mechanism in the NPC, one for soluble proteins based on Nup62 and potentially Nup98 and the other one for membrane proteins based on Nup188 and Nup205. This would be consistent with the model that membrane proteins pass the NPC through a route with a different size control mechanism than soluble cargo, such as the previously proposed lateral channel of the NPC.

4.9 The ER and NE proteins Nesprin-1 and SIGMAR1 affect LBR targeting

Two potentially interesting new regulators of INM protein targeting are identified in the screen: Nesprin1 (SYNE1) and SIGMAR1. The ONM protein Nesprin-1 is a component of LINC (Linker of the Cytoskeleton and Nucleoskeleton) complex and through interaction with the INM SUN protein believed to be involved in the maintenance of nuclear organization and structural integrity. There are nine isoforms of Nesprin-1, one of which (Nesprin-1alpha), is reported to be localized also in the INM where it interacts with emerin and lamin a (Mislov et al., 2002). SIGMAR1 (Sigma non-opioid intracellular receptor 1) is a protein receptor localized through the ER and NE membranes involved in different cellular functions like lipid transport from the endoplasmic reticulum and calcium signaling through ITP3R-dependent calcium efflux at the endoplasmic reticulum (Kekuda et al., 1996; Jbilo et al., 1997).

In future work it is important to first validate the phenotype seen after Nesprin-1 and SIGMAR1 depletion and excluding siRNA off target effects. Addressing which isoforms contribute to Nesprin-1 phenotype by rescue experiments using specific isoform can guide more functional follow up experiments whereas SIGMAR1 expression and localization still needs to be confirm in HeLa cell lines.

4.10 The diffusion retention model is sufficient to explain LBR targeting

The phenotypes I observed in the screen and their experimental validation suggest that LBR targeting can almost completely be explained with the diffusion retention model of INM protein targeting. The model predicts no asymmetric effects on import and export rates after knocking down different nucleoporins. In addition, none of the knock down of 17 members of the importin α/β family affected LBR INM targeting, including importin-α-16 (KPNA4-16), that has been proposed to support INM targeting of LBR (Braunagel et al., 2007).

This model is also supported by the evidence provided by Target-INM-Δ60LBR lacking the binding regions for different nuclear substrates (lamin B, histones and DNA binding domains) but still containing three NLS signals. Target-INM-Δ60LBR is largely localized in the ER membrane when the protease is active indicating that the

NLS signals are not sufficient to confer efficient INM localization, which rather requires the presence of the first 60 aa domain of LBR.

The sole evidence against a pure diffusion retention model I could find is the mild reduction in reporter accumulation after knock down of Importin β1 (KPNB1). However based on the kinetic signature of the importin β1 phenotype, the mathematical model predicts it to be caused by an increased export of the reporter rather than a decreased import, suggesting that importin β1 might normally regulate retention after an INM protein has reached the nucleus, rather than its translocation through the NPC. This prediction could be tested in future experiments, analogous to the FRAP validation experiments performed for the LMNA KD phenotype, the model predicted to be due to decreased export. FRAP experiments of the NE in cells depleted of importin β1 should show a faster fluorescence recovery after photobleaching.
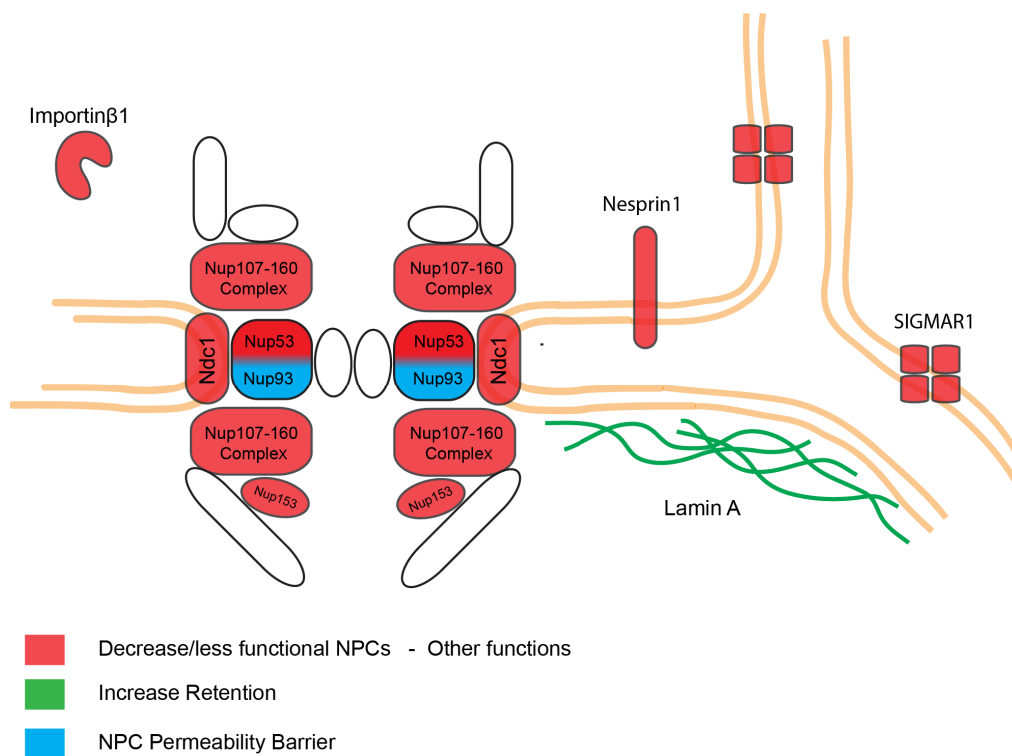
Figure 4.1 Mapping of screen hits in the NPC and NE. The colors genes that after cause decrease (red) and increase (green) translocation of the reporter or permeability of the NPC to the uncleaved form of the reporter (blue).

Abbreviations

NPC: Nuclear Pore Complex

INM: Inner Nuclear Membrane

ONM: Outer Nuclear Membrane

NE: Nuclear Envelope

ER: Endoplasmic Reticulum

HCV: Hepatite C Virus

CMPK: Chicken Muscle Pyruvate Kinase

LBR: Lamin B Receptor

Lap2β: Lamin associated polypeptide 2 β

Tor1AIP1: Torsin 1 A Interacting Protein 1

FRAP: Fluorescence Recovery After Photobleaching

CHX: Cycloheximide

Bibliography

Adam SA, Marr RS and Gerace L. (1990) Nuclear protein import in permeabilized mammalian cells requires soluble cytoplasmic factors. *J Cell Biol.* 111:807-16.

Aebi U, Cohn J, Buhle L and Gerace L. (1986) The nuclear lamina is a meshwork of intermediate-type filaments. *Nature* 323:560-4.

Akey, CW and Radermacher M. (1993). Architecture of the Xenopus nuclear pore complex revealed by three-dimensional cryo-electron microscopy. *J. Cell Biol. 122*, 1–19.

Akhtar A. and Gasser SM. (2007) The nuclear envelope and transcriptional control. *Nat Rev Genet.* 8:507-17.

Anderson DJ and Hetzer MW (2008) Reshaping of the endoplasmic reticulum limits the rate for nuclear envelope formation. *J Cell Biol.* 182:911-24.

Anderson DJ, Vargas JD, Hsiao JP and Hetzer MW.(2009) Recruitment of functionally distinct membrane proteins to chromatin mediates nuclear envelope formation in vivo. *J Cell Biol.* 186:183-91

Antonin W, Ellenberg J and Dultz E. (2008) Nuclear pore complex assembly through the cell cycle: regulation and membrane organization. *FEBS Lett.* 582(14):2004-16

Antonin W, Ungricht R, Kutay U. (2011) Traversing the NPC along the pore membrane: targeting of membrane proteins to the INM. *Nucleus.* 2(2):87-91.

Asencio C, Davidson IF, Santarella-Mellwig R, Ly-Hartig TB, Mall M, Wallenfang MR, Mattaj IW and Gorjánácz M. (2012) Coordination of kinase and phosphatase activities by Lem4 enables nuclear envelope reassembly during mitosis. *Cell.* 150(1):122-35.

Audhya A, Desai A, and Oegema K. (2007) A role for Rab5 in structuring the endoplasmic reticulum. *J Cell Biol.* 178:43-56.

Beaudouin J, Gerlich D, Daigle N, Eils R and Ellenberg J (2002) Nuclear envelope breakdown proceeds by microtubule-induced tearing of the lamina. *Cell* 108:83-96.

Beck M, Förster F, Ecke M, Plitzko J.M, Melchior F, Gerisch G, Baumeister W and Medalia O. (2004) Nuclear pore complex structure and dynamics revealed by cryoelectron tomography. *Science.* 306(5700):1387-90.

Beck M, Lucić V, Förster F, Baumeister W. and Medalia O. (2007) Snapshots of nuclear pore complexes in action captured by cryo-electron tomography. *Nature* 449:611-5.

Bengtsson L and Otto H. (2008) LUMA interacts with emerin and influences its distribution at the inner nuclear membrane. *J Cell Sci.* 121:536-48

Bergmann JE and Singer SJ. (1993) Immunoelectron microscopic studies of the intracellular transport of the membrane glycoprotein (G) of vesicular stomatitis virus in infected Chinese hamster ovary cells. *J Cell Biol.* 97(6):1777-87.

Bione S, Maestrini E, Rivella S, Mancini M, Regis S, Romeo G and Toniolo D. (1994) Identification of a novel X-linked gene responsible for Emery-Dreifuss muscular dystrophy. *Nat Genet.* 8:323-7.

Braunagel SC, Williamson ST, Ding Q, Wu X and Summers MD. (2007) Early sorting of inner nuclear membrane proteins is conserved. *Proc Natl Acad Sci U S A* 104:9307-12.

Brohawn SG, Partridge JR, Whittle JR and Schwartz TU (2009) The nuclear pore complex has entered the atomic age. *Structure.* 17(9):1156-68.

Jokhi V, Ashley J, Nunnari J, Noma A, Ito N, Wakabayashi-Ito N, Moore MJ, Budnik V. (2013) Torsin mediates primary envelopment of large ribonucleoprotein granules at the nuclear envelope. *Cell Rep.* 3(4):988-95.

Burke B and Stewart CL. (2006) The laminopathies: the functional architecture of the nucleus and its contribution to disease. *Annu Rev Genomics Hum Genet.* 7:369-405

Cabrita LD, Gilis D, Robertson AL, Dehouck Y, Rooman M and Bottomley SP (2007) Enhancing the stability and solubility of TEV protease using in silico design *Protein Sci.* 16:2360-7

Capelson M, Liang Y, Schulte R, Mair W, Wagner U, and Hetzer MW.(2010) Chromatin-bound nuclear pore components regulate gene expression in higher eukaryotes. Cell. 140:372-83.

Casolari JM, Brown CR, Komili S, West J, Hieronymus H and Silver PA. (2004) Genome-wide localization of the nuclear transport machinery couples transcriptional status and nuclear organization. *Cell.* 117:427-39.

Chaudhary N and Courvalin JC. (1993) Stepwise reassembly of the nuclear envelope at the end of mitosis. *J Cell Biol.* 122:295-306.

Collas P, Courvalin JC and Poccia D. (1996) Targeting of membranes to sea urchin sperm chromatin is mediated by a lamin B receptor-like integral membrane protein. *J Cell Biol.* 135:1715-25

Collinet C, Stöter M, Bradshaw CR, Samusik N, Rink JC, Kenski D., Habermann B, Buchholz F, Henschel R., Mueller MS, Nagel WE, Fava E, Kalaidzidis Y and Zerial M (2010) Systems survey of endocytosis by multiparametric image analysis. *Nature* 464(7286):243-9.

Courvalin JC, Segil N, Blobel G and Worman HJ. (1992) The lamin B receptor of the inner nuclear membrane undergoes mitosis-specific phosphorylation and is a substrate for p34cdc2-type protein kinase. *J Biol Chem.* 267:19035-8.

Crisp M, Liu Q, Roux K, Rattner JB, Shanahan C, Burke B, Stahl PD and Hodzic D. (2006) Coupling of the nucleus and cytoplasm: role of the LINC complex. *J Cell Biol.* 172:41-53.

Daigle N, Beaudouin J, Hartnell L, Imreh G, Hallberg E, Lippincott-Schwartz J, Ellenberg J. (2001) Nuclear pore complexes form immobile networks and have a very low turnover in live mammalian cells. *J Cell Biol.* 154:71-84.

D'Angelo MA, Anderson DJ, Richard E and Hetzer MW (2006) Nuclear pores form de novo from both sides of the nuclear envelope. *Science* 312:440-3

D'Angelo MA, Raices M, Panowski SH and Hetzer MW (2009) Age-dependent deterioration of nuclear pore complexes causes a loss of nuclear integrity in postmitotic cells. *Cell.* 136:284-95.

D'Angelo MA, Gomez-Cavazos JS, Mei A, Lackner DH, Hetzer MW. (2012) A change in nuclear pore complex composition regulates cell differentiation. Dev Cell. 2012 Feb 14

Dauer WT and Worman HJ. (2009) The nuclear envelope as a signaling node in development and disease. *Dev Cell.* 17(5):626-38.

Dechat T, Pfleghaar K, Sengupta K, Shimi T, Shumaker DK, Solimando L. and Goldman RD. (2008) Nuclear lamins: major factors in the structural organization and function of the nucleus and chromatin. *Genes Dev.* 22(7):832-53.

Deng M, Hochstrasser M.(2006) Spatially regulated ubiquitin ligation by an ER/nuclear membrane ligase. *Nature.*443(7113):827-31.

Dixon JR, Selvaraj S, Yue F, Kim A, Li Y, Shen Y, Hu M, Liu JS and Ren B. (2012) Topological domains in mammalian genomes identified by analysis of chromatin interactions. *Nature.* 485(7398):376-80.

Doucet CM, Talamas JA and Hetzer MW (2010) Cell cycle-dependent differences in nuclear pore complex assembly in metazoa. *Cell* 141:1030-41

Dreger M, Bengtsson L, Schöneberg T, Otto H and Hucho F. (2001) Nuclear envelope proteomics: novel integral membrane proteins of the inner nuclear membrane. *Proc Natl Acad Sci U S A.* 98:11943-8

Dreger M, Otto H, Neubauer G, Mann M and Hucho F. (1999) Identification of phosphorylation sites in native lamina-associated polypeptide 2 beta. *Biochemistry* 38:9426-34.

Dultz E, Ellenberg J. (2007) Nuclear envelope. *Curr Biol.* 17(5):R154-6

Dultz and Ellenberg. Live imaging of single nuclear pores reveals a unique assembly mechanism in interphase. *J. Cell Biol. 191*, 15–22.

Dultz E, Zanin E, Wurzenberger C, Braun M, Rabut G, Sironi L and Ellenberg J (2008) Systematic kinetic analysis of mitotic dis- and reassembly of the nuclear pore in living cells. *J Cell Biol.* 180:857-65

Ellenberg J, Siggia ED, Moreira JE, Smith CL, Presley JF, Worman HJ and Lippincott-Schwartz J. (1997) Nuclear membrane dynamics and reassembly in living cells: targeting of an inner nuclear membrane protein in interphase and mitosis. *J Cell Biol.* 138(6):1193-206.

Erfle H, Neumann B, Rogers P, Bulkescher J, Ellenberg J and Pepperkok R. (2008) Work flow for multiplexing siRNA assays by solid-phase reverse transfection in multiwell plates. J Biomol Screen. 13(7):575-80

Fahrenkrog B and Aebi U. (2003) The nuclear pore complex: nucleocytoplasmic transport and beyond. *Nat Rev Mol Cell Biol.* 4:757-66.

Fornerod, M., Ohno, M., Yoshida, M. and Mattaj, I.W. (1997) CRM1 is an export receptor for leucine-rich nuclear export signals. *Cell 90:*1051-1060

Frey S and Görlich D. (2007) A saturated FG-repeat hydrogel can reproduce the permeability properties of nuclear pore complexes. *Cell* 130(3):512-23.

Furukawa K, Panté N, Aebi U, Gerace L. (1995) Cloning of a cDNA for lamina-associated polypeptide 2 (LAP2) and identification of regions that specify targeting to the nuclear envelope. *EMBO J.* 14:1626-36.

Galy V, Mattaj IW and Askjaer P (2003) Caenorhabditis elegans nucleoporins Nup93 and Nup205 determine the limit of nuclear pore complex size exclusion in vivo. *Mol Biol Cell.* 14(12):5104-15

Gardner JM, Smoyer CJ, Stensrud ES, Alexander R, Gogol M, Wiegraebe W, Jaspersen SL.(2011) Targeting of the SUN protein Mps3 to the inner nuclear membrane by the histone variant H2A.Z. J *Cell Biol.* 193(3):489-507.

Gorjánácz M and Mattaj IW. (2009) Lipin is required for efficient breakdown of the nuclear envelope in Caenorhabditis elegans. *J Cell Sci.* 122:1963-9

Guarda A, Bolognese F, Bonapace IM and Badaracco G. (2009) Interaction between the inner nuclear membrane lamin B receptor and the heterochromatic methyl binding protein, MeCP2. *Exp Cell Res.* 315:1895-903.

Guelen L, Pagie L, Brasset E, Meuleman W, Faza MB, Talhout W, Eussen BH, de Klein A, Wessels L, de Laat W and van Steensel B. (2008) Domain organization of human chromosomes revealed by mapping of nuclear lamina interactions. *Nature* 453(7197):948-51.

Güttinger S, Laurell E, Kutay U. (2009) Orchestrating nuclear envelope disassembly and reassembly during mitosis. *Nat Rev Mol Cell Biol.* 10:178-91

Han GS, O'Hara L, Carman GM and Siniossoglou S. (2008) An unconventional diacylglycerol kinase that regulates phospholipid synthesis and nuclear membrane growth. *J Biol Chem.* 283:20433-42.

Harris CA, Andryuk PJ, Cline S, Chan HK, Natarajan A, Siekierka JJ and Goldstein G. (1994) Three distinct human thymopoietins are derived from alternatively spliced mRNAs. *Proc Natl Acad Sci U S A.* 91:6283-7.

Harris CA, Andryuk PJ, Cline SW, Mathew S, Siekierka JJ and Goldstein G. (1995) Structure and mapping of the human thymopoietin (TMPO) gene and relationship of human TMPO beta to rat lamin-associated polypeptide 2. *Genomics* 28:198-205.

Harel A, Chan RC, Lachish-Zalait A, Zimmerman E, Elbaum M and Forbes DJ. (2003) Importin beta negatively regulates nuclear membrane fusion and nuclear pore complex assembly. *Mol Biol Cell.* 14:4387-96

Heessen S. and Fornerod M. (2007) The inner nuclear envelope as a transcription factor resting place. *EMBO Rep.* 8:914-9.

Held M, Schmitz MHA, Fischer B, Walter T, Neumann B, Olma MH, Peter M., Ellenberg J., and D.W. Gerlich (2010) CellCognition: time-resolved phenotype annotation in high-throughput live cell imaging. *Nat Meth.* 7: 747–754.

Hellemans J, Preobrazhenska O, Willaert A, Debeer P, Verdonk PC, Costa T, Janssens K, Menten B, Van Roy N, Vermeulen SJ, Savarirayan R, Van Hul W, Vanhoenacker F, Huylebroeck D, De Paepe A, Naeyaert JM, Vandesompele J, Speleman F, Verschueren K, Coucke PJ and Mortier GR. (2004) Loss-of-function mutations in LEMD3 result in osteopoikilosis, Buschke-Ollendorff syndrome and melorheostosis.*Nat Genet.* 36:1213- 8

Hériché J.K., J.G. Lees, I. Morilla, T. Walter, B. Petrova, M.J. Roberti, M.J Hossain, P. Adler, J.M. Fernández, M. Krallinger, C.H. Haering, J. Vilo, A. Valencia, J.A. Ranea, C. Orengo and J. Ellenberg (2014) Integration of biological data by kernels on graph nodes allows prediction of new genes involved in mitotic chromosome condensation. Mol. Biol. Cell 25(16) 2522-2536.

Hetzer M, Gruss OJ, and Mattaj IW. (2002) The Ran GTPase as a marker of chromosome position in spindle formation and nuclear envelope assembly. *Nat Cell Biol.* 4:177-84

Hieda M, Isokane M, Koizumi M, Higashi C, Tachibana T, Shudou M, Taguchi T, Hieda Y, Higashiyama S. (2008) Membrane-anchored growth factor, HB-EGF, on the cell surface targeted to the inner nuclear membrane. *J Cell Biol* 180(4):763-9.

Hinshaw, JE, Carragher BO and Milligan RA (1992). Architecture and design of the nuclear pore complex. *Cell 69*, 1133–1141.

Hirota T, Gerlich D, Koch B, Ellenberg J and Peters JM. (2004) Distinct functions of condensin I and II in mitotic chromosome assembly. *J Cell Sci.* 117:6435-45.

Hodzic DM, Yeater DB, Bengtsson L, Otto H and Stahl PD. (2004) Sun2 is a novel mammalian inner nuclear membrane protein. *J Biol Chem.* 279:25805-12

Hofemeister H, O'Hare P. (2005) Analysis of the localization and topology of nurim, a polytopic protein tightly associated with the inner nuclear membrane. *J Biol Chem.* 280:2512-21

Hoffmann K, Dreger CK, Olins AL, Olins DE, Shultz LD, Lucke B, Karl H, Kaps R, Müller D, Vayá

A, Aznar J, Ware RE, Sotelo Cruz N, Lindner TH, Herrmann H, Reis A and Sperling K. (2002) Mutations in the gene encoding the lamin B receptor produce an altered nuclear morphology in granulocytes (Pelger-Huët anomaly) *Nat Genet.* 31:410-4

Horn HF, Brownstein Z, Lenz DR, Shivatzki S, Dror AA, Dagan-Rosenfeld O, Friedman LM, Roux KJ, Kozlov S, Jeang KT, Frydman M, Burke B, Stewart CL and Avraham KB. (2013) The LINC complex is essential for hearing. *J Clin Invest.* 123(2):740-50.

Hülsmann BB, Labokha AA, Görlich D. (2012) The permeability of reconstituted nuclear pores provides direct evidence for the selective phase model. *Cell.*150(4):738-51.

Isokane M, Hieda M, Hirakawa S, Shudou M, Nakashiro K, Hashimoto K, Hamakawa H, Higashiyama S.(2008) Plasma-membrane-anchored growth factor pro-amphiregulin binds A-type lamin and regulates global transcription. *J.Cell Sci* 121(Pt 21):3608-18

Jbilo O, Vidal ., Paul R, De Nys N, Bensaid M, Silve S, Carayon P, Davi D, Galiegue S, Bourrie B, Guillemot JC, Ferrara P, Loison G, Maffrand JP, Le Fur G and Casellas P. (1997) Purification and characterization of the human SR 31747A-binding protein. A nuclear membrane protein related to yeast sterol isomerase." *J. Biol. Chem.* 272:27107-27115

Johnson DC, Baines JD. (2011) Herpesviruses remodel host membranes for virus egress. *Nat Rev Microbiol.* 9(5):382-94.

Katta SS, Smoyer CJ, Jaspersen SL. (2014) Destination: inner nuclear membrane.*Trends Cell Biol.* 24(4):221-9.

Kekuda R., Prasad PD., Fei YJ., Leibach FH. and Ganapathy V. (1996) Cloning and functional expression of the human type 1 sigma receptor (hSigmaR1) Biochem. Biophys. Res. Commun. 229:553-558

Kervrann C, Legland D. and Pardin L. (2004) Robust incremental compensation of the light attenuation with depth in 3D fluorescence microscopy. Journal of Microscopy 214: 297–314.

King MC, Lusk CP, Blobel G.(2006) Karyopherin-mediated import of integral inner nuclear membrane proteins. *Nature.* 442(7106):1003-7

Kaiser C., E.Y. Dobrikova, S.S. Bradrick , M. Shveygert, J.T. Herbert, and M. Gromeier (2008) Activation of cap-independent translation by variant eukaryotic initiation factor 4G in vivo. *RNA.* 2008 14(10):2170-82. doi: 10.1261/rna.1171808.

Kalverda B, Pickersgill H, Shloma VV, Fornerod M. (2010) Nucleoporins directly stimulate expression of developmental and cell-cycle genes inside the nucleoplasm. *Cell.* 140:360-71.

Kerr AR, Schirmer EC.(2011) FG repeats facilitate integral protein trafficking to the inner nuclear membrane. *Commun Integr Biol.* 4(5):557-9

Korfali N, Wilkie GS, Swanson SK, Srsen V, Batrakou DG, Fairley EA, Malik P, Zuleger N, Goncharevich A, de Las Heras J, Kelly DA, Kerr AR, Florens L and Schirmer EC (2010) The leukocyte nuclear envelope proteome varies with cell activation and contains novel transmembrane proteins that affect genome architecture *Mol Cell Proteomics.* 9(12):2571-85

Korfali N, Wilkie GS, Swanson SK, Srsen V, de Las Heras J, Batrakou DG, Malik P, Zuleger N, Kerr AR, Florens L and Schirmer EC. (2012) The nuclear envelope proteome differs notably between tissues. *Nucleus* 3(6):552-64.

Krüger A, Batsios P, Baumann O, Luckert E, Schwarz H, Stick R, Meyer I, Gräf R. (2012) Characterization of NE81, the first lamin-like nucleoskeleton protein in a unicellular organism. *Mol Biol Cell.* 23(2):360-70.

Krull S, Thyberg J, Björkroth B, Rackwitz HR and Cordes VC. (2004). Nucleoporins as components of the nuclear pore complex core structure and Tpr as the architectural element of the nuclear basket. *Mol Biol Cell.* 15(9):4261-77.

Lamarre D, Anderson PC, Bailey M, Beaulieu P, Bolger G, Bonneau P, Bös M, Cameron DR, Cartier M, Cordingley MG, Faucher AM, Goudreau N, Kawai SH, Kukolj G, Lagacé L, LaPlante SR, Narjes H, Poupart MA, Rancourt J, Sentjens RE, St George R, Simoneau B, Steinmann G, Thibeault D, Tsantrizos YS, Weldon SM, Yong CL and Llinàs-Brunet M (2003) An NS3 protease inhibitor with antiviral effects in humans infected with hepatitis C virus. *Nature.* 426:186-9

Ledeen RW and Wu G. (2006) Sphingolipids of the nucleus and their role in nuclear signaling. *Biochim Biophys Acta.* 1761:588-98.

Lénárt P, Rabut G, Daigle N, Hand AR, Terasaki M and Ellenberg J. (2003) Nuclear envelope breakdown in starfish oocytes proceeds by partial NPC disassembly followed by a rapidly spreading fenestration of nuclear membranes. *J Cell Biol.* 160:1055-68

Liang Y, Chiu PH, Yip KY, Chan SY.(2011) Subcellular localization of SUN2 is regulated by lamin A and Rab5. *PLoS One.* 6(5):e20507.

Lin F, Blake DL, Callebaut I, Skerjanc IS, Holmer L, McBurney MW, Paulin-Levasseur M and Worman HJ.(2000) MAN1, an inner nuclear membrane protein that shares the LEM domain with lamina-associated polypeptide 2 and emerin. *J Biol Chem.*

Lin F, Morrison JM, Wu W and Worman HJ. (2005) MAN1, an integral protein of the inner nuclear membrane, binds Smad2 and Smad3 and antagonizes transforming growth factor-beta signaling. *Hum Mol Genet.* 14:437-45

Lin MZ, Glenn JS and Tsien RY (2008) A drug-controllable tag for visualizing newly synthesized proteins in cells and whole animals. *Proc Natl Acad Sci U S A.* 105:7744-9.

Liu Q, Pante N, Misteli T, Elsagga M, Crisp M, Hodzic D, Burke B, Roux KJ. (2007) Functional association of Sun1 with nuclear pore complexes. *J Cell Biol* 178(5):785-98.

Loïodice I, Alves A, Rabut G, Van Overbeek M, Ellenberg J, Sibarita JB, Doye V. (2004) The entire Nup107-160 complex, including three new members, is targeted as one entity to kinetochores in mitosis. *Mol Biol Cell.* 15(7):3333-44.

Lu W, Gotzmann J, Sironi L, Jaeger VM, Schneider M, Lüke Y, Uhlén M, Szigyarto CA, Brachner A, Ellenberg J, Foisner R, Noegel AA, and Karakesisoglou I. (2008) Sun1 forms immobile macromolecular assemblies at the nuclear envelope. *Biochim Biophys Acta.* 1783:2415-26.

Lu X, Shi Y, Lu Q, Ma Y, Luo J, Wang Q, Ji J, Jiang Q and Zhang C. (2010) Requirement for lamin B receptor and its regulation by importin {beta} and phosphorylation in nuclear envelope assembly during mitotic exit. *J Biol Chem.* 285(43):33281-93.

Lusk CP, Blobel G, King MC. (2007) Highway to the inner nuclear membrane: rules for the road. *Nat Rev Mol Cell Biol* 8(5):414-20

Ma Y, Cai S, Lv Q, Jiang Q, Zhang Q, Sodmergen, Zhai Z and Zhang C. (2001) Lamin B receptor plays a role in stimulating nuclear envelope production and targeting membrane vesicles to chromatin during nuclear envelope assembly through direct interaction with importin beta. *J Cell Sci.* 120:520-30.

Maimon T, Elad N, Dahan I and Medalia O. (2012) The human nuclear pore complex as revealed by cryo-electron tomography. *Structure*, 20:998-1006.

Mall M, Walter T, Gorjánácz M, Davidson IF, Nga Ly-Hartig TB, Ellenberg J and Mattaj IW. Mitotic lamin disassembly is triggered by lipid-mediated signaling. *J Cell Biol.* 198(6):981-90.

Malone CJ, Fixsen WD, Horvitz HR and Han M. (1999) UNC-84 localizes to the nuclear envelope and is required for nuclear migration and anchoring during C. elegans development. *Development*. 126:3171-81.

Manilal S, Nguyen TM, Sewry CA, and Morris GE (1996) The Emery-Dreifuss muscular dystrophy protein, emerin, is a nuclear membrane protein *Hum Mol Genet.* 5:801-8.

Mans BJ, Anantharaman V, Aravind L, Koonin EV. (2004) Comparative genomics, evolution and origins of the nuclear envelope and nuclear pore complex. *Cell Cycle* 3(12):1612-37

Margalit A, Brachner A, Gotzmann J, Foisner R. and Gruenbaum Y. (2007) Barrier-to-autointegration factor--a BAFfling little protein. *Trends Cell Biol.* 17:202-8.

Martins S, Eikvar S, Furukawa K and Collas P. (2003) HA95 and LAP2 beta mediate a novel chromatin-nuclear envelope interaction implicated in initiation of DNA replication. *J Cell Biol.* 160:177-88.

Maul HM, Hsu BY, Borun TM and Maul GG (1973) Effect of metabolic inhibitors on nuclear pore formation during the HeLa S3 cell cycle. *J Cell Biol* 59:669-76.

Matsuura, Y. and Stewart, M. (2004) Structural basis for the assembly of an nuclear export complex *Nature* 432:872-877

Meinema AC, Laba JK, Hapsari RA, Otten R, Mulder FA, Kralt A, van den Bogaart G, Lusk CP, Poolman B, Veenhoff LM. (2011) Long unfolded linkers facilitate membrane protein import through the nuclear pore complex. *Science.* 333(6038):90-3.

Melcon G, Kozlov S, Cutler DA, Sullivan T, Hernandez L, Zhao P, Mitchell S, Nader G, Bakay M, Rottman JN, Hoffman EP and Stewart CL.(2006) Loss of emerin at the nuclear envelope disrupts the Rb1/E2F and MyoD pathways during muscle regeneration. *Hum Mol Genet.* 15:637-51.

Mislow JM, Holaska JM, Kim MS, Lee KK, Segura-Totten M, Wilson KL and McNally EM. (2002) Nesprin-1alpha self-associates and binds directly to emerin and lamin A in vitro. *FEBS Lett.* 525:135-40.

Mohr D, Frey S, Fischer T, Güttler T and Görlich D (2009) Characterisation of the passive permeability barrier of nuclear pore complexes. *EMBO J.* 28: 2541-53.

Murthi A and Hopper AK. (2005) Genome-wide screen for inner nuclear membrane protein targeting in Saccharomyces cerevisiae: roles for N-acetylation and an integral membrane protein. *Genetics.* 170:1553-60.

Newport JW, Wilson KL and Dunphy WG. (1990) A lamin-independent pathway for nuclear envelope assembly. *J Cell Biol* 111:2247-59.

Nichols RJ, Wiebe MS and Traktman P. (2006) The vaccinia-related kinases phosphorylate the N' terminus of BAF, regulating its interaction with DNA and its retention in the nucleus. *Mol Biol Cell.* 17:2451-64

Nikolakaki E, Meier J, Simos G, Georgatos SD and Giannakouros T. (1997) Mitotic phosphorylation of the lamin B receptor by a serine/arginine kinase and p34(cdc2). *J Biol Chem.* 272:6208-13.

Nili E, Cojocaru GS, Kalma Y, Ginsberg D, Copeland NG, Gilbert DJ, Jenkins NA, Berger R, Shaklai S, Amariglio N, Brok-Simoni F, Simon AJ and Rechavi G. (2001) Nuclear membrane protein LAP2beta mediates transcriptional repression alone and together with its binding partner GCL (germ-cell-less). *J Cell Sci.* 114:3297-307

Ohba T, Schirmer EC, Nishimoto T, Gerace L. (2004) Energy- and temperature-dependent transport of integral proteins to the inner nuclear membrane via the nuclear pore. *J Cell Biol.* 167(6):1051-62.

O'Hara L, Han GS, Peak-Chew S, Grimsey N, Carman GM and Siniossoglou S (2006) Control of phospholipid synthesis by phosphorylation of the yeast lipin Pah1p/Smp2p Mg2+-dependent phosphatidate phosphatase. *J Biol Chem.* 281:34537-48

Osada S, Ohmori SY and Taira M. (2003) XMAN1, an inner nuclear membrane protein, antagonizes BMP signaling by interacting with Smad1 in Xenopus embryos. *Development.* 130:1783-94.

Ostlund C, Ellenberg J, Hallberg E, Lippincott-Schwartz J and Worman HJ (1999) Intracellular trafficking of emerin, the Emery-Dreifuss muscular dystrophy protein. *J Cell Sci.* 112:1709-19.

Ostlund C, Sullivan T, Stewart CL, Worman HJ. (2006) Dependence of diffusional mobility of integral inner nuclear membrane proteins on A-type lamins. *Biochemistry* 45(5):1374-82.

Pan D, Estévez-Salmerón LD, Stroschein SL, Zhu X, He J, Zhou S and Luo K. (2005) The integral inner nuclear membrane protein MAN1 physically interacts with the R-Smad proteins to repress signaling by the transforming growth factor-{beta} superfamily of cytokines. *J Biol Chem.* 280:15992-6001

Padmakumar VC, Libotte T, Lu W, Zaim H, Abraham S, Noegel AA, Gotzmann J, Foisner R and Karakesisoglou I. (2005) The inner nuclear membrane protein Sun1 mediates the anchorage of Nesprin-2 to the nuclear envelope. *J Cell Sci.* 118:3419-30.

kaPeric-Hupkes D, Meuleman W, Pagie L, Bruggeman SW, Solovei I, Brugman W, Gräf S, Flicek P, Kerkhoven RM, van Lohuizen M, Reinders M, Wessels L and van Steensel B. (2010) Molecular maps of the reorganization of genome-nuclear lamina interactions during differentiation. *Mol Cell.* 38(4):603-13.

Peters R. (2005) Translocation through the nuclear pore complex: selectivity and speed by reduction-of-dimensionality. *Traffic* 6(5): p. 421-7.

Polioudaki H, Kourmouli N, Drosou V, Bakou A, Theodoropoulos PA, Singh PB, Giannakouros T and Georgatos SD (2001) Histones H3/H4 form a tight complex with the inner nuclear membrane protein LBR and heterochromatin protein 1. *EMBO Rep.* 2:920-5

Powell L, Burke B. (1990) Internuclear exchange of an inner nuclear membrane protein (p55) in heterokaryons: in vivo evidence for the interaction of p55 with the nuclear lamina. *J Cell Biol.* 111 (6 Pt 1):2225-34.

Powers M.A., D.J. Forbes J.E. Dahlberg, and Lund E. (*1997)* The vertebrate GLFG nucleoporin, Nup98, is an essential component of multiple RNA export pathways. *J. Cell Biol.* 136*:241–250.*

Prüfert K, Vogel A and Krohne G. (2004) The lamin CxxM motif promotes nuclear membrane growth. *J Cell Sci.* 1176105-16

Rabut G, Doye V and Ellenberg J. (2004) Mapping the dynamic organization of the nuclear pore complex inside single living cells. *Nat Cell Biol.* 6:1114-21.

Ralle T, Grund C, Franke WW and Stick R. (2004) Intranuclear membrane structure formations by CaaX-containing nuclear proteins. *J Cell Sci.* 117:6095-104

Raju GP, Dimova N, Klein PS and Huang HC. (2003) SANE, a novel LEM domain protein, regulates bone morphogenetic protein signaling through interaction with Smad1. *J Biol Chem.* 278:428-37

Reichelt R, Holzenburg A, Buhle EL Jr, Jarnik M, Engel A, and Aebi U. (1990) Correlation between structure and mass distribution of the nuclear pore complex and of distinct pore complex components. *J Cell Biol.* 110:883-94.

Ribbeck K and Görlich D. (2001) Kinetic analysis of translocation through nuclear pore complexes. *EMBO J.* 20:1320-30.

Rolls MM, Stein PA, Taylor SS, Ha E, McKeon F and Rapoport TA. (1999) A visual screen of a GFP-fusion library identifies a new type of nuclear envelope membrane protein. *J Cell Biol.* 146:29-44.

Rout MP, Aitchison JD, Suprapto A, Hjertaas K, Zhao Y and Chait BT (2000). The yeast nuclear pore complex: composition, architecture, and transport mechanism. *J. Cell Biol. 148*, 635–651.

Roux KJ, Crisp ML, Liu Q, Kim D, Kozlov S, Stewart CL and Burke B.(2009) Nesprin 4 is an outer nuclear membrane protein that can induce kinesin-mediated cell polarization. *Proc Natl Acad Sci U S A.* 106:2194-9

Sabariegos R, Picazo F, Domingo B, Franco S, Martinez MA and Llopis J. (2009) Fluorescence resonance energy transfer-based assay for characterization of hepatitis C virus NS3-4A protease activity in live cells. *Antimicrob Agents Chemother.* 53:728-34.

Sachdev R., Sieverding C, Flötenmeyer M and Antonin W. 2012 The C-terminal domain of Nup93 is essential for assembly of the structural backbone of nuclear pore complexes. *Mol Biol Cell.* 23(4):740-9. doi: 10.1091/mbc.E11-09-0761.

Saksena S, Shao Y, Braunagel SC, Summers MD and Johnson AE. (2004) Cotranslational integration and initial sorting at the endoplasmic reticulum translocon of proteins destined for the inner nuclear membrane. *Proc Natl Acad Sci U S A.* 101:12537-42

Savas, JN, Toyama BH, Xu T, Yates JR and Hetzer MW (2012). Extremely long-lived nuclear pore proteins in the rat brain. *Science 335*, 942.

Schindelin J, Arganda-Carreras I, Frise E, Kaynig V, Longair M, Pietzsch T, Preibisch S, Rueden C, Saalfeld S, Schmid B, Tinevex JY, White DJ, Hartenstein V, Eliceiri K, Tomancak P and Cardona A (2012) Fiji: an open-source platform for biological-image analysis. *Nat Meth.* 9: 676–682.

Schirmer EC, Florens L, Guan T, Yates JR, Gerace L. (2003). Nuclear membrane proteins with potential disease links found by subtractive proteomics. *Science* 301(5638):1380-2

Simpson JC, Joggerst B, Laketa V, Verissimo F, Cetin C, Erfle H, Bexiga MG, Singan VR, Hériché JK, Neumann B, Mateos A, Blake J, Bechtel S, Benes V, Wiemann S, Ellenberg J and Pepperkok R. (2012) Genome-wide RNAi screening identifies human proteins with a regulatory function in the early secretory pathway. *Nat Cell Biol.* 14(7):764-74.

Solovei I, Wang AS, Thanisch K, Schmidt CS, Krebs S, Zwerger M, Cohen TV, Devys D, Foisner R, Peichl L, Herrmann H, Blum H, Engelkamp D, Stewart CL, Leonhardt H, and Joffe B. (2013) LBR and lamin A/C sequentially tether peripheral heterochromatin and inversely regulate differentiation. *Cell.* 152(3):584-98.

Somech R, Shaklai S, Geller O, Amariglio N, Simon AJ, Rechavi G and Gal-Yam EN (2005) The nuclear-envelope protein and transcriptional repressor LAP2beta interacts with HDAC3 at the nuclear periphery, and induces histone H4 deacetylation. *J Cell Sci.* 118:4017-25

Sosa BA, Rothballer A, Kutay U, Schwartz TU. (2012) LINC complexes form by binding of three KASH peptides to domain interfaces of trimeric SUN proteins. *Cell.*149(5):1035-47.

Soullam B, Worman HJ. (1993) The amino-terminal domain of the lamin B receptor is a nuclear envelope targeting signal. *J Cell Biol.* 120(5):1093-100.

Soullam B and Worman HJ (1995) Signals and structural features involved in integral membrane protein targeting to the inner nuclear membrane. *J Cell Biol.* 130:15-27.

Speese SD, Ashley J, Jokhi V, Nunnari J, Barria R, Li Y, Ataman B, Koon A, Chang YT, Li Q, Moore MJ, Budnik V. (2012) Nuclear envelope budding enables large ribonucleoprotein particle export during synaptic Wnt signaling. *Cell.* 149(4):832-46.

Starr DA and Han M. (2002) Role of ANC-1 in tethering nuclei to the actin cytoskeleton. *Science* 298:406-9

Strambio-De-Castillia C, Niepel M and Rout MP (2010) The nuclear pore complex: bridging nuclear transport and gene regulation. *Nat Rev Mol Cell Biol.* 11:490-501.

Stewart, M (2007) Molecular mechanism of the nuclear protein import cycle. *Nat. Rev. Mol. Cell. Biol.* 8:195-208

Szymborska A, de Marco A, Daigle N, Cordes VC, Briggs JA and Ellenberg J (2013) Nuclear pore scaffold structure analyzed by super-resolution microscopy and particle averaging. *Science.* 341(6146):655-8.

Walther TC, Alves A, Pickersgill H , Loïodice I, Hetzer M, Galy B, Hülsmann BB., Köcher T, Wilm M , Allen T, Mattaj IW and Doye V (2003). The conserved Nup107-160 complex is critical for nuclear pore complex assembly. *Cell.* 113(2):195-206.

Walter T, Held M, Neumann B, Hériché JK, Conrad C, Pepperkok R and Ellenberg J (2010) Automatic identification and clustering of chromosome phenotypes in a genome wide RNAi screen by time-lapse imaging. *Journal of Structural Biology.* 170: 1–9.

Wang Q, Du X, Cai Z and Greene MI. (2006) Characterization of the structures involved in localization of the SUN proteins to the nuclear envelope and the centrosome. *DNA Cell Biol.* 25:554-62

Waterham HR, Koster J, Mooyer P, Noort Gv G, Kelley RI, Wilcox WR, Wanders RJ, Hennekam RC and Oosterwijk JC. (2003) Autosomal recessive HEM/Greenberg skeletal dysplasia is caused by 3 beta-hydroxysterol delta 14-reductase deficiency due to mutations in the lamin B receptor gene. *Am J Hum Genet.* 72:1013-7

Weiss K. (2003) Regulating access to the genome: nucleocytoplasmic transport throughout the cell cycle. *Cell.* 112:441-51

Wilhelmsen K, Litjens SH, Kuikman I, Tshimbalanga N, Janssen H, van den Bout I, Raymond K and Sonnenberg A. (2005) Nesprin-3, a novel outer nuclear membrane protein, associates with the cytoskeletal linker protein plectin. *J Cell Biol.* 171:799-810.

Wilkie GS, Korfali N, Swanson SK, Malik P, Srsen V, Batrakou DG, de las Heras J, Zuleger N, Kerr AR, Florens L and Schirmer EC. (2011) Several novel nuclear envelope transmembrane proteins identified in skeletal muscle have cytoskeletal associations. *Mol Cell Proteomics.* 10(1):M110.003129.

Wilson K.L. and Foisner R. (2010) Lamin-binding Proteins. *Cold Spring Harb Perspect Biol.* 2 (4): a 00554.

Wong X, Luperchio TR and Reddy KL. (2014) NET gains and losses: the role of changing nuclear envelope proteomes in genome regulation. *Curr Opin Cell Biol.* 28:105-20.

Worman HJ. (2006) Inner nuclear membrane and regulation of Smad-mediated signaling. *Biochim. Biophys Acta* 1761(5-6):626-31

Worman HJ, Evans CD and Blobel G. (1990) The lamin B receptor of the nuclear envelope inner membrane: a polytopic protein with eight potential transmembrane domains. *J Cell Biol.* 111:1535-42.

Wu W, Lin F and Worman HJ (2002) Intracellular trafficking of MAN1, an integral protein of the nuclear envelope inner membrane. *J Cell Sci.* 115:1361-71.

Talamas JA and Hetzer MW. (2011) POM121 and Sun1 play a role in early steps of interphase NPC assembly. *J Cell Biol.* 2011 194(1):27-37.

Tapley EC and Starr DA. (2013) Connecting the nucleus to the cytoskeleton by SUN-KASH bridges across the nuclear envelope. *Curr Opin Cell Biol.* 25(1):57-62.

Terasaki M, Campagnola P, Rolls MM, Stein PA, Ellenberg J, Hinkle B and Slepchenko B. (2001) A new model for nuclear envelope breakdown. *Mol Biol Cell.* 12:503-10.

Theerthagiri, G., Eisenhardt N, Schwarz H, and Antonin W (2010) The nucleoporin Nup188 controls passage of membrane proteins across the nuclear pore complex. *J. Cell Biol.* 189:1129–1142. doi:10.1083/jcb.200912045

Tu LC and Musser SM. (2011) Single molecule studies of nucleocytoplasmic transport. Biochim Biophys Acta. 1813(9):1607-18.

Turgay Y, Ungricht R, Rothballer A, Kiss A, Csucs G, Horvath P and Kutay U. (2010) A classical NLS and the SUN domain contribute to the targeting of SUN2 to the inner nuclear membrane. *EMBO J.* 29:2262-75

Turgay Y, Champion L, Balazs C, Held M, Toso A, Gerlich DW, Meraldi P and Kutay U. (2014) SUN proteins facilitate the removal of membranes from chromatin during nuclear envelope breakdown. *J.Cell Biol.* 204(7):1099-109.

Ulbert S, Platani M, Boue S and Mattaj IW. (2006) Direct membrane protein-DNA interactions required early in nuclear envelope assembly. *J Cell Biol.* 173:469-76.

Voeltz GK, Prinz WA, Shibata Y, Rist JM and Rapoport TA.(2006) A class of membrane proteins shaping the tubular endoplasmic reticulum. *Cell* 124:573-86

Yang L, Guan T and Gerace L. (1997) Integral membrane proteins of the nuclear envelope are dispersed throughout the endoplasmic reticulum during mitosis. *J Cell Biol.* 137:1199-210.

Yao J, Fetter RD, Hu P, Betzig E, Tjian R. (2011) Subnuclear segregation of genes and core promoter factors in myogenesis. *Genes Dev.* 25(6):569-80.

Ye Q. and Worman HJ (1994) Primary structure analysis and lamin B and DNA binding of human LBR, an integral protein of the nuclear envelope inner membrane. *J Biol Chem.* 15;269(15):11306-11.

Zhang R, Durkin J, Windsor WT, McNemar C, Ramanathan L and Le HV (1997) Probing the substrate specificity of hepatitis C virus NS3 serine protease by using synthetic peptides. *J Virol.* 71:6208-13.

Zhang Q, Skepper JN, Yang F, Davies JD, Hegyi L, Roberts RG, Weissberg PL, Ellis JA and Shanahan CM. (2001) Nesprins: a novel family of spectrin-repeat-containing proteins that localize to the nuclear membrane in multiple tissues. *J Cell Sci.* 114:4485-98.

Zhou Z, Du X, Cai Z, Song X, Zhang H, Mizuno T, Suzuki E, Yee MR, Berezov A, Murali R, Wu SL, Karger BL, Greene MI and Wang Q. (2012) Structure of Sad1-UNC84 homology (SUN) domain defines features of molecular bridge in nuclear envelope. *J Biol Chem.* 287(8):5317-26.

Zhou XX, Chung HK, Lam AJ and Lin MZ. (2012) Optical control of protein activity by fluorescent protein domains. *Science* 338(6108):810-4

Zuleger N, Kelly DA, Richardson AC, Kerr AR, Goldberg MW, Goryachev AB, Schirmer EC (2011) System analysis shows distinct mechanisms and common principles of nuclear envelope protein dynamics. *J Cell Biol.* 193(1):109-23.

Zuleger N, Boyle S, Kelly DA, de las Heras JI, Lazou V, Korfali N, Batrakou DG, Randles KN, Morris GE, Harrison DJ, Bickmore WA and Schirmer EC. (2013) Specific nuclear envelope transmembrane proteins can promote the location of chromosomes to and from the nuclear periphery. *Genome Biol.* 14(2):R14.

Zullo JM, Demarco IA, Piqué-Regi R, Gaffney DJ, Epstein CB, Spooner CJ, Luperchio TR, Bernstein BE, Pritchard JK, Reddy KL and Singh H. (2012) DNA sequence-dependent compartmentalization and silencing of chromatin at the nuclear lamina. *Cell.* 149(7):1474-87.

Acknowledgements

First at all I would like to thank Jan Ellenberg for the opportunity to be part of his lab and for guiding me through my PhD with constant support and motivation.

I´m grateful to my thesis advisory committee – Iain Mattaj, Rainer Pepperkok and Oliver Gruss for their valuable input and to Ed Hurt and Edward Lemke for participating in the defense.

Many thanks go to all past and current Ellenberg lab members. It has been a great long time with all of you and each of you contributes to the friendly atmosphere in the lab. A special thank goes to Antonio for his inestimable help in my project and as well as to Wani, Julius and Bianca. I cannot forget Faba, from the ALMF, for her help in setting up my screen.

I have no enough "thank you" for Petr for taking interest in my work since the beginning and helping with the project. I´ve been extremely admired of your attitude to listen, your understanding power and the never ending propensity to teach and help me and other people. I extremely enjoy discussing the "non-scientific world" in all its flavors and the time spent together outside EMBL. I feel very lucky to have you as a colleague and I consider you a truly friend.

Foremost the amazing people that I met during the last 4 years made this PhD one of the most valuable experience of my life. The following lines are for you. Yuri, I could not now imagine all the past time without your heavy presence. You have been of great support in many occasions. I learnt from you how to do sit-ups in the gym and how to cook hamburgers and well…yes…I also learnt that differences and distances are vanishing when people cultivate the real value of life. I deeply hope this will be true also for the future time. I would not be in such a great shape without Claudia and Erika that contribute respectively 1/4 and 3/4 to the "increase" of my body mass by feeding me in countless dinners where I discovered two equally beautiful person. Bianca, I´m happy that the distance did not dilute but consolidate our friendship and I will always remember our dances of "Saltarello" and wait for many more. I would like to thank Rodolfo for his introspective questions and for sharing some

unforgettable and as well as expensive emotions in Baden-Baden Festspielhaus. A great thank you to Marzia; between coffee breaks I found in her an infinite source of advices and comforting words.

Avrei volute ringraziare chi mi ha insegnato ad andare sulla mia prima bici e coloro che mi hanno insegnato ad amare le colline intorno a Camartoni 1…con loro sento se ne sia andata un po´della mia saggezza .

Alla (unica) zia preferita Mara. Ne e´passato di tempo dalla lepre e tartaruga nel corridoio di casa ma continuo a correre anche grazie a te che so credi in me e al tuo costante supporto (non solo emotivo !!!!).

L´infinitamente piccolo che ho raggiunto non sarebbe stato possibile senza due galattiche persone. Mamma, la piu´ tenace e positiva, e Babbo (mio), il piu´sensibile e intelligente. Siete insieme qualcosa di unico e meraviglioso.